

Nicole Pfefferkorn

Master Thesis 2018: E12 supervised by  
Univ.-Prof. Dipl.-Ing. Dr.mont. Gerhard Thonhauser

# Update of the Geomechanical Pre-Drill Model of the Stripping T1/T1a Wellbore

Model Building and Comparison



*This thesis is dedicated to my grandparents.  
They gave me all they could to make me the person I am today.  
And to Emanuel.*





# Affidavit

I declare in lieu of oath that I wrote this thesis and performed the associated research myself using only literature cited in this volume.

# Eidesstattliche Erklärung

Ich erkläre an Eides statt, dass ich diese Arbeit selbständig verfasst, andere als die angegebenen Quellen und Hilfsmittel nicht benutzt und mich auch sonst keiner unerlaubten Hilfsmittel bedient habe.

---

Nicole Pfefferkorn, 23 April 2018



# Abstract

This thesis covers the methodology of the geomechanical model building and describes the requirement to continuously update a model with newly gained data from recently drilled wellbores. Such geomechanical models are used during well planning to predict important parameters like mud weight, pore pressure, in-situ stresses and favorable drilling direction, to enhance the safety of the drilling operation and reduce non-productive time and expenditures.

On the basis of the Stripfing Tief 1 wellbore, drilled in the central Vienna Basin, the differences between the pre- and post-drill model are evaluated and by this the improvements which arise from integrating new data into the already existing model (provided by Baker Hughes), could be demonstrated. For a better understanding of the geomechanical model building itself, first the general methodology with necessary explanations of input parameters and workflow steps is described, to afterwards illustrate in more detail how the model building is done for the specific case of the Stripfing Tief 1 wellbore. Here the focus is on the post-drill model workflow steps which significantly differ from the pre-drill ones because the quantity of new data allows for more appropriate analysis methods or a more exact determination. For the post-drill model, built during the accomplishment of this thesis with the JewelSuite™ program, this especially applies to pore pressure, minimum and maximum horizontal stress and stress direction. Those same parameters are addressed in a literature study where the applicability of the leak-off test analysis to determine the minimum horizontal stress and the possible generation mechanism of the overpressure, predicted and discovered in the Stripfing Tief 1 wellbore, are evaluated. Recommendations how to further improve the geomechanical model of the studied Stripfing Tief 1 wellbore by enhancing the quality of selected input parameters can be found in the respective sections as part of the discussion.



# Zusammenfassung

Diese Arbeit umfasst die Methodik des Erstellens eines geomechanischen Modells und beschreibt die Notwendigkeit des kontinuierlichen Aktualisierens mit neu erworbenen Daten von jüngst abgeteuften Bohrungen. Solche geomechanischen Modelle werden während der Planungsphase der Bohrvorhaben eingesetzt, um wichtige Parameter wie Spülgewicht, Porendruck, in-situ Spannungen, und einen möglichst vorteilhaften Bohrlochverlauf vorherzusagen, um die Sicherheit des Bohrvorhabens zu erhöhen und nicht-produktive Arbeitszeit und finanzielle Ausgaben zu verringern.

Anhand der Stripfing Tief 1 Bohrung, welche im zentralen Wiener Becken abgeteuft wurde, werden die Unterschiede zwischen dem vor und nach dem Bohren erstellten geomechanischen Modell erörtert und die Verbesserungen, welche durch das Einbeziehen von neu erworbenen Daten in das bereits existierende Modell (erstellt durch Baker Hughes) erreicht werden können, dargestellt. Um den eigentlichen Vorgang des Erstellens eines geomechanischen Modells besser verstehen zu können, wird zuerst die allgemeine Methodik, mit zugehörigen Erklärungen der Eingabeparameter und Arbeitsschritte, beschrieben, um drauffolgend die Erstellung des Modells für den spezifischen Fall der Stripfing Tief 1 Bohrung darzustellen. Hierbei liegt der Fokus auf den Arbeitsschritten des nach dem Bohren erstellten Modells, welche sich merklich von denen des vor dem Bohren erstellten Modells unterscheiden. Diese angesprochenen Unterschiede entstehen durch die Anzahl neuer Daten, welche passendere Analysemethoden oder exaktere Bestimmungen zulässt. Für das im Anschluss des Bohrvorhabens erzeugte Modell, welches im Zuge dieser Arbeit, mit dem Programm JewelSuite™, erstellt wurde, sind es vor allem die Parameter Porendruck, minimaler und maximaler horizontaler Stress und die Stressrichtung, für die diese bemerkbaren Unterschiede zutreffen. Eben diese Parameter werden in einer Literaturstudie, die sich mit der Anwendbarkeit der Analyse von Leak-Off Tests zum Zweck der Bestimmung des minimalen horizontalen Stresses und dem möglichen Entstehungsprozess des für die Stripfing Tief 1 Bohrung vorhergesagten und angetroffenen Überdruckes beschäftigt, evaluiert. Empfehlungen wie das Modell der Stripfing Tief 1 Bohrung in weiterer Folge durch die Verbesserung der Qualität ausgewählter Eingabeparameter weiterentwickelt werden kann, können im jeweiligen Absatz des Kapitels „Discussion“ gefunden werden.



# Acknowledgements

First, I would like to express my sincerely thanks to Dr. Leopold Bräuer, Dr. Mira Persaud and Nikolaus Bartl MSc, who gave me the opportunity to write my master thesis in such an extremely interesting topic. They supported me throughout the whole thesis with knowledge and encouragement and they admitted me as a full member of their team. I am truly grateful for your help.

Furthermore, I would like to express my gratitude to my supervisor at university Univ.-Prof. Dipl.-Ing. Dr. mont. Thonhauser for his advice and assistance during my studies and especially during writing this thesis.

Special thanks go to my colleagues in OMV for their support not only with know-how but also with kindness and the feeling of solidarity. Being a part of your group felt comfortable and I enjoyed it.

Thank you, Gerhard, for your patience and the geological support.

My family and friends deserve special acknowledgement for all the provided support and affection. You enrich my life every day.

We met because we both have a passion for this business. Thank you for being on my side, my beloved companion.





# Contents

Chapter 1 Introduction .....	1
Chapter 2 Geology .....	5
Chapter 3 Methodology of Building a Post-Drill Geomechanical Model – OMV Standard Workflow .....	9
3.1 Data Acquisition and Quality Check .....	11
3.2 Lithology Estimation .....	12
3.3 Vertical Stress Determination.....	13
3.4 Pore Pressure Prediction.....	13
3.5 Least Principal Stress Determination .....	15
3.6 Rock Properties Evaluation .....	16
3.6.1 Unconfined Compressive Strength.....	17
3.6.2 Internal Friction .....	17
3.6.3 Young’s Modulus .....	18
3.6.4 Poisson’s Ratio .....	18
3.6.5 Biot’s Coefficient.....	19
3.7 Horizontal Stress Orientation Estimation .....	19
3.7.1 Borehole Breakouts.....	20
3.7.2 Drilling Induced Tensile Fractures .....	24
3.7.3 Drilling Enhanced Fractures and Tensile Regions.....	26
3.8 Maximum Horizontal Stress Determination.....	26
3.9 Drilling Event Analysis .....	30
3.10 Verification of the Geomechanical Model.....	33
Chapter 4 Post-Drill Geomechanical Model for the Stripfing T1/T1a Well .....	35
4.1 Data Acquisition and Quality Check (Post-Drill).....	35
4.2 Lithology Estimation (Post-Drill) .....	39
4.3 Vertical Stress Determination (Post-Drill).....	41
4.4 Pore Pressure Prediction (Post-Drill) .....	43
4.5 Minimum Horizontal Stress Determination (Post-Drill).....	47
4.6 Maximum Horizontal Stress Magnitude and Azimuth Determination, Including Rock Properties Evaluation (Post-Drill) .....	52
4.7 Verification of the Geomechanical Model (Post-Drill) .....	60
4.8 Evaluation of Data Received from Sidetrack Drilling Occurrence .....	65
Chapter 5 Discussion .....	69

5.1 Comparison of Pre- and Post-Drill Model.....	69
5.1.1 Data Acquisition and Quality Check (Comparison).....	69
5.1.2 Lithology Estimation (Comparison) .....	70
5.1.3 Vertical Stress Determination (Comparison).....	71
5.1.4 Pore Pressure Prediction (Comparison) .....	72
5.1.5 Minimum Horizontal Stress Determination (Comparison).....	74
5.1.6 Rock Properties Evaluation (Comparison).....	76
5.1.7 Maximum Horizontal Stress Azimuth Determination (Comparison) .....	76
5.1.8 Maximum Horizontal Stress Determination (Comparison).....	77
5.1.9 Verification of the Geomechanical Model (Comparison) .....	77
5.1.10 Recommendations – Fulfilled or still suggested .....	78
5.2 Evaluation of Potential Reasons for the Overpressure Occurrence Encountered During Drilling the STR T1/T1a Wellbore .....	79
5.3 Estimation of Leak-Off Test Results as a Method for Minimum Horizontal Stress Determination.....	88
Chapter 6 Conclusion.....	97
Appendix .....	99

# Chapter 1 Introduction

To incorporate the geomechanical principles and integrate the opportunities arising from the application of that specific scientific field into the planning and drilling of a wellbore, brings several benefits not only to drilling but also to completion and production of wells in nearly all drilling campaigns. The most common method to include the geomechanical approach into the drilling subject is the generation of geomechanical models which are used to predict important information required for safe and cost-effective drilling procedures. Although the field of application is wide, the general workflow for the generation of the basic model is approximately the same for every geomechanical model and includes the determination of the stratigraphy, lithology, pore pressure, rock properties, in-situ stresses and stress direction and the verification of these parameters by the utilization of compressive borehole failures and geomechanically relevant drilling events. Apart from slight differences in model building arising from distinct approaches of the model building workflow in various companies, a decisive factor influencing the procedure of the different workflow steps is the fact whether the analysis deals with a pre- or a post-drill model. The generation of a pre-drill geomechanical model supports several decisions during the planning phase of a wellbore. For the drilling engineering planning phase this includes without limitation mud weight planning, fracture gradient prediction, most advantageous casing design, most favorable drilling inclination and azimuth and root cause analyses to identify zones or formations where special care needs to be taken because events like instabilities, lost circulations and inflows into the wellbore are to be expected. The building of such a drilling practice optimizing model requires a wide range of offset well data which describe the rock properties, stresses, pressures and drilling events in the geological region of the wellbore and in addition to that, offset well logs which can be depth stretched to fit the anticipated stratigraphy of the generic pre-drill wellbore model. Using these widespread information, the model of the synthetic well can be generated by combining the data delivered by the offset wells to a conclusive and verifying entirety.

In contrast to establishing a model prior to the drilling operation, a post-drill model is created after the wellbore has been drilled and all gathered information has been collected. Hence, this kind of a geomechanical model is obvious less dependent on offset well data and represents the prevailing conditions around the well as realistic as possible. However, determined by the extend of collected and measured data, the post-drill model utilizes assumptions and information from the pre-drill model if they are supposed to be conclusive. Such a post-drill model can thereby be considered to be an update of the pre-drill model and enhances the quality of the statements drawn from the forecasting model.

The wellbore which has been studied during the accomplishment of this thesis is named Stripfing Tief 1 (STR T1; with the associated sidetrack Stripfing Tief 1a) and is located in the central Vienna Basin north-east of Vienna. This well was planned as an exploration well to drill a large antiform, known as the Tallesbrunn high, which has been drilled several times before by a number of offset wells of the STR T1 wellbore. However, none of the key offset wellbores reached the important Upper Triassic reservoir rock, called the Hauptdolomit. Drilling events, experiences and measurements indicated several problematic zones along the planned well path of the STR T1 wellbore, including zones of lost circulation and/or inflows and abnormally high pressured zones. To minimize the

## Introduction

risks, non-productive time and costs associated with the drilling operation, a pre-drill geomechanical model was commissioned. This model was built by geomechanical engineers of Baker Hughes GMI Geomechanics Services who supplied the applicable model generated with the in-house software as well as the corresponding report (Geomechanical Earth Model (GEM) for the Stripfing Tief Area, Austria, 2012) and thereby provided the best geomechanical knowledge at that time and delivered the basis for a continuous update of this model (Zheng, Schulze, and Blumenthal 2012). As briefly described above, offset well data was used to create a model for the STR T1 well which summarized the important information which could be extracted from the offset well data sets. Thus, it was possible to determine all necessary parameters of a geomechanical model, namely stratigraphy and lithology, overburden stress, pore pressure, least principal stress, rock properties, maximum horizontal stress and maximum horizontal stress direction and to verify the model with the drilling experience documented for the key offset wells. However, the lack of important logging data, tests and general information made it necessary to include results and equations of other (geological comparable) geomechanical models into the pre-drill model building workflow. As a consequence of that fact several parameters of the model providing the opportunity to be improved if newly gained data from logging and measurements become available. To be more exact, the conduction of the workflow steps according to the OMV standard procedure for geomechanical model building requires a minimum selection of data which preferentially can be provided by the offset wells. For the STR T1/T1a pre-drill model the quantity of data from the offset wells was not sufficient to generate the model without applying results and assumptions from the Schönkirchen geomechanical earth model. This pertains especially for the minimum and maximum horizontal stress and stress direction determination. But the application of different equations borrowed from Schönkirchen GEM can also be found for modeling steps like vertical stress and unconfined compressive strength determination.

Like mentioned above, it is possible or rather preferable to continuously update such a geomechanical model by integrating data from accordingly drilled wells in the geological suitable setting. This is exactly what has been done during conducting the practical part of this thesis. After the STR T1/T1a wellbore was drilled and several logging runs were completed, a large amount of new data was acquired which describes the conditions in the near wellbore surrounding. This information includes data which partially has not been available for the pre-drill model building workflow, however also logs which were already available from offset wells have been logged and deliver a more accurate description of the well than the depth stretched ones, generated for the predicting model, do. The above stated differences between pre- and post-drill model for a single wellbore make the purpose of this thesis evident. The overall objective this thesis pursues is the update of the already generated pre-drill model which provides a suitable basis for this project. In more detail, this includes the generation of a completely new model with logging data and information gathered during drilling, however the assumptions and equations used during the pre-drill model workflow are tried to be kept constant because they were assumed to be valid for the geological setting of the STR T1/T1a wellbore. The list below shows the considerable workflow steps which are different for the post-drill model because the newly gained data allowed for other approaches to determine these parameters and because of that these steps represent important objectives:

- Pore pressure prediction with normal compaction trend and Eaton's Method and the additional evaluation of the pore pressure from kill mud weight calculations and drilling events
- Least principal stress determination by the Effective Stress Method, where the leak-off pressure analysis was used to determine minimum horizontal stress calibration points
- Image log analyses to determine the maximum horizontal stress direction and to ascertain input values for the maximum horizontal stress determination and model verification
- Maximum horizontal stress determination by the Effective Stress Method, where the stress polygon analysis was used to determine maximum horizontal stress calibration points

Additional to the creation of the post-drill model itself, the comparison of both models, where similarities and differences were figured out, is covered in this thesis. Moreover, the special pore pressure situation anticipated and discovered in the STR T1/T1a wellbore, gave rise to address the overpressure generation for this special case. For that reason, a brief literature study covering the subject of overpressure generation mechanisms was part of the theoretical part of the thesis. During the practical part, namely the model building, an overpressure generation mechanism was discussed as well and the procedure to evaluate the overpressure is described as part of the literature study. The last subject which arose during the model generation was the applicability of leak-off tests to determine calibration points for the least principal stress evaluation. A short literature study and an evaluation of the leak-off test results of the Stripfing well was conducted to address this last objective.

After this first introduction chapter, the description of the Stripfing Tief 1 geology will follow to get an overview of the geological background and the necessity of this drilling campaign. The structure of the succeeding chapters, where the methodology of the standard and the specific workflow is explained is subdivided into the same sections to simplify the understanding of the procedure and to allow for a general applicability. This classification follows the consecutive workflow steps executed during the model building by using the JewelSuite™ program to facilitate the reproducibility of the methodology. Nearly the same subdivision can also be found for the comparison of the models as one of the sections of the discussion chapter. Furthermore, the discussion includes the literature studies and analyses of the overpressure and leak-off test issue and is followed by the last concluding chapter.



## Chapter 2 Geology

The Stripfing Tief 1/Tief 1a wellbore has been planned as an exploration well with the intent to drill a large antiform in the central Vienna Basin where it was expected to discover the Upper Triassic Norian reservoir rock. This antiform which is known as the Tallesbrunn high, has already been drilled in the 1960ies and 1970ies. The Zwerndorf gas field and the sour gas field Baumgarten are located in this regional high, which was assumed to show a typical Northern Calcareous Alps stratigraphic succession, namely Neogene, Middle Triassic and Haselgebirge (Juvavic nappe), Upper Cretaceous and Jurassic (Tirolic nappe). For the offset wells (except the Zwerndorf T1) of the STR T1/T1a well it could not be managed to drill deeper than the Jurassic formations, but the stratigraphy of the Northern Calcareous Alps allowed to reason that the Upper Triassic formations underlying the Jurassic ones. This Upper Triassic formations have also been detected for example in the Gänserndorf Übertief 3 wellbore, where however, no Jurassic sequence has been drilled above. By the help of this exploration well, the forecasted stratigraphy should have been approved and the target formations (primary target: Hauptdolomit, secondary target: Steinalmkalk/-dolomite) should have been drilled. A new 3D seismic of the Vienna Basin showed the already known regional high in the structural map of the Pre-Neogene as well as in the structural map illustrating the Upper Cretaceous (Gosau) base. From this information, the geologists derived that the Tallesbrunn high was not formed by carbonates of the Middle Triassic but is caused by a deformation in the Triassic level of the Tirolic nappe. The fact that all stratigraphic levels are showing the same deformation indicates that the anticline structure was formed in post Gosauian times. Figure 1 is showing the seismic section of the Tallesbrunn high from south-west to north-east including the interpretation of the Neogene base, the Upper Cretaceous Gosau base and the expected top of the Upper Triassic Hauptdolomit as primary target. The Stripfing T1 wellbore has been planned to drill this clearly visible structure and the flat reflectors and explore the underlying formations which have not been reached by the offset wells. (Strauss and König 2015)

According to that seismic, OMV geologists developed several potential interpretations (Figure 2) which would explain the structure and the flat reflectors seen on the seismic plot. Three of these models were chosen to be realistic, where one of them was favored. For two of the models it was assumed that the flat reflectors represent geological features (Figure 2, 1 and 2) and that either the complete structure is formed by the Gosau including Jurassic and Triassic formation in form of olistoliths (Figure 2, 1) or that the structure is built by Jurassic formation including a Triassic olistolith (Figure 2, 2). The third option, which was selected to be the favored one, stated that the flat reflectors are not real and that the structure is the result of a thrust stack (Figure 2, 3 and Figure 3). The Jurassic formation in this case is of much smaller extend, but is assumed to represent an inverted basin containing a Triassic olistolith like it also was assumed for option number two. (Strauss and König 2015)

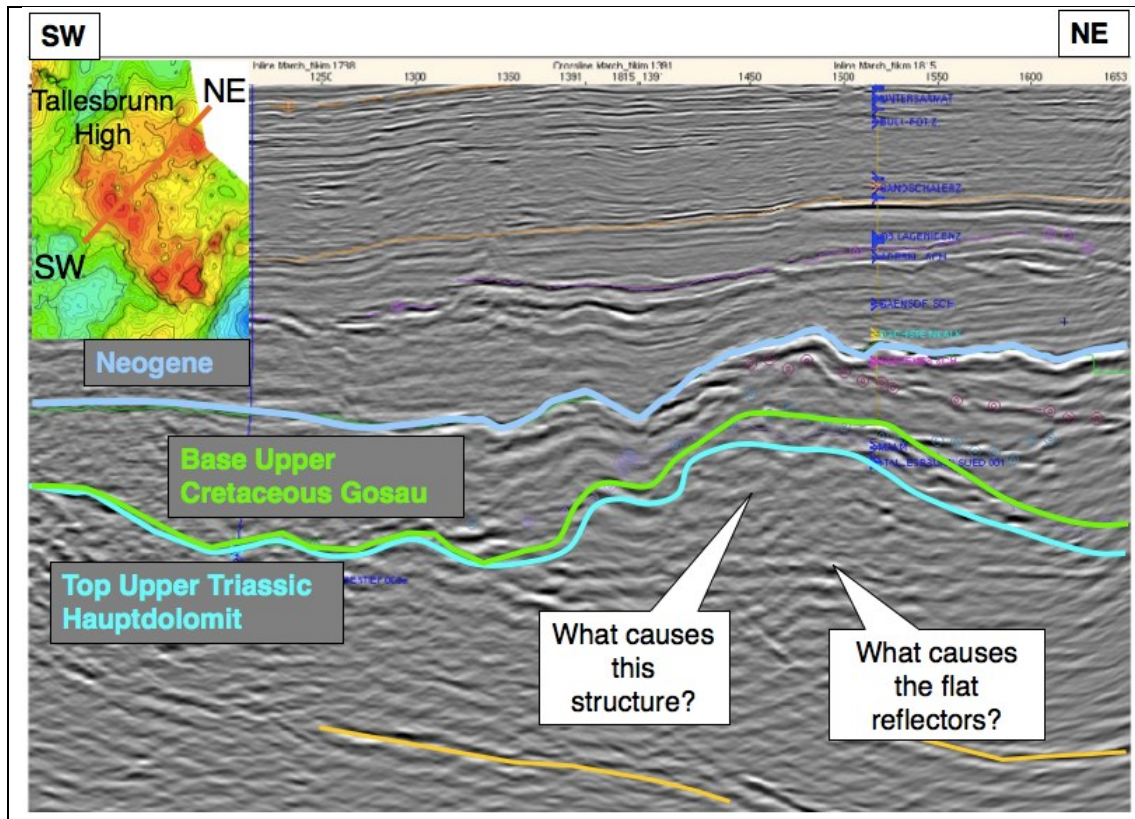


**Figure 1:** Seismic section of the Tallesbrunn high from SW to NE. Pictures, interpretations and explanations are borrowed from the AAR prepared by Strauss and König (2015).

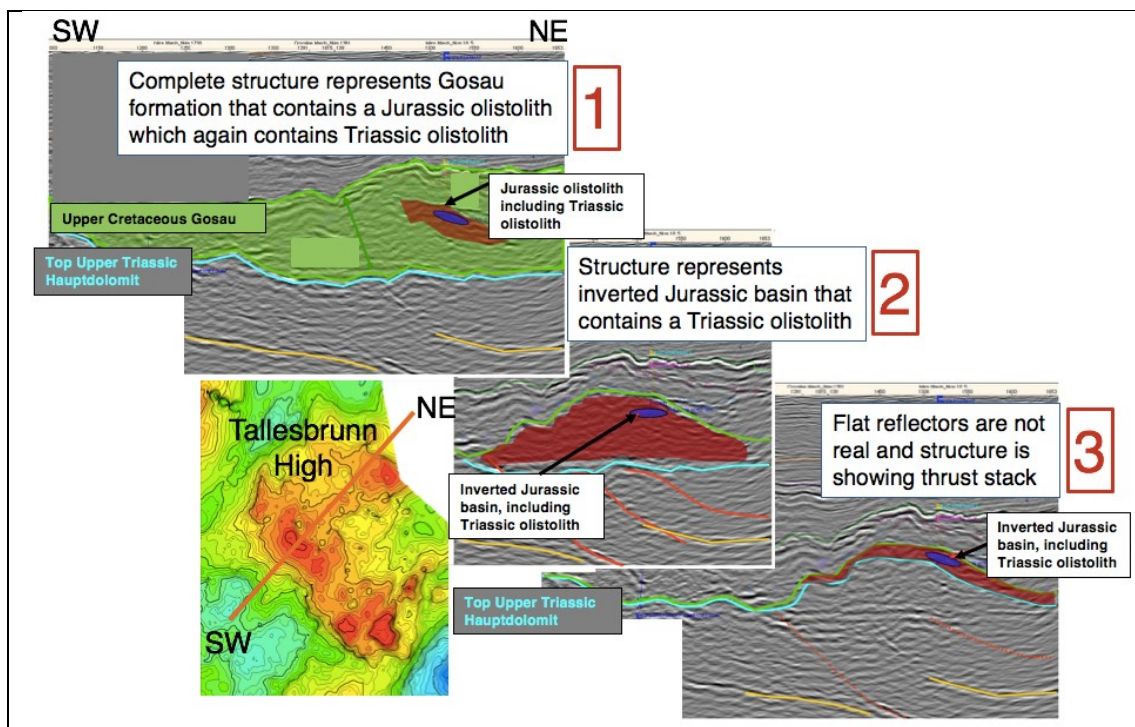


**Figure 2:** Potential geological interpretations of the seismic, explaining the noticeable structure and the flat reflectors. Pictures, interpretations and explanations are borrowed from AAR prepared by Strauss and König (2015).



The situation which was eventually found during drilling (Figure 4) was similar to the model which stated that the structure shows an inverted Jurassic basin with a Triassic olistolith embedded in the Jurassic sequence (Figure 2, version 2). The expected Upper Triassic Hauptdolomit however, was not found encased in the inverted Jurassic basin, but Middle Triassic rock of 1500m thickness had been drilled. After this unexpected large section of Middle Triassic rock, the well returned to the normal stratigraphy and found Upper Triassic Kössen formation below the Jurassic surrounding the olistolith. A similarity to the stratigraphy of the Zwerndorf T1 well is recognizable, where the Jurassic sections were drilled and Middle Triassic formation was reached below, which later on was interpreted as an olistolith (Strauss 2015). However, for the STR T1 it was managed to drill through the olistolith and reach the lower part of the Jurassic sequence (containing the olistolith) and Upper Triassic formation underlying this Middle Triassic and Jurassic formations (Strauss 2015). It is expected that below this formation, Upper Triassic Hauptdolomit (primary target) will follow, which could not be proven because the wellbore did not reach this depth due to technical problems.

By the evaluation of the information gathered during drilling, the assumption that the Tallesbrunn high is not caused by Middle Triassic carbonates could be disproved. The antiformal structure consists of an allochthonous Middle Triassic gliding complex which was in the first instance interpreted as an olistolith. Eventually another potential explanation of the origin of the Middle Triassic complex was considered. An individual nappe or thrust sheet, likely originating from the overthrusting of the Tirolic nappe by the Juvavic nappe, could be responsible for the occurrence of this Middle Triassic body embedded in Jurassic sequence (Knoop 2015). A final decision which event has caused this special stratigraphy was not stated as of this writing.

Detailed information on the stratigraphy of the STR T1 wellbore can be found in section 4.2 (Table 5) where also the lithology determination is described. Further geological information which has been relevant for the model building workflow and analysis, is mentioned in the respective context.

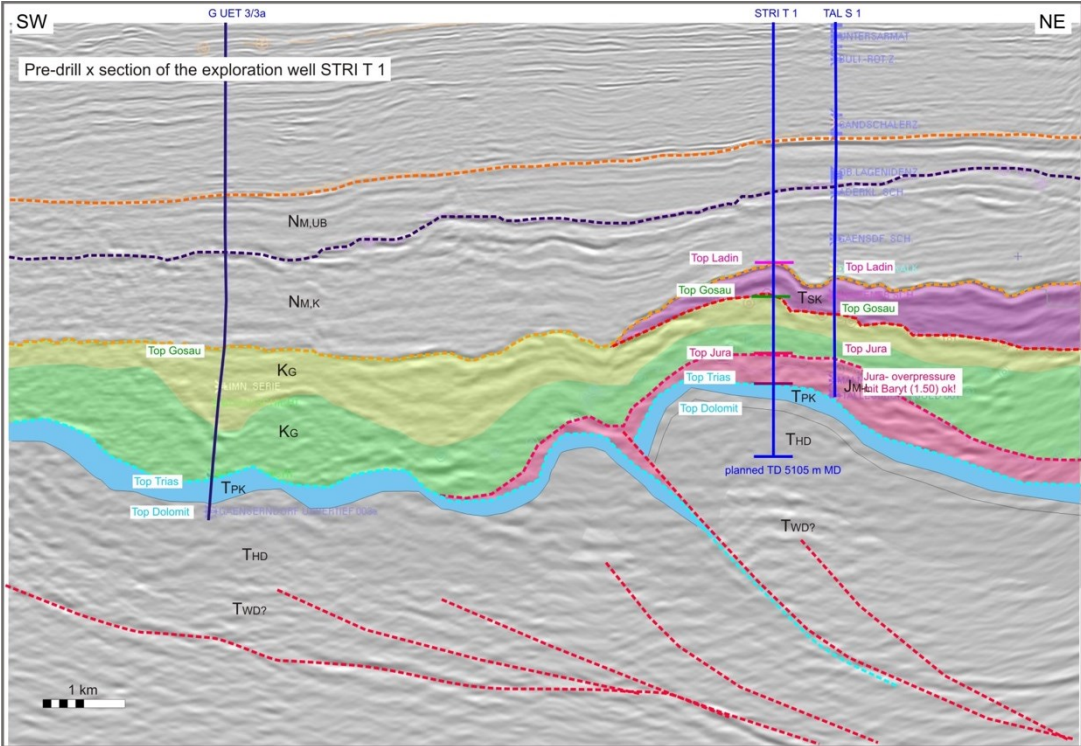


**Figure 3:** Interpretation of the seismic section of the STR T1 well, pre-drill. Pictures, interpretations and explanations are borrowed from AAR prepared by Strauss and König (2015).

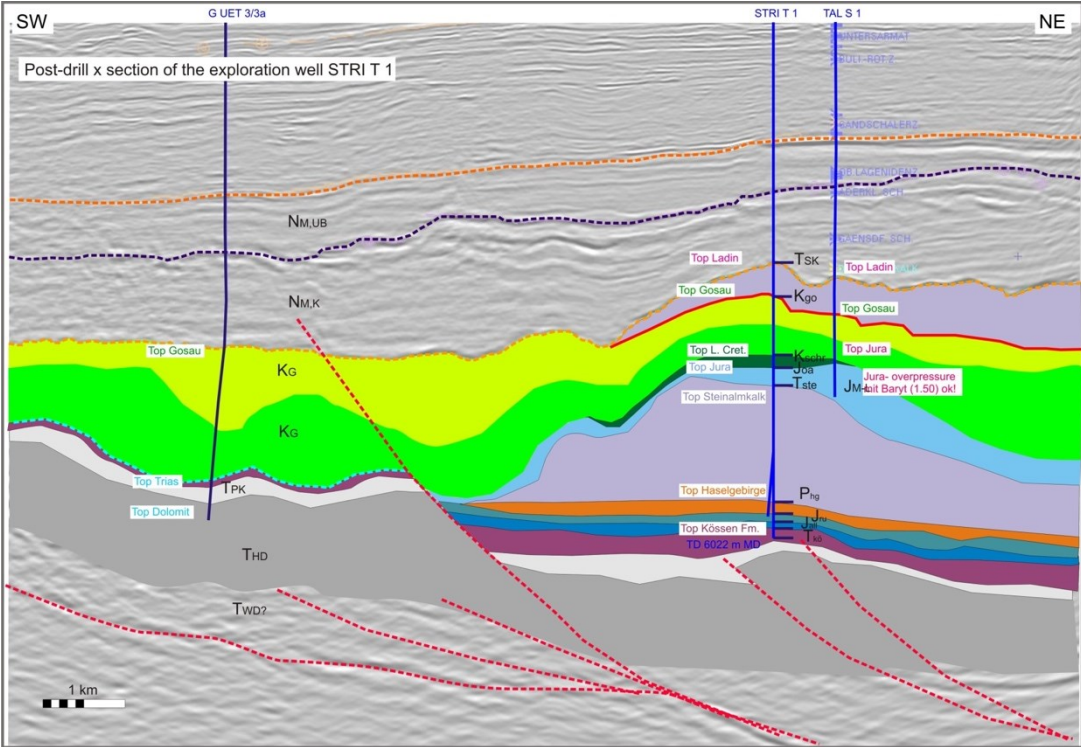


**Figure 4:** Interpretation of the seismic section of the STR T1 well, post-drill. Pictures, interpretations and explanations are borrowed from AAR prepared by Strauss and König (2015).

# Chapter 3 Methodology of Building a Post-Drill Geomechanical Model – OMV Standard Workflow

The development of a geomechanical model is not a regular practice done ahead or during every well planning. It is more a tool which is used for wells or regions where problems during drilling are expected or have already been experienced. The most common method is the development of a geomechanical earth model (GEM), where data of several offset wells is used to build a geomechanical model for a notional well where all information is combined. The GEM can then be used as a reference for the development of a model for wells drilled in this region. Models done in the planning phase of the wells are called pre-drill models and will help to predict for example wellbore failure, mud weights, best possible drilling direction, loss zones and zones of high pore pressure. Using a model as an instrument to get a forecast of the pressure and stresses in the earth will enable a much more safer drilling and can reduce NPT and costs. But even the best model is not able to predict the actual situation in the borehole hundred percent. As it was seen in the Stripfing T1/T1a case, the prediction can be fairly good for several sections. But it is also possible that the forecast is not matching with the model for other sections because of various reasons. During drilling, lots of different sets of data are collected. This data including log data, local measurements (e.g. LOTs, formation tests, pressure tests), recorded drilling events, geological data, cutting analysis and image data will later be used to update the pre-drill model with the real data gathered during drilling. Applying and updating geomechanical models can help to enhance future drilling projects by minimizing drilling problems such as stuck pipe incidents, tight holes, wellbore instabilities, losses, wellbore gains and kick events belonging to geomechanical uncertainties. By allowing a more accurate prediction of the pore pressure, stresses and stress direction, a better prediction of wellbore stability can be achieved and the MW curve for future drilling operations can be forecasted more applicable. Such an update or post-drill model can then be used to clarify open questions, confirm assumptions of the pre-drill model and improve the forecasted guesses. Figure 5 below shows an overview of the steps done successively to build a geomechanical model. In the following chapters, the workflow steps and the required input parameters are described in more detail. First the general tasks for an arbitrary model are explained to afterwards illustrate how the workflow steps have been accomplished for the case of the STR T1 wellbore.

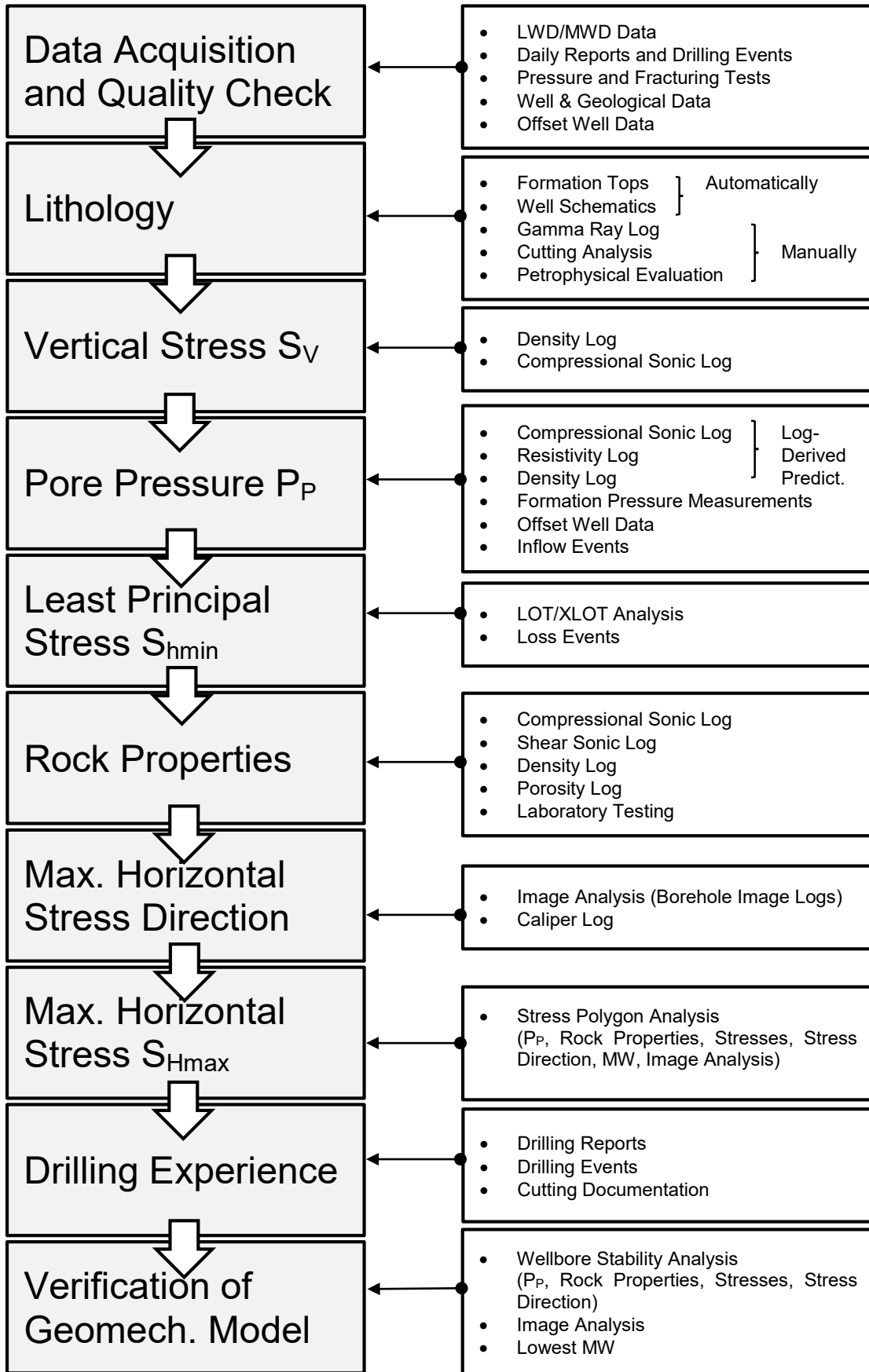


**Figure 5:** Overview of the workflow steps which are conducted during model building. The parameters on the right side act as input data for the individual workflow steps.

## 3.1 Data Acquisition and Quality Check

The starting point of a conclusive model is the collection of all useful information and data. This outranges the information gathered by logging while drilling (LWD) and measurement while drilling (MWD). Also, drilling and geological information like daily reports are an important source of information acting as input data for the different model workflow steps, as well as for the verification of the model at the end of the entire workflow.

For models built from data of recently drilled wells the quality check of the logging data is mostly already done by the petrophysicist who is handing over the processed data. Nevertheless, a second check of conclusiveness is advisable. It is also of importance to be well informed about the processing which was done and the necessity why it was done. To give an example, the petrophysicists using bad hole flags to show logging intervals where some data is not reliable because of the dependency of the logging equipment on a in gauge hole. This will also be important for the model building, because it is possible that calculated logs used for modeling show unrealistic values because of an impractical value of the input log. Therefore, it is useful to have such sections identified to not rely on erroneous data falsifying the outcome. For models using older data it may be useful to have a broader quality check of the data in case this was not done before.

The knowledge of quality and uncertainty of the information is an important factor for the wellbore stability analysis because the identification of the parameters with the highest uncertainty will help to adapt the model in an appropriate way. The stability analysis and the verification of the model require the change of input parameters, preferentially the most uncertain one (see 3.10).

The range of information which is valuable for a post-drill model is wide. It contains without limitation, information gathered from reports, logging data, measurement while drilling data, data from leak-off and pressure tests, drilling data like mud losses, kicks, inflows and stuck pipe events, as well as offset well data which can for example be suitable for calibration.

Before starting with the construction of the model, coordinate and unit system should be set up and useful data must be loaded in. These data include:

- Well data (well survey, well location, reference setting, trajectory, wellbore schematic data (well depth, casing size))
- Formation tops
- Logs
- Calibration data (also possible to add these data later)

The logs are needed over the entire depth of the wellbore. For this purpose, often several logs of the same property need to be combined to generate a single curve. Also, trend lines can be added in case data is missing or is not representing the logged parameter in an appropriate way. If different curves of the same parameter are available (e.g. density log, pseudo density calculated from sonic log and regional density data) a log can be composed out of these. It is possible to assemble the curve by choosing the most valid curve for dedicated depth ranges or using just one of the available logs as composite log. These log compositions are usually done graphically and the selected curves are then used

## Lithology Estimation

throughout the complete workflow. Several composite logs can be generated for the model workflow. It is not required to include all of them into the model, though. The composite logs which can be assembled are:

- Gamma Ray
- Density
- Acoustic (Compressional Sonic Slowness)
- Shear Acoustic (Shear Sonic Slowness)
- Caliper
- Resistivity
- Porosity
- Effective Porosity
- Velocity (Compressional Sonic Velocity)
- Shear Velocity (Shear Sonic Velocity)
- Rate of Penetration
- Drilling Exponent

Another useful application included in the JewelSuite™ program is the conversion of logs. This application is beneficial for model building because the slowness logs can be converted into velocity logs, which are required later in the workflow procedure. Furthermore, pressure and stress logs can be expressed in pressure (e.g. MPa) as well as mud weight (e.g. SG) units and it is possible to convert the original logs into logs with the alternative unit system.

## 3.2 Lithology Estimation

After loading all practical logs and data into JewelSuite™, the construction of the lithology should be done. It is important to mention that it is always possible to go back and forth during the workflow and change inputs, used formulas and methods and update the model as soon as new data becomes available. The only thing which is important is that all following steps must be recalculated. This can be done automatically or manually.

The lithology determination can be done automatically. In this case the zonation model is calculated based on the existing tops and well schematic information which has been inserted before. If the adaption to real lithology is possible, like in post-drill models where information about the drilled lithology is available through gamma ray logging and cutting analysis, the manual mode should be selected to build a zonation model as truthful as possible. Therefore, the lithology construction for the post-drill model is done by employing the evaluation of the petrophysicist and the cutting analysis from the geologist and building an as accurate as possible lithology log. To adjust the lithology, the gamma ray cut-off value for discriminating between two different lithology types can be changed. This cut-off value classifies the parts below and above a determined gamma ray value to the respective lithology. By lowering or raising this cut-off value the proportion of the two lithology types can be adapted. In case there are more than two lithology types present in the formation or section, the selection is restricted to the two main ones. If required, the insertion of zonation is possible to represent the actual lithology in an appropriate way, especially if the lithology is changing within the formations given by the geologist.

### 3.3 Vertical Stress Determination

Generally, a geomechanical model is built from the surface down to the TD of the wellbore. However, logging in most cases is not starting directly from the surface and it is also possible that logging is not performed to the end of the wellbore. If this is the case, it is necessary to correlate the logs with other available ones taking the dominant lithology into account or to use trend lines to fill the missing sections. This is not just relevant for density logs but for all logs which will be used during model building.

The vertical stress which is also called overburden pressure or lithostatic pressure describes the pressure or stress which the overlying rock exerts on the underlying formation simply by its weight. To build the overburden density curve throughout the whole length of the wellbore, the bulk density composite log and if needed the pseudo density log can be used. The pseudo density curve, which is calculated from the sonic slowness log should be used in sections where the results of the bulk density log show incorrect readings because of the dependency of the density logging tool on the condition of the borehole. If density data is missing it is also possible to fit a trend line to the overburden density curve, like for example an exponential extrapolation trend line for the section above and below the logged wellbore depth. By combining the bulk and the pseudo density curve together with the applied trend line the composite overburden density curve can be generated. The vertical stress or the vertical stress gradient can then be determined by integrating the composite overburden density log from the surface down to true depth by using equation ( 1), where  $S_v$  describes the vertical stress [Pa],  $\rho$  the rock density [ $\text{kg/m}^3$ ],  $z$  the depth [m] and  $g$  the gravitational acceleration [ $\text{m/s}^2$ ].

$$S_v = \int_0^z \rho(z) g dz \quad (1)$$

### 3.4 Pore Pressure Prediction

The determination of the pore pressure, also called pore pressure prediction (PPP) is a very essential part of the model building because the pore pressure is a crucial input parameter for workflow steps such as in-situ stress calculations (stress magnitudes are closely linked to the pore pressure magnitude), physical rock property determinations and stability analysis. Moreover, an as exact as possible pore pressure determination helps minimizing risks during drilling because an adjustment of the mud weight to the prevailing pore pressure can be implemented as precise as possible.

It is feasible to predict the pore pressure from shale properties derived from logging data such as sonic and resistivity logs. By the analysis of acoustic travel time, Hottmann and Johnson (1965) ascertained that the porosity in a shale decreases as a function of depth. This can be represented by the normal compaction trend (NCT) which illustrates the change of logging parameters (density, resistivity, sonic slowness and velocity) as a function of burial depth. The fluid pressure for NCT is assumed to be hydrostatic. If intervals with abnormal compaction are present, the measurements of the log properties diverge from the NCT. Too high porosity and too high transit time relative to its depth for example indicate an abnormal high fluid pressure.

## Pore Pressure Prediction

There are several methods for PPP with JewelSuite™, like Eaton's Method, Equivalent Depth Method, Ratio Pore Pressure Method and Bower's Method. In the OMV workflow the PPP with Eaton's Method is common practice. The application of the NCT is the requirement for the implementation of Eaton's Method to predict the pore pressure, because the trend line and the deviation from this trend line are delivering the input values of the physical properties used during the Eaton calculation to determine the pore pressure from different shale properties. In the JewelSuite™ workflow, applying Eaton's method, a PPP is possible from density, sonic and resistivity logs by applying equation ( 2 ) and ( 3 ), published by Eaton in 1972 and 1975.

$$P_p = S_V \left[ (S_V - P_{NCT}) \left( \frac{x_{obs}}{x_{NCT}} \right)^{1.2} \right] \quad (2)$$

$$P_p = S_V \left[ (S_V - P_{NCT}) \left( \frac{\Delta t_{NCT}}{\Delta t_{obs}} \right)^3 \right] \quad (3)$$

In these equations,  $P_p$  represents the pore pressure [MPa or SG],  $S_V$  the overburden pressure [MPa or SG],  $P_{NCT}$  the pressure for normally compacted shales [MPa or SG] (equals the hydrostatic pressure),  $x_{obs}$  the measurement of resistivity [ohm.m] or density [g/cm<sup>3</sup>] obtained from well logging,  $x_{NCT}$  the measurement of resistivity [ohm.m] or density [g/cm<sup>3</sup>] at normal (hydrostatic) pressure and  $\Delta t_{obs}$  and  $\Delta t_{NCT}$  the sonic compressional transit time measurement [μs/ft] obtained from well logging and at hydrostatic pressure, respectively. Due to difficulties to determine the shale resistivity and density for hydrostatic pressure conditions, the approach of drawing a normal compaction trend line to the respective log is used. Like stated above, using NCT lines, the pore pressure is solely estimated in shale intervals (sections with high GR lithology). By employing a NCT line to the composite logs for density, sonic slowness, formation resistivity and sonic velocity and using these trend lines together with the logging data as input values for the Eaton Method, pore pressure predictions for these logs are calculated. This is done by fitting a trend line to each of these logs and a resulting pore pressure curve for every input log is calculated. The depth track should show TVD during this process because NCT is just valid for TVD and not MD. The trend lines can be adjusted and repositioned until the different pore pressure curves match to a certain extend of contentment. With this resulting pore pressure curves, a general user defined pore pressure curve can now be constructed and manually adapted with self-determined accuracy. For this workflow, it is helpful to have direct measurements of pore pressure values to calibrate the interpretation to fixed pore pressure values. Such measurements can be for example formation pressure tests or well tests. Moreover, inflow/kick events are adjuvant to predict the pore pressure for the depth where the event occurred, with a very good accuracy. For this purpose, the kill mud weight which is going to be calculated for well control purpose, is taken as a reference point for the pore pressure.

Another source of information for PPP can be offset well data, like pore pressure measurements in wells where the same horizons were drilled. Prerequisites to use these data are that the measurements are taken approximately at the same depth, in the same formation and that there is no geological event separating the wells from each other in a geological sense (e.g. fault plane as barrier for hydraulic connection). If the region of interest is a well-known and highly explored field of activity, like it is the case for the Vienna Basin, pore pressures can also be empirical values.



Due to the fact that the pore pressure is in correlation with wellbore breakouts (wellbore collapse) and the fracture pressure, the accuracy of the borehole failure prediction increases with increasing accuracy of the pore pressure prediction.

### 3.5 Least Principal Stress Determination

The least principal stress represents the smallest one of the three in-situ stresses in the earth. Depending on the stress regime the least principal stress can be the minimum horizontal (for normal faulting and strike-slip faulting) or the overburden (for reverse faulting) stress. In the Vienna Basin, it is assumed that the predominant stress regime is normal faulting. This would imply that the least principal stress equals the minimum horizontal stress in this region.

There are three possible methods how the horizontal stresses can be determined using JewelSuite™ from Baker Hughes. These three methods are called Effective Stress Method, Stress Contrast and  $S_{Hmax}$  Equilibrium Ratio. The Effective Stress Method is the practice how the minimum horizontal stress determination from the overburden stress, the pore pressure and  $S_{Hmin}$  calibration points is done within the geomechanical department of OMV. These calibration points are minimum horizontal stress interpretations from hydraulic fracturing (HF), LOT or extended LOT (XLOT) executions. However, a determination of the minimum horizontal stress from HF is not a general practice within OMV and in this thesis the focus is on  $S_{Hmin}$  determination from LOTs or XLOTs. For this purpose, it is necessary to analyze the pressure vs. volume data of the leak-off tests and to determine the most reliable and meaningful pressure value which can be extracted from this data. The leak-off test description in section 5.3 explains in detail why it is possible to have more than one potential pressure value which can be used for the minimum horizontal stress determination and a closer look on LOT procedure and data analysis is given. Generally, the fracture closure pressure (FCP) is the most adequate magnitude for least principal stress determination, followed by the instantaneous-shut-in pressure (ISIP). However mostly the LOP is the one which is ascertained from the pressure vs. volume data, because the practical execution of these tests often differs from the execution and extension that would be needed to evaluate the other pressure measurements.

The pressure values determined from LOTs are subsequently utilized to develop the minimum horizontal stress curve using the effective stress ratio (ESR) method. For this purpose, the determined pressure values (FCP, ISIP, FPP or LOP) are taken as input values for the ESR equation ( 4). Together with the pore pressure ( $P_p$ ) and the vertical stress ( $S_v$ ) at the depth of interest, unitless effective stress ratio points are calculated and plotted to be illustrated. The values for  $S_v$  and  $P_p$  were estimated during the preceding model steps. By interpolation and extrapolation of the discrete values from top hole to TD (by adding a trend line to the local measurement points) an ESR curve is generated which afterwards can be used to calculate the minimum horizontal stress from top to bottom, using the same equation. Input values are now ESR, pore pressure and vertical stress, to get  $S_{Hmin}$  as resulting curve in mud weight (SG) and pressure (MPa) units. The units for the pressure and stress input parameters, respectively can be pressure (e.g. MPa) as well as mud weight (SG) units, but have to be the same for the individual calculations.

$$ESR_{min} = \frac{S_{hmin} - P_p}{S_v - P_p} \quad (4)$$

Assuming there is already a pre-drill model or a geomechanical earth model in place, like it has been the case for the Stripfing T1 wellbore, the ESR of these models can be used as a reference value to match the trend in this region (assess whether the unitless effective stress ratio points determined from LOT pressures match with the forecasted regional trend).

The magnitude of the maximum horizontal stress as well as the orientation of the stresses is another highly important task. The determination of the stress direction is done by the evaluation of image logs and caliper measurements. Within OMV's geomechanical department this is done manually by screening all existing image logs and precisely picking of breakouts and fractures to get a meaningful and as exact as possible direction of stress. The direction of the minimum horizontal stress is parallel to the breakout azimuth and perpendicular to the azimuth of the drilling induced tensile fractures, which, one the other hand is parallel to the maximum horizontal stress direction. The determination of the maximum horizontal stress magnitude also requires the analysis of the image logs, because the stress direction as well as the borehole breakout width and position are input values for the workflow which must be conducted to assess the maximum horizontal stress. Furthermore, the determination of the rock properties is required to get additional input parameters for this assessment. In the following section these rock properties and their calculation or determination are explained in more detail.

### 3.6 Rock Properties Evaluation

The calculation or determination of the rock properties is the next essential part of the model building. These parameters are input values and logs respectively for all following steps, including maximum stress magnitude determination, wellbore stability analysis and the model verification. The rock properties include elastic constants like Young's Modulus (E) and Poisson's Ratio ( $\nu$ ) and rock strength data like unconfined compressive strength (UCS) and angle of internal friction ( $\mu_i$ ). These basic parameters for any geomechanical model building can be determined from laboratory core measurements if cores have been taken during drilling. Assuming no cores have been taken and considering that it is not possible to log the whole wellbore depth, general correlations can be used to determine the rock properties for the geomechanical model. Whenever it is possible, correlations should be adjusted to the specific region by conducting lab tests to get an appropriate match of calculated and true rock property values, though. Typical logs required to calculate the rock properties are compressive and shear sonic (slowness/velocity) logs, porosity logs and bulk density logs. Based on these logs, the rock properties can be computed along the wellbore for the different formations. Changes in the magnitude of the curves showing natural variations of properties like strength (UCS) or stiffness (Young's Modulus) of the respective formation.

The JewelSuite™ program allows to choose from preset, general accepted formulas or to enter a user defined formula for each rock property for every single rock type. The input logs for the calculations must be chosen to generate rock property logs based on the definitions which have been made in the rock type form of the program.

For some of the rock properties, like internal friction and Biot's Coefficient, fixed values are used instead of calculated ones which would depend on logging data as input values.

These fixed values can be rock type dependent and stay constant for distinct lithology types like it is the case for the internal friction or a standard value is taken like it is mostly done for the Biot's Coefficient which often is assumed to be 1.

An important subject to mention in this context is the difference between static and dynamic moduli in geomechanical modeling. Which ones should be used as input parameters for calculations and why is either of them the better choice?

If a rock or rock sample experiences short time scale deformation (fractions of seconds) like it is the case for (acoustic) logging, the dynamic elastic moduli can be derived from log measurements, whereas for long time scale deformation like lab testing of cores (time scales in the order of hours to days), the static values can be determined from laboratory testing results. During OMV's model building workflow these static values are required for many of the applications. However, dynamic moduli are generally the gathered values because it is easier and cheaper to collect logging data than to conduct laboratory measurements. Laboratory measurements are expensive and core samples are taken mostly in the reservoir section and not throughout the whole well path. Therefore, static moduli are nearly always derived from the dynamic moduli by empirical relationships or calibration. Conversion factors are rock type dependent and range between 1 to 4, where rock types with lower stiffness (lower Young's Modulus) tend to have larger conversion factors (Zheng, Schulze, and Blumenthal 2012). In the ideal case the log derived values can be calibrated based on laboratory measurements. If no lab tests are available, accepted equations can be used to derive the static values from dynamic ones.

### 3.6.1 Unconfined Compressive Strength

The unconfined compressive strength of a rock is a measure of the strength of the rock which is determined during an unconfined uniaxial compressive stress tests. During such a test, the sample is axially compressed until it fails, without applying any radial stress ( $S_1 > 0$ ,  $S_2 = S_3 = 0$ ). The stress at which the failure occurs defines the axial compressive stress the rock sample can withstand under unconfined conditions. Furthermore, the UCS is one of the two parameters which are used to describe the linearized Mohr-Coulomb failure envelop. With the help of the laboratory tests, empirical correlations between the UCS and physical properties like sonic travel time, density, Young's Modulus and porosity are developed for the dedicated regions and lithology types. There are several known rock strength equations for different geological regions with various validation ranges for the respective input parameter. A good overview of different rock strength equations is for example presented in the book "Reservoir Geomechanics" from Zoback (2010). Despite the availability of already developed empirical equations, the correlation of these equations to rock tests is indispensable and should be carried out to adapt the published equations to the present geological setting.

### 3.6.2 Internal Friction

The internal friction ( $\mu_i$ ) is the other one of the two parameters (UCS and  $\mu_i$ ) which are used to describe the linearized Mohr-Coulomb failure envelop. Within this failure envelop, the internal friction is used to describe the slope of the failure line. Several equations are available in the JewelSuite™ program for the determination of the internal friction. These equations depend on compressional sonic velocity or gamma ray logs as input parameters. To not depend the entire rock strength parameters on sonic logs alone, it is not unusual to take fixed internal friction values for different rock types. The stronger the rock, the higher its friction coefficient should be.

### 3.6.3 Young's Modulus

The Young's Modulus is one of the five elastic moduli used to describe the linear proportional relationship between stress and strain in elastic behaving rocks. In idealized deformation measurements, Young's Modulus can be described as the stiffness of a rock in unconfined uniaxial compression tests ( 5).

$$E = \frac{S_{11}}{\varepsilon_{11}} = \frac{\text{axial stress}}{\text{axial strain}} \quad (5)$$

In geomechanical modeling, the Young's Modulus (usually given in GPa) can be determined by the application of equation ( 6). The input logs for this calculation are shear ( $v_s$ ) and compressional sonic ( $v_p$ ) velocity [m/s], derived from sonic slowness logs, and density [ $\text{kg/m}^3$ ]. Since the dynamic Young's Modulus is derived from log measurements, the resulting values for  $E_{\text{dynamic}}$  are larger than the values for  $E_{\text{static}}$  which are normally derived from laboratory measurements.

$$E_{\text{dynamic}} = \rho v_s^2 \frac{(3v_p^2 - 4v_s^2)}{v_p^2 - v_s^2} \quad (6)$$

If, however no laboratory measurements have been conducted on cores, known relationships must be used to evaluate the static Young's Modulus.

### 3.6.4 Poisson's Ratio

The Poisson's Ratio is another one of the five elastic moduli applied within the theory of linear elasticity and can be described as the ratio of lateral expansion to axial shortening in idealized deformation measurements ( 7).

$$\nu = \frac{\varepsilon_{33}}{\varepsilon_{11}} = \frac{\text{lateral expansion}}{\text{axial strain}} \quad (7)$$

The values for the Poisson's Ratio for rocks typically vary between 0.15 – 0.25. For weak porous rock  $\nu$  approaches to zero, whereas for unconsolidated sand  $\nu$  approaches to 0.5. Incompressible fluids also have a Poisson's Ratio of 0.5. By applying compressional and shear sonic log measurements, Poisson's Ratio can be calculated by using the compressional sonic velocity ( $v_p$ ) and the shear sonic velocity ( $v_s$ ) as input values for equation ( 8), shown below.

$$\nu_{\text{dynamic}} = \frac{v_p^2 - 2v_s^2}{2(v_p^2 - v_s^2)} \quad (8)$$

In the JewelSuite™ program, the factor between dynamic and static Poisson's Ratio is assumed to be 1 ( $\nu_{\text{stat}} = \nu_{\text{dyn}}$ ).

### 3.6.5 Biot's Coefficient

The Biot's Coefficient is used to describe the influence of the change in confining pressure on the pore pressure when the fluid has no possibility to escape from the pore space. The Biot's Coefficient can be applied for porous, fluid-saturated rock and is described by equation ( 9), where  $C_g$  and  $C_b$  describe the compressibility [ $\text{Pa}^{-1}$ ] of the individual solid grain of the rock and of the rock itself, respectively. Due to the fact, that the compressibility of the individual grain ( $C_g$ ) is smaller than or equal to the compressibility of the rock itself,  $\alpha$  has a magnitude between 0 and 1 ( $0 \leq \alpha \leq 1$ ). For a solid rock like quartzite which shows no interconnected porosity, the Biot Coefficient is 0, which means that the rock behavior is not influenced by the pore pressure. For a highly porous, compliant rock (e.g. uncemented sand), however the influence of the pore pressure on the rock behavior is maximized and the Biot Coefficient shows a value of 1, which is in most cases taken as the standard value for modeling. (Zoback 2010)

$$\alpha = 1 - \frac{C_g}{C_b} \quad (9)$$

## 3.7 Horizontal Stress Orientation Estimation

To ascertain the orientation of the minimum and the maximum horizontal stress the interpretation of the image data should be carried out. Image data shows different features which can be used to interpret the stress direction. A careful analysis of these features is the prerequisite for a reliable stress orientation prediction. Characteristics (borehole wall artefacts) belonging to key seating, washouts, tools touching the borehole wall or similar events solely depending on drilling activity, should be distinguished from characteristics belonging to geomechanical relevant events, to make sure just to include geomechanical occurrences into the evaluation of the stress orientation. The major features for the stress direction evaluation are borehole breakouts (BO) and drilling induced tensile fractures (DITF). More circumstantial features like drilling enhanced fractures (DEF) and tensile regions can be helpful in case no other features can be determined with a certain extend of accuracy. To enhance the detection of borehole breakouts on the image logs, caliper logs are used. On the basis of the caliper logging data, it is easier to differentiate between geomechanical relevant BOs and borehole wall artefacts belonging to drilling activity. It is also possible to determine the direction of the minimum horizontal stress from caliper logs alone in case no image logging has been conducted. However, the appropriate method to evaluate the stress direction of recently drilled wells is image analysis in combination with caliper logging results.

In case the well is vertical, the orientation of BOs and DITFs can directly be adopted as minimum respectively maximum horizontal stress orientation. For arbitrary deviated wellbores, such a relation between the orientation of the compressive (BO) and tensile failures (DITF) and the orientation of the far-field stresses is not existing. Breakouts are not always forming in the direction of the minimum horizontal stress like it can be observed for vertical wellbores. In arbitrary oriented wellbores, the breakout position depends on the magnitude and the orientation of the three principal stresses and on the wellbore orientation in relation to the stress field. Also, the orientation of the drilling induced tensile fractures is different for arbitrary deviated wellbores, where the tensile fractures initiate at the point around the wellbore where the minimum principal stress (which varies around the borehole wall) is tensile. These tensile fractures which are called

en echelon fractures form over the range of the angle where the wellbore is under tension. To conclude it can be said that the direction determination of the compressive and tensile wellbore failures which can be seen on the image logs differs significantly in vertical and deviated holes. Hence to derive the stress direction from BO and DITF observations of deviated wells is not as uncomplicated as it is for vertical wells. (Zoback 2010)

This thesis is not covering this subject in greater detail. For more information about stress determination in deviated wells, literature like “Reservoir Geomechanics” from Zoback (2010) can be recommended. In the following sections a vertical wellbore is assumed.

The wellbore breakouts and drilling induced tensile fractures are the most important and most meaningful characteristics for the stress orientation analysis with the help of image logs and will be used within the model building workflow. How to determine the different features on the image logs, where to pay attention to and what kind of information can be extracted from the image log analysis will be discussed in the following sections.

### 3.7.1 Borehole Breakouts

Features like breakouts and drilling induced tensile fracture form at the wellbore wall due to stress concentrations around the wellbore. These stress concentrations around a vertical well drilled parallel to the overburden stress ( $S_v$ ) are the result of the removal of material during drilling which therefore is no longer able to support the far-field stresses. The stresses prevailing at the wellbore wall are called hoop stress, radial stress and axial stress and can be calculated from the minimum and maximum horizontal stress, the pore pressure, the mud weight, the wellbore radius and the thermal stress (Kirsch Equations). At the azimuth of the minimum horizontal stress, the hoop stress reaches its maximum (increased compressive stress) and at the azimuth of the maximum horizontal stress the hoop stress reaches its minimum (decreased compressive stress). The hoop stress is the stress with the largest variation around the wellbore and because of that the most important one in terms of wellbore failure. In case this hoop stress concentration around the wellbore wall exceeds the rock strength, borehole breakouts will form over a finite width determined by the extend of the wellbore section where the hoop stress exceeds the rock strength. The azimuth of the minimum horizontal stress in this case defines the azimuth of origin of the breakouts. As mentioned above, these breakouts can be detected by the analysis of the image logs (combined with caliper logs) or by the evaluation of caliper logs alone if no image logs are available. Nevertheless, identifying BOs using images in combination with caliper data is much easier to comprehend and execute. Albeit the determination or picking of breakouts, tensile fractures and enhanced fractures (see 3.7.2 and 3.7.3) is a very subjective perception and the outcome of the picking of features can be diverse if two different persons pick the breakouts of the same section or even if the engineer has a second look on the features he or she picked before. Staying consistent throughout the whole logging interval is of high importance to get conclusive results. The picture below (Figure 6) depicts an example of breakouts picked on an image log of the Stripfing T1 well. This shown image log is a GVR™ log of the 12.25in section of the Stripfing wellbore. The three image logs on the left side show the same borehole section, but different depth of investigation. The first one on the left side visualizes the deepest investigation depth, the one to the right the shallowest one. The third and the fourth image (rightmost) show the same log, with and without picked breakouts. This availability of different investigation depths existing for GVR™ logs is quite useful because it can be detected whether the features which are visible on the logs are occurrences close to the borehole wall and fade out with increasing distance from the wall or whether these are

features which are also existing at greater distance apart from the wellbore. Features which belong to geomechanical events should exist close to the wall of the wellbore. For FMI™ logs (an example can be seen in Figure 7) only one depth of investigation of the borehole image is available. The wellbore image is split up in four images with missing sections in between. It is obvious that not the whole borehole section is visible even though the resolution is much better for the FMI™ than for the GVR™ logs. On the pictures below (Figure 6) which show a section of the GVR™ logging run, it is visible that the breakouts used for geomechanical analysis must be picked accurately and it is not reasonable to pick a single box around the borders of a continuous breakout. This principle of operation is crucial because the extend (width) and the position (azimuth) of the breakouts are input parameters not only for stress orientation prediction but also for the maximum horizontal stress determination and the wellbore failure prediction.

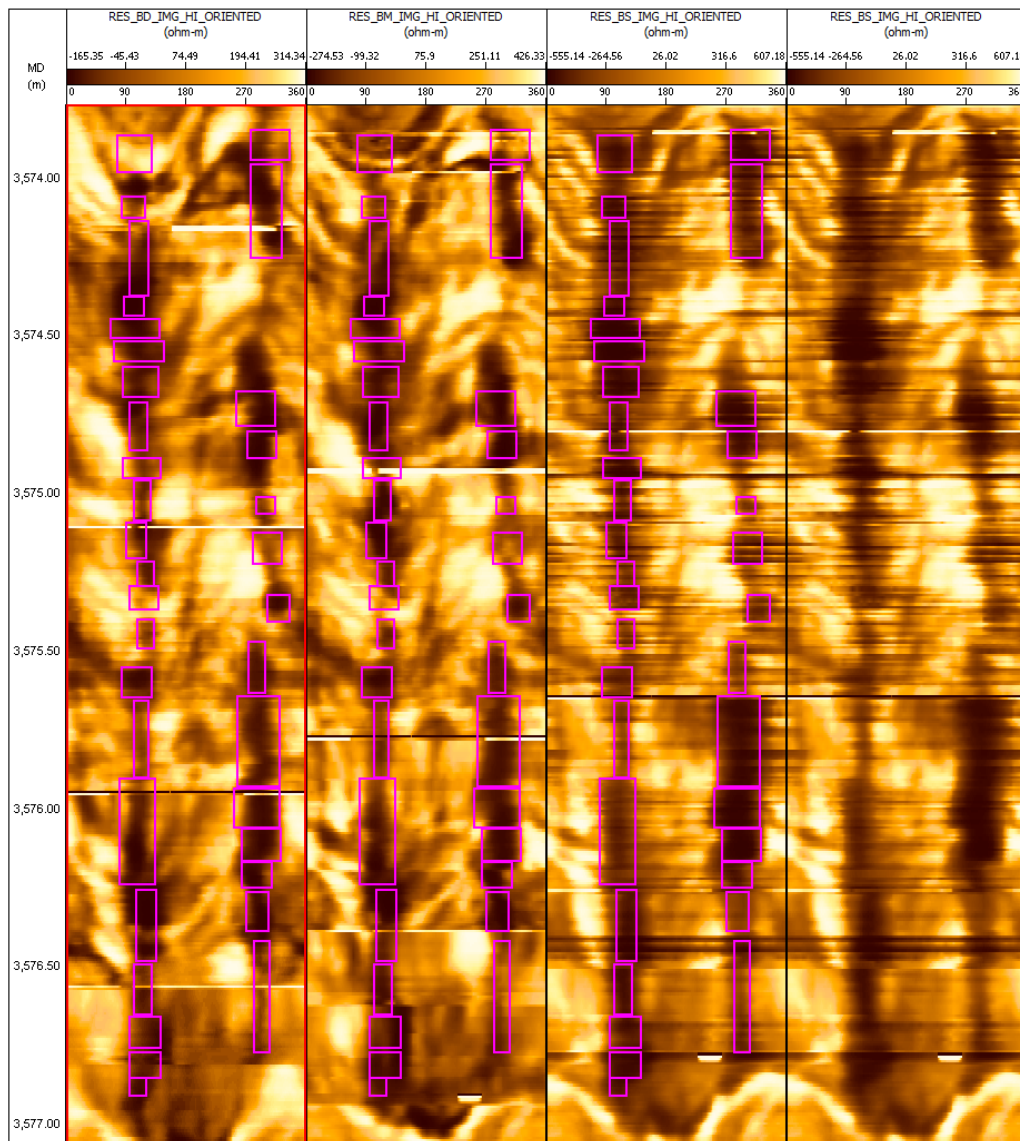


**Figure 6:** Borehole section of the Stripfing T1 wellbore, logged with a GVR™ LWD tool. The four pictures are showing the same section, but different depths of investigation, with the deepest depth of investigation on the left side. The third and the fourth log show the same investigation depth, with and without picked breakouts. The magenta boxes represent the breakouts picked by the use of the Imager™ program.

## Horizontal Stress Orientation Estimation

The procedure how the occurring breakouts should be picked is as follows:

1. As accurate as possible with as few as possible boxes
2. Boxes should be placed stacked (on top of each other) and not in juxtaposition
3. Breakouts may just be picked if the opposite breakout approximately 180° apart is visible (slightly vertical offset is possible)

How this can look like for GVR™ logs is shown in the picture above (Figure 6). For FMI™ logs, it is often necessary to just pick parts of the breakouts instead of complete ones, simply because the other part of the BO is located in the missing part of the image and it is not possible to assess where the BO ends within this hidden section of the wellbore.

Accordingly, a second version of picked breakouts must be generated. In this version, solely breakouts which are convincing and where the outer borders are visible on the image log may be chosen. Figure 7 shows a FMI™ log of the 17.5in section of the Stripfing T1 well. Here it can be seen that just the parts of the borehole are visible where the pads of the tool are touching the wellbore wall. This implies that parts of occurring breakouts or even complete breakouts are not visible because the image log is not recording them. In contrast to the GVR™ logs where the complete breakouts can be detected, often just fractions of breakouts can be picked. If, however the borders of the breakouts can be seen on two neighboring image stripes, it is possible to pick the feature across the missing section. Due to the fact that the FMI™ image logs showing noticeable void space, less breakouts for stress determination (BO where borders can be detected) can be identified in relation to the GVR™ image log, albeit the accuracy of BOs picked on the FMI™ image logs is superior to the one from the GVR™ logs because the image is of noticeable better quality. Nevertheless, if selected breakouts are not convincing regardless of on which type of image log they are visible, it is better to not include them into the stress direction analysis.

Having two different versions of breakouts (one version where all breakouts are picked and one version where only the breakouts are picked where the complete breakout can be identified) is a necessity because the version containing all detected breakouts is used in the wellbore stability calculation of the model workflow and the second version provides the input data for the maximum horizontal stress orientation and magnitude determination. Hence version number one gives a quantitative measurement of how often and where rock fails, but the determined width of these breakouts is frequently just a part of the entire BO width. For the evaluation of the stress direction though a precise as possible BO azimuth is indispensable because selecting parts of the BO may deliver azimuth values which are falsifying the outcome.

The image analysis program (Imager™) is able to calculate and plot the distribution of the azimuths of the picked BOs and by this allow the determination of the stress direction. Moreover, the selected BOs can be imported into the JewelSuite™ program where they are used in the wellbore stability workflow (see 3.10).



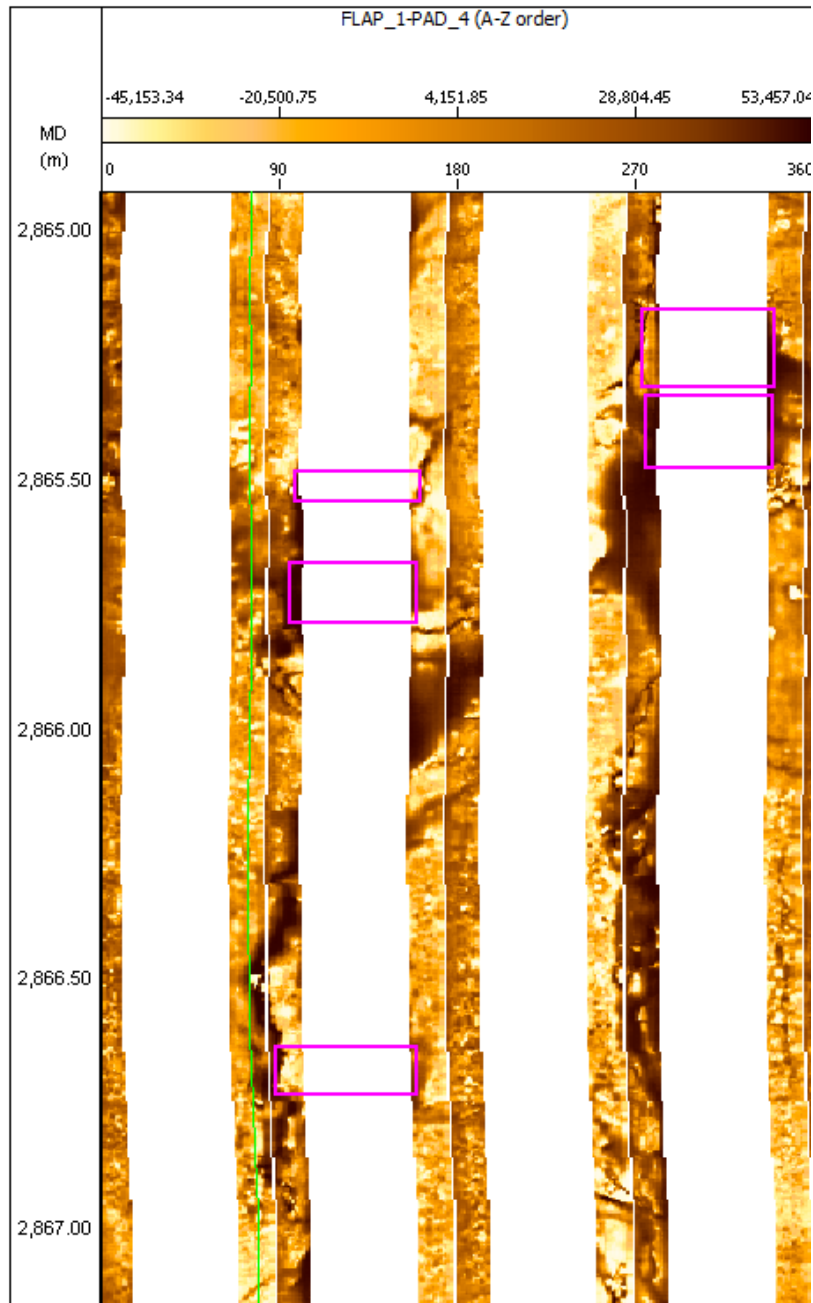


**Figure 7:** Borehole section of the Stripfing T1 wellbore, logged with a FMI™ wireline logging tool.

The magenta boxes are representing breakouts which could be seen on the neighboring image stripes and because of that were picked across the missing part of the borehole circumference.

The most common way of acquiring borehole images is the conduct of resistivity image logging either by using LWD or WL tools. A typical WL logging tool which was also used for the Stripfing T1 well is the Formation MicroImager™ from Schlumberger. These wireline electrical images generated by WL tools like FMI™ have high resolutions and can represent more geological features than a LWD tool with lower resolution. However, LWD tools like the GVR™ (geoVISION resistivity™ from Schlumberger), which was also used for one section of the Stripfing T1 well, can measure data while drilling with nearly no delay, so the image shows the borehole in a not deteriorated or altered condition (Lei et al. 2007).

## Horizontal Stress Orientation Estimation

Three typical FMI™ logs are shown in Figure 8, starting with the log of the 17.5in hole on the left, to the 12.25in hole in the middle and the smallest hole size of 8.5in to the right. On this picture, it is visible that a FMI™ image log is not showing the whole borehole wall like the GVR™ does. The coverage of the log is dependent on the borehole size and increases with decreasing hole size. The missing parts of the borehole wall are resulting from the limited size of the pads on the logging tool. If the size of the borehole decreases, the fraction of the hole circumference which is occupied by the pads increases and a larger part of the borehole can be detected on the logging images.

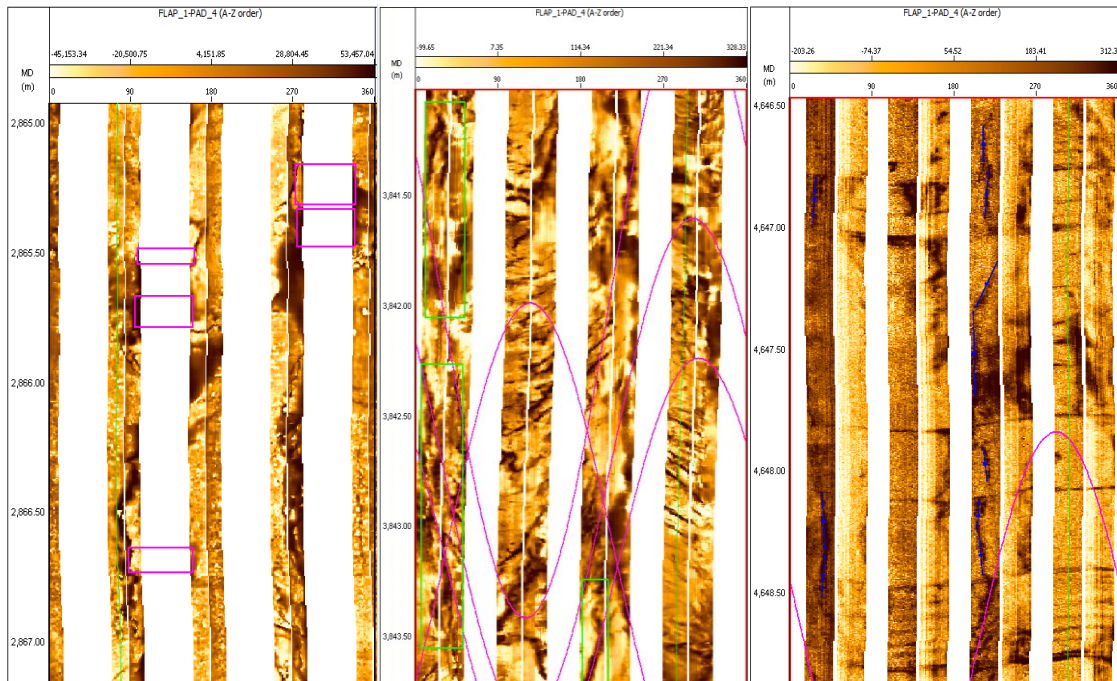


**Figure 8:** Examples of borehole sections of the STR T1 well with different hole diameters, logged with FMI™ wireline logging.

The dependency of the proportion of depict to not visible borehole wall on the borehole diameter for FMI™ logging tools is shown. A decrease in hole diameter entails an increase in visible borehole wall on the image log.

### 3.7.2 Drilling Induced Tensile Fractures

The detection of the azimuth of the drilling induced tensile fractures (DITF) on image logs is another method for the direct indication of the stress orientation. The azimuth of the DITFs however indicates the maximum horizontal stress direction. As explained in the section 3.7.1, the hoop stress reaches its minimum at the azimuth of the maximum horizontal stress. If this hoop stress decreases or the pressure difference (mud weight minus pore pressure) in the well increases, the wellbore can go into tension locally and DITFs form in the direction of  $S_{Hmax}$ . These DITFs just form very close to the wellbore wall (in a range of mm to one cm) and because of that, image logs are the only way to detect whether DITFs are present at the wellbore wall (Zoback 2010). For vertical wells the picking of DITFs is a quite simple but again subjective task. Drilling induced tensile fractures form  $180^\circ$  apart from each other, comparable with the formation of breakouts. To distinguish between drilling induced tensile fractures and drilling enhanced fractures (3.7.3), the application of a sinusoidal curve is used. Drilling enhanced fractures can be fitted on such a sinusoidal curve like it can be seen in Figure 9. Drilling induced tensile fractures cannot. According to the fact that DITFs form in the direction of the maximum

horizontal stress and breakouts form in the direction of minimum horizontal stress, DITFs and BOs form  $90^\circ$  apart from each other. It is possible that both occur at the same depth. If this is the case, the containment of the magnitude of the maximum horizontal stress with the help of the stress polygon analysis can be even more precise (see 3.8). In the picture below (Figure 9) the difference between DITFs and DEFs is visible. The associated ( $180^\circ$  apart) induced fractures tend in the same direction and because of that cannot be fitted on a sinusoidal curve, compared with the enhanced fractures which tend towards each other and fit on such a curve. DITFs may just be picked if both associated fractures are visible (slight vertical offset is possible) like it has been the approach for the picking of the breakouts.

Just like it should be done during the procedure applied for the BO selection, it is useful to sort out the picked DITFs and generate a second version where just DITFs with high confidence are chosen to base the maximum horizontal stress direction determination on reliable data. Again, the distribution of the azimuths can be calculated and plotted by the program to determine the likeliest value for the azimuth of the maximum horizontal stress.

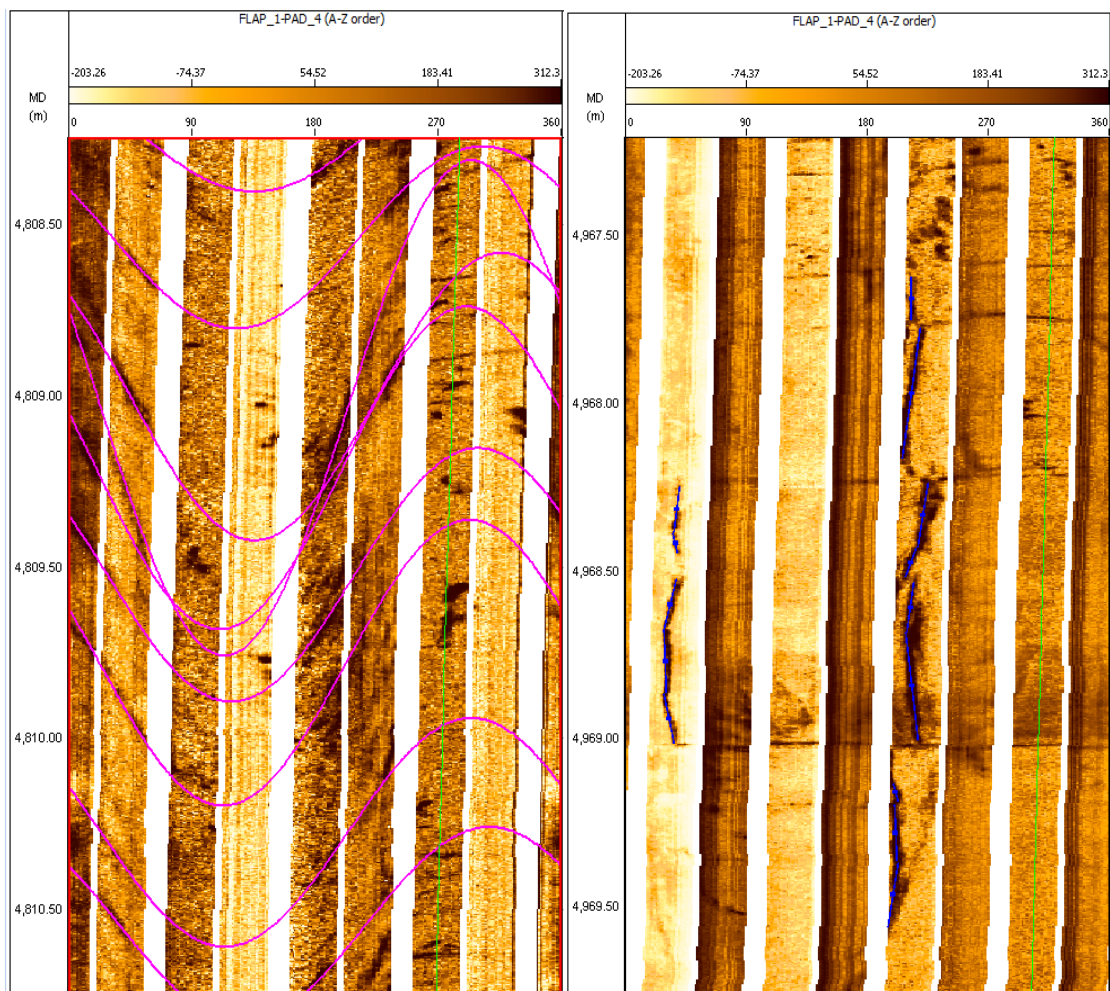


**Figure 9:** Borehole sections of the STR T1 well, showing drilling enhanced fractures on the left and drilling induced tensile fractures on the right. Matching pairs of drilling enhanced fractures ( $180^\circ$  apart) point in the opposite direction and can be fitted on a sinusoidal curve (magenta sinusoids on the left). Drilling induced tensile fractures ( $180^\circ$  apart) point in the same direction and can be picked by using straight lines (blue lines on the right).

### 3.7.3 Drilling Enhanced Fractures and Tensile Regions

Like it has been explained above, by the help of the Imager™ software from Baker Hughes, the borehole images can be displayed and the features which are visible on these images can be picked. Breakouts will be picked by dragging boxes around it and DITFs will be picked with straight lines. The determination of the maximum horizontal stress magnitude and direction as well as the wellbore stability analysis can be accomplished based on this data. However, also drilling enhanced fractures (DEF) and tensile regions can be picked with the help of this program.

Assuming, that no breakouts or drilling induced tensile fractures can be detected, it is also possible to evaluate the stress direction from drilling enhanced fractures or tensile regions. But anyway, the selection of these borehole features should be done for the sake of completeness.

Like explained at the outset of the last section, drilling enhanced fractures must be distinguished from DITFs. Drilling enhanced fracture are pre-existing natural fractures which open in the borehole due to drilling activity. These fractures are not striking parallel to the vertical stress, but have an inclined appearance. This is the reason why they can be fitted on a sinusoid to be picked on the image log. The strike direction of the DEF corresponds to the orientation of the maximum horizontal stress, like the one for the DITF does (Nie et al. 2013). The last features which can be valuable for the azimuth determination are tensile regions which are selected by dragging a box around them. Tensile regions, like shown in the middle picture of Figure 8 as green boxes, are used to qualify regions where a large amount of tensile fractures is visible and because of the wealth of fractures it is not possible to identify and pick individual ones. Also for these features, the Imager™ program enables the user to plot the distribution of the azimuths of the different characteristics and thereby provides the determination of the horizontal stress direction.

The determined maximum horizontal stress azimuth together with the previously defined and calculated rock properties, overburden stress and pore pressure are the input values for the following maximum horizontal stress determination.

## 3.8 Maximum Horizontal Stress Determination

The magnitude of the maximum horizontal stress cannot be determined directly but must be modeled from the occurrence of wellbore failure. The application of the stress polygon is the used method to estimate the maximal horizontal stress. To identify the magnitude of  $S_{Hmax}$ , several input parameters must be determined prior to apply this method. By deploying this procedure, a possible range of  $S_{Hmax}$  values (a low and a high maximum horizontal stress value) for a dedicated depth is identified instead of a single value. Afterwards the Effective Stress Method is applied to convert the read  $S_{Hmax}$  values to unitless effective stress ratio points by applying equation ( 10 ) and fitting a trend line through the set of ESR values to determine an ESR curve from surface to TD of the wellbore. This curve acts as the input for the maximum horizontal stress determination by the ESR equation ( 10 ). This workflow of using the Effective Stress Method works analogously to the minimum horizontal stress determination which was accomplished before (see 3.5). The units for the pressure and stress input parameters, respectively can



be pressure [e.g. MPa] as well as mud weight [SG] units, but have to be the same for the individual calculations.

$$ESR_{max} = \frac{S_{Hmax} - P_p}{S_v - P_p} \quad (10)$$

The low and the high maximum horizontal stress values are determined by the application of the stress polygon, like stated above. The input parameters for the stress polygon analysis include for instance overburden stress, maximum horizontal stress direction, pore pressure, BO width (from image analysis) and elastic parameters like Young's Modulus and Poisson's Ratio. UCS and minimum horizontal stress ranges are used to contain the maximum horizontal stress on the constructed stress polygon to receive a maximum horizontal stress range. Each generated stress polygon which is valid for a certain depth uses dedicated input parameters determined at exactly this depth.

In OMV's geomechanical workflow the SFIB™ program from Baker Hughes is used for the stress polygon analysis. The outcome values of this analysis are then transferred into the JewelSuite™ program to calculate and display the unitless ESR points and the ESR curve to determine the maximum horizontal stress. The best practice to do a stress polygon analysis is the following:

1. Detecting conclusive breakout zones or single breakouts on the image logs for stress modeling

Selecting a breakout zone with several demonstrative breakouts makes it necessary to form an average value for the breakout width and select one BO out of this zone of breakouts which matches best with the average width which was calculated before. This BO represents the average breakout which is chosen as the representative one and it can be proceeded similarly to the process for a single picked BO.

2. Collecting all input parameters for the depth of the selected BO

Identify the dedicated depth for the chosen breakout and collect all necessary input parameters for the stress polygon analysis at this depth. These input parameters are calculated or determined in the steps before and include:

- a. Vertical Stress
- b. Horizontal Stress Direction
- c. Pore Pressure
- d. Biot's Coefficient
- e. Wellbore Azimuth
- f. Wellbore Deviation
- g.  $\Delta$ Pressure = Mud Weight – Pore Pressure
- h. Breakout Width
- i. Failure Criterion
- j. Internal Friction
- k. Poisson's Ratio
- l. Sliding Friction

## Maximum Horizontal Stress Determination

3. Insert these input parameters into the SFIB™ program and generate the stress polygon for the appropriate depth

For the calculation of the stress polygon the failure criterion is an important input parameter. For selected BOs which have formed in sandstone or shale formations the Modified Lade failure criterion (often works better for softer rock) is the one which should be chosen, for limestone and dolomite Mohr Coulomb failure criterion (works better for brittle rock) is the prevailing one. Another parameter which was not mentioned before is the sliding friction which can be expressed as the ratio of shear to effective normal stress. Sliding friction describes the slip on a pre-existing fault and normally ranges from 0.6 to 1. This input value is assumed to be 0.6 for all stress polygon calculations.

4. Determine the range of minimum horizontal stress and formation strength to contain the  $S_{Hmax}$  values from the stress polygon

A possible range for the  $S_{hmin}$  and the UCS must be inserted to generate an area within the stress polygon where the stress state can be located at the chosen breakout depth. For this reason, it is useful to have a closer look on the variation of the  $S_{hmin}$  and UCS values in the surrounding of the chosen depth instead of taken an overall percentage which is added and subtracted to generate a range of  $S_{hmin}$  and UCS from a single read value.

In the picture below (Figure 10), the x-axis of the stress polygon represents the  $S_{hmin}$  whereas the  $S_{Hmax}$  is plotted on the y-axis. The UCS values are represented by the red lines crossing the stress polygon.

5. Read a minimum and a maximum possible value for  $S_{Hmax}$  from the stress polygon and transfer the values into JewelSuite™

To read the low and the high value of the maximum horizontal stress, the lowermost and the uppermost possible  $S_{Hmax}$  value within the determined area (red square) must be assessed. Solely values within the stress polygon are valid. The occurrence of tensile failures (negative hoop stress represented as blue lines) can additionally be helpful to contain the  $S_{Hmax}$  values more precise. If DITFs are visible at the depth of interest, it is also necessary to stay to the right of the zero tension line, within the determined area (red square) and the stress polygon margin.

6. Calculate the maximum horizontal stress from  $S_{Hmax}$  calibration points by the Effective Stress Method

Like it has already been done for the minimum horizontal stress determination, the Effective Stress Method is used to calculate the maximum horizontal stress. The low and high  $S_{Hmax}$  values are used, together with the pore pressure and the overburden stress, to calculate unitless ESR points. By the application of a trend line, a  $ESR_{max}$  curve for the whole borehole length is generated and a maximum horizontal stress curve can be determined by again applying the ESR equation.

7. Determining the stress regime from the stress polygon

Another information which can be ascertained from the stress polygon is the stress regime of the region around the wellbore. Depending on the position of the

determined area (red square) within the stress polygon, the stress regime can be read from the polygon. Also, it is possible to determine the stress regime by applying the ESR formulas like it can be seen in Table 1 below (Anderson’s theory of faulting (Anderson 1951)).

Stress Regime	Minimum ESR	Maximum ESR
Normal Faulting	$\frac{S_{hmin} - P_p}{S_v - P_p} < 1$	$\frac{S_{Hmax} - P_p}{S_v - P_p} < 1$
Strike-Slip Faulting	$\frac{S_{hmin} - P_p}{S_v - P_p} < 1$	$\frac{S_{Hmax} - P_p}{S_v - P_p} > 1$
Reverse Faulting	$\frac{S_{hmin} - P_p}{S_v - P_p} > 1$	$\frac{S_{Hmax} - P_p}{S_v - P_p} > 1$

**Table 1:** Determination of the stress regime by applying the effective stress ratio, after Anderson’s theory of faulting (Anderson 1951).

The identified stress regime should correspond with the overall stress regime of the geological region. It should be kept in mind that a change in the stress regime is possible, but it is unlikely that the stress regime is changing several times within the depth of a wellbore.

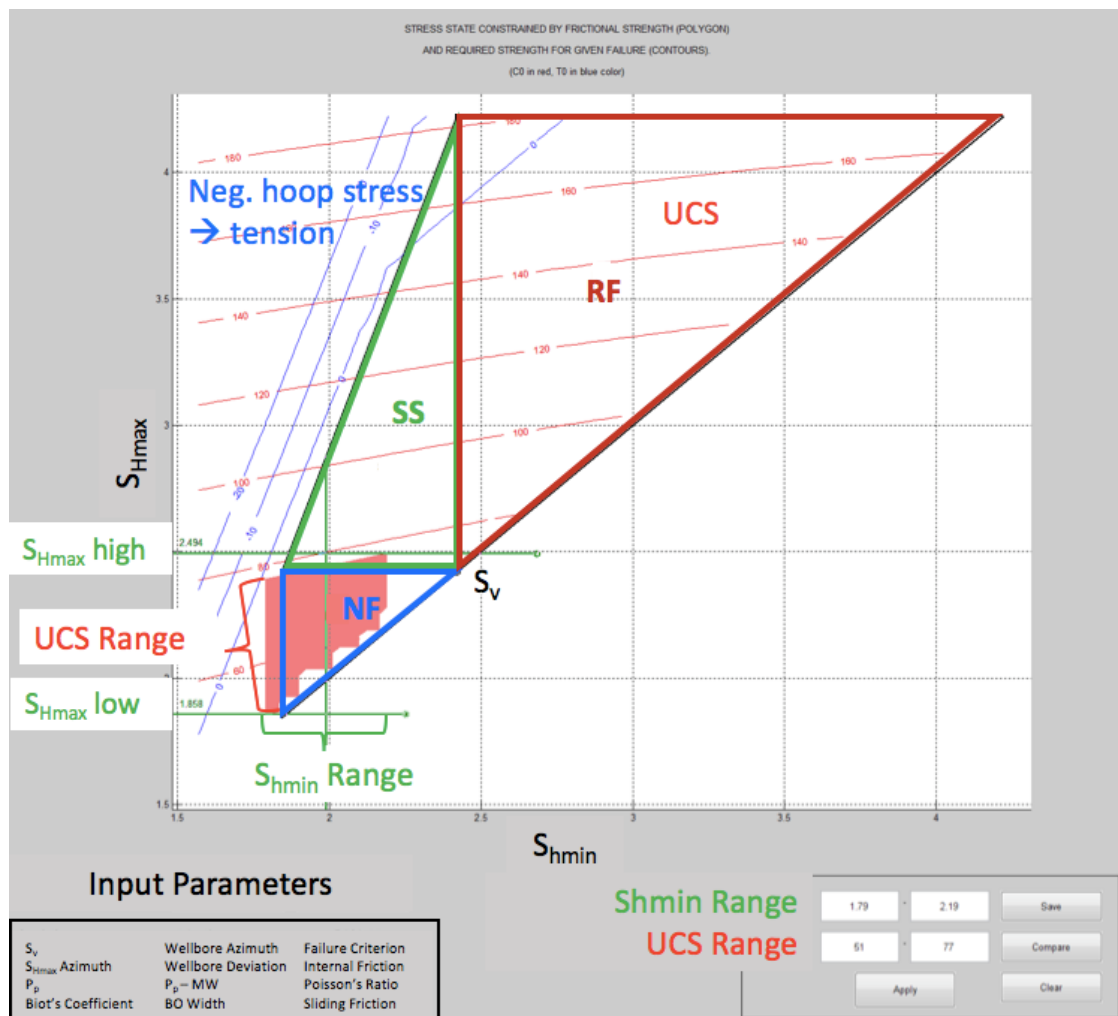


**Figure 10:** Exemplary stress polygon plot generated by the use of the SFIB™ program.

The stress polygon is plotted in a maximum vs. minimum horizontal stress diagram. The outer borders of this polygon are contained by the possible horizontal stress magnitudes which are valid for a dedicated depth, for a given pore pressure and coefficient of friction (in this thesis 0.6). The stress regimes, namely normal faulting, strike-slip faulting and reverse faulting, defined by Anderson (Anderson 1951), can be identified from the plot. Furthermore, the input parameters for the stress polygon analysis and the resulting maximum horizontal stress values are represented.

### 3.9 Drilling Event Analysis

The gathering of all information which can be included into the drilling event analysis is a time consuming but essential task. Information about drilling procedure, drilling events and other related occurrences can be found in nearly all recordings, presentations and reports. Hence it is quite important to comb through all available data with reasonable care and collect as much information as possible which can be helpful for e.g. pore pressure prediction and wellbore stability determination. Furthermore, drilling event analysis is an adequate source of information for the calibration and verification of the geomechanical model. Tellez et al. 2012 gave an example of how available drilling information can be used for the interpretation and determination of geomechanical data (Table 2).

Available Data	Interpretation
Daily Drilling Reports	Root-Cause Analysis
Drilling Events	Pore Pressure and Minimum Horizontal Stress Determination and Model Verification
Digital Leak-Off Test Data	Minimum Horizontal Stress Determination
Cutting Documentation	Determination of failure and possible causes of failure by analysis of caving appearance
Root-Cause Analysis of Drilling Events	Differentiation between Geomechanical and Operational Events and Future Risk Mitigation

**Table 2:** Evaluation of collected drilling data, cf. Tellez et al. 2012.

The first exercise to complete is the analysis of the daily drilling and geological reports (DDR/DGR) where all important and relevant data should be filtered and noted. In the geomechanical department of the OMV an Excel file with special applications is the basis for the gathering of all crucial data. Information of special geomechanical importance should be lifted out as input information for the compilation of mud weight vs. depth and time vs. depth curves. Based on this file it is later possible to easily and quickly validate data which has been read or found in reports or presentations and check for special occurrences at special depths, mud weights or dates. This means a detailed and accurate



implemented template is very helpful at all steps of the model building because an easy and quick check of information is possible without time consuming repeated screening of input documents. With the help of this data it is possible to identify the main reasons of wellbore instabilities and the problematic formations which are prone to drilling problems. In these wellbore sections, it is of high importance to develop a conclusive prediction because often these are areas of uncertain pore pressure or stress values or areas where the mud weight and the pore pressure are close together switching between over- and underbalance. Analyzing the drilling events and determining problematic zones encountered during drilling will help to adapt the pore pressure curve (see 3.4) and verify the results of the following wellbore stability analysis (see 3.10).

Important drilling events for calibration and verification extracted from reports can include:

- Leak-Off Tests (Minimum Horizontal Stress)
- Lost Circulation (Minimum Horizontal Stress)
- Total Losses (Minimum Horizontal Stress)
- Tight Holes (Drilling Practice or Borehole Instabilities)
- Stuck Pipe (Pore Pressure (Different. Sticking) or Instabilities)
- Kicks/Gains (Pore Pressure)
- Drilling Breaks (Pore Pressure)
- Torque/Drag (Drilling Practice or Instabilities)
- Reaming (No Clear Indication)
- Connection Gas (Pore Pressure)
- Gas Readings (Pore Pressure)

For the entered drilling events, it is possible to select date, mud weight and type (point or interval, LOT, P<sub>p</sub>). In case the event occurred over an interval, also the base MD can be entered. This is possible for the Excel file as well as for the drilling events workflow step of the JewelSuite™ program.

How important and meaningful these drilling events are for the model workflow cannot be rated generally. This must be assessed from the engineer for every model and workflow step. Often this also depends on the information which is reported and general principles within the company. Reaming is a typical event where it is necessary to assess the data in a general drilling context. The question which arises with reaming is: What are the guidelines for reaming? Is reaming just done in case of arising hole problems or is there a standard specified in the company where reaming is done on a regular basis? This shows an example for what is stated above. It is important to analyze the information with care and thinking about the usefulness is a prerequisite.


For each incident/event the associated depth and MW can be specified to visualize these information as a plot. For the Excel file evaluation, this can be the time vs. depth and the MW vs. depth plot. In the JewelSuite™ program the drilling events can be plotted in a MW vs. depth log which can be outlined along with other curves like the pore pressure log. Since the events are displayed on a mud weight scale it can be seen whether the event occurred during drilling or during operations where another mud weight was present (e.g. reaming after deeper sections have already been drilled). The drilling events can be differentiated by the selected color codes to get an overview of the frequency of the events and to identify the wellbore depths where problems are encountered during drilling.

Drilling Event Analysis

These drilling events will be used in the next steps together with images and caliper logs to verify the results of the wellbore stability analysis. For this usage, it is very important to have an understanding, whether the drilling events occurred because of geomechanical problems or whether other not geomechanical related incidents (e.g. wrong mud selection) are the reason for instabilities.

Despite the fact that LOT data is included in drilling events, the results of the LOT analysis were already required for the least principal stress determination (see 3.5) and must be added separately as calibration points during this model step.

The cutting analysis can deliver a good evidence for geomechanical problems, by screening the cuttings across the shaker and identifying the cavings (distinguished from normal cuttings by size, shape and morphology difference) which can relate the actual failure to geomechanical features. In the table below (Table 3) a short overview of typical failures and causes is listed.

Caving Appearance	Causes of Failure	Examples
Splintery Cavings (Shale)	Due to tensile failure when $P_p$ in shale exceeds the MW, especially in massive shales	
Shear Failure	Due to effective wellbore stress exceeding the rock strength, MW is not sufficient to reduce wellbore stresses	
Platy/Tabular Cavings	Due to rock strength anisotropy (weakly bedded or fissile)	
Blocky Cavings (Rubble)	Due to stress and time-dependent mud penetration into fractures, associated with brittle rock	
Chemical Instabilities (Mushy Cavings)	Due to stress and time-dependent water penetration into shale and/or swelling	

**Table 3:** Interpretation of caving appearance as a method to determine the causes of failure.

Information borrowed from an OMV internal wellbore stability presentation (done by GMI) and the document “Diagnosing Wellbore Failure”, published by Halliburton 2017.

For the caving analysis, good documentations are required such as photographs and descriptions together with the detailed depth declaration, where care must be taken on the time delay of the cavings, to determine the exact depth at which the cavings have formed.

At this point in the model workflow, nearly all input parameters have been collected and inserted into the model. The following verification of the geomechanical model just requires the import of the breakout data to conduct the wellbore stability workflow and the final verification of the model.

## 3.10 Verification of the Geomechanical Model

In the last step of the model workflow, it must be demonstrated, that the built model is conclusive and that the assumptions made and formulas used, deliver a model which verifies with the detected wellbore failures and drilling events. The verification of a geomechanical post-drill model is done by comparing the real compressive wellbore failures seen on image and caliper logs with the predicted wellbore failures along the well trajectory, calculated during the model workflow. These mechanical failures of the wellbore are caused by the interaction between in-situ stresses, pore pressure, rock and fluid properties and drilling practice (Zheng, Schulze, and Blumenthal 2012).

First, a wellbore stability prediction must be carried out, where the wellbore failure is calculated based on several previously determined characteristics. These characteristics are the input values for the first step of the failure calculation (called the wellbore stability preparation), namely pore pressure, stresses, azimuth of the maximum horizontal stress, UCS, static Poisson's Ratio, internal friction, tensile strength, Biot's Coefficient, failure criteria and the critical BO width. The following step is called "Check MW" and requires the generation of a special mud weight curve. This mud weight curve represents the minimum mud weight the borehole has experienced during image logging. For this reason, it is useful to collect information about the image logging runs. When they were conducted and what has been the lowest mud weight the borehole has seen until this date. With this information, it is possible to build a mud weight curve with the lowest seen mud weight before image data has been collected. By this it is prevented to over- or underestimate the rock strength, because the same failure at higher mud weights would implement the presence of a weaker rock and vice versa.

Finally, the observed breakouts should be imported into the program to display them together with the caliper log next to the calculated wellbore failure. In section 3.7 picking the wellbore BOs has already been discussed. Like explained in this chapter, there are two different versions of selected BOs. The version which was used for maximum horizontal stress direction and magnitude determination solely uses the breakouts where the borders can be detected. For the wellbore stability prediction, it is more useful to take the version where all picked breakouts are included, because for this analysis the quantity is also of importance.

The outcome of this wellbore failure calculation represents a computed failure along the wellbore. This modeled failure occurrence must eventually be compared to the true wellbore failure seen on image and caliper logs and it should be assessed how good this current model with present input values, formulas and criterions is matching with the observed wellbore failure. The question which arises when thinking about matching of calculated and real wellbore failure could read as follows:

## Verification of the Geomechanical Model

*What is the requirement for a good match?*

Overall the model should match with reality with a reasonable accuracy. Reasonable accuracy in this context means that the calculated trend follows the reality and noticeable departures from the trend should be represented on the calculated wellbore failure log.

Depending on how good the wellbore failures are matching, an adaption of parameters must be executed to a greater or lesser extent. The emerging question relating to this subject could be:

*If the calculated and the detected wellbore failure logs do not match, which parameters should be changed?*

It is advisable that first the parameters with the highest uncertainty would do well to be changed. Parameters with higher certainties should be held constant or changed as one of the later options.

In case the prediction of compressive failure at the wellbore wall is not matching with the observed failure on the image and caliper logs (BO existence and/or BO width) or with the drilling experience, a change in pore pressure and/or UCS can adjust the calculated failure to get a match with the observed BO existence and width. Which one of the parameters should be changed depends, like discussed above, on the certainty of the parameter. During this step, it is common to go back and forth to see which changes fit best. Once the calculated and detected breakouts match satisfyingly the verification is completed and the model can be used for further applications enhancing for example well planning and drilling operations.

In this context, it should also be mentioned that it is possible that a conclusive model which is verifying with desired accuracy was built but it is not an accurate representation of the conditions that are present in this wellbore region. However, the more calibration points and measurements (like e.g.  $S_{hmin}$ ,  $P_p$  and lab testing) are available the closer the model approaches to reality.

# Chapter 4 Post-Drill Geomechanical Model for the Stripfing T1/T1a Well

Based on the general within OMV used workflow which was described above (Chapter 3, Methodology of Building a Post-Drill Geomechanical Model – OMV Standard Workflow), the post-drill model for the Stripfing T1/T1a well was built. For this wellbore, a pre-drill model was done by Baker Hughes GMI which was the basis for the model generated during this thesis. General assumptions made during the pre-drill model workflow were adopted and it was tried to stay as close as possible to this prediction. The data input for the pre-drill model by Baker Hughes GMI came from seven different offset wells and the Schönkirchen GEM. The pre-drill model workflow as well as the structure of the model is described in the report “Geomechanical Earth Model (GEM) for the Stripfing Tief Area, Austria” (Zheng, Schulze, and Blumenthal 2012).

## 4.1 Data Acquisition and Quality Check (Post-Drill)

With the help of the gained data by logs, tests and drilling experience the model has been updated and a post-drill model was developed to merge all gained data and previously made assumptions for a more accurate description of the wellbore parameters, especially wellbore stresses and pore pressure and to verify whether assumed data and equations can be used to describe the conditions in this region.

All useful data which contributes to an improvement of the model was collected, applied and inserted into the program to enhance the exactness of the interpretation, make deviations from the pre-drill model visible and deliver a conclusive post-drill model which can be applied as an input for future pre-drill models near the Stripfing area. The data which has been used is listed in the table below (Table 4).

<b>Input Data</b>	<b>Main Fields of Application</b>
Daily Reports	$P_p$ , Verification
GR Log	Lithology
Density Log	$S_v$ , $P_p$ , Rock Properties
Compressional Sonic Slowness Log	$S_v$ , $P_p$ , Rock Properties
Shear Sonic Slowness Log	Rock Properties
Resistivity Log	$P_p$
Drilling Events, LOTs	$P_p$ , $S_{hmin}$ , Verification
Image Logs	$S_{Hmax}$ , $S_{Hmax}$ direction, Verification

**Table 4:** Input data available for the post-drill model building of the Stripfing T1 wellbore.

Data Acquisition and Quality Check (Post-Drill)

The starting point of the model building was the gathering of information about the Striping T1 wellbore. The best way to start is to peruse the daily drilling and geological reports where it is easiest to enter the topic and where an overview of the drilling practice, including possible problems, can be gained. The most important information is transferred to a pre-built Excel file which is supplied by OMV's geomechanical department. The outcome of this work is the presentation of the drilling events in a mud weight vs. depth plot (Figure 11) and a time vs. depth plot (Figure 12) where it is possible to detect encountered drilling problems and the most time-consuming operations during drilling.

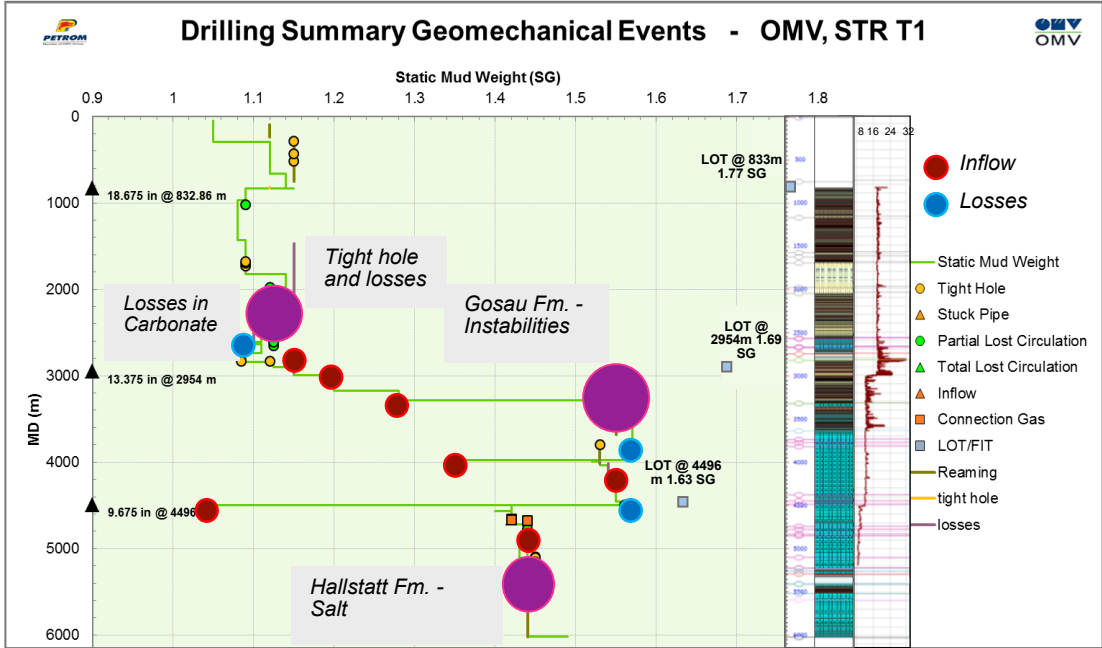


**Figure 11:** Geomechanical relevant drilling events collected during drilling the STR T1 well.

Characteristic inflow (red) and loss (blue) events as well as zones of substantial drilling problems (magenta) are highlighted in the mud weight vs. depth plot. To the right of this plot, the lithology and the caliper log are visible.

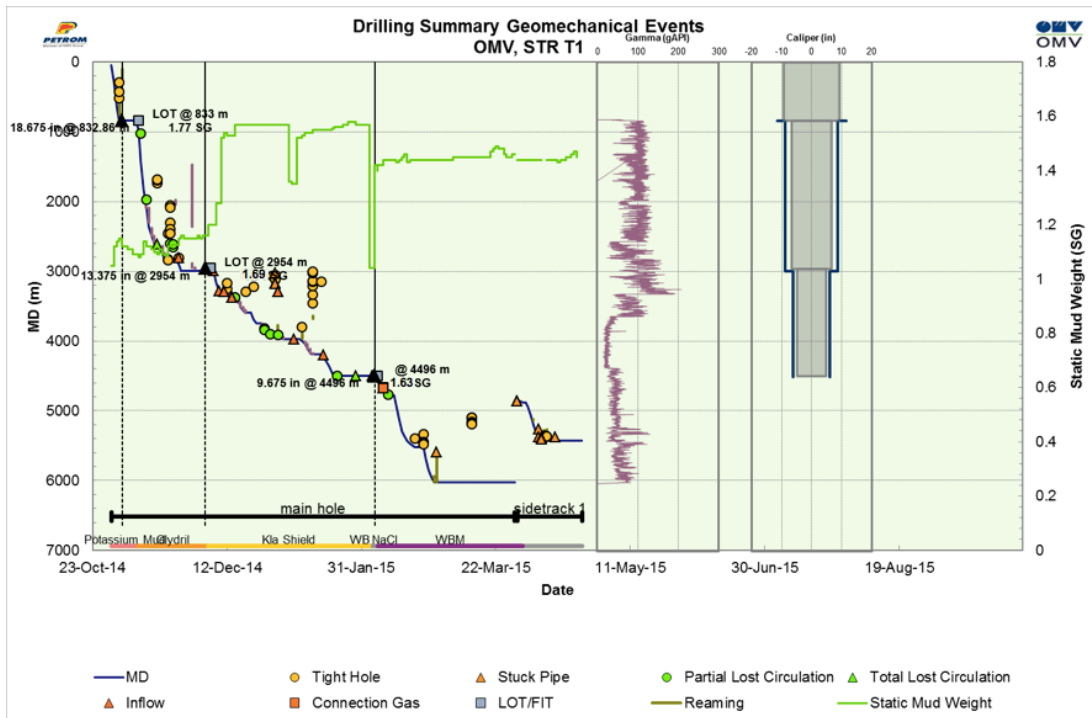


**Figure 12:** Time vs. depth plot of the STR T1 wellbore, including the geomechanical relevant drilling events.

Inserting this geomechanical relevant data into JewelSuite™ also delivers a mud weight vs. depth plot (Figure 13) where all inserted drilling events can be shown. This drilling events can be helpful for the pore pressure evaluation (3.4 and 4.4) as well as for the verification of the model (3.10 and 4.7) at the end of the modeling workflow. Drilling events of special interest are kick events, which allow a precise determination of the pore pressure by calculating the kill mud weight which is assumed to be equal to the pore pressure (3.4 and 4.4) and LOTs which are used to determine the minimum horizontal stress (3.5 and 4.5). Losses and gains were used to adapt the pore pressure curve below or above the mud weight in use, respectively, where the kick events and the LOT results were assumed to be fixed pore pressure and minimum horizontal stress calibration points, respectively. In the picture below (Figure 13) the JewelSuite™ mud weight versus depth plot which is generated during the model workflow can be seen. Similar to the plot which is generated during the interpretation of the drilling events by the help of the Excel program, the different drilling events at dedicated depth or depth ranges are plotted against the reported mud weight and problematic regions can be identified easily.

Although the whole model workflow is done in JewelSuite™, different preliminary work steps are done with the help of other programs like Excel, Imager™ and SFIB™ and the results gained from the analyses supported by these programs are imported into JewelSuite™ and used for further evaluations. The workflow steps where the mentioned programs are utilized are for example the maximum horizontal stress magnitude and direction determination and the model verification at the very end of the workflow. In the previous as well as the present chapter the procedures are explained in greater detail.

Data Acquisition and Quality Check (Post-Drill)

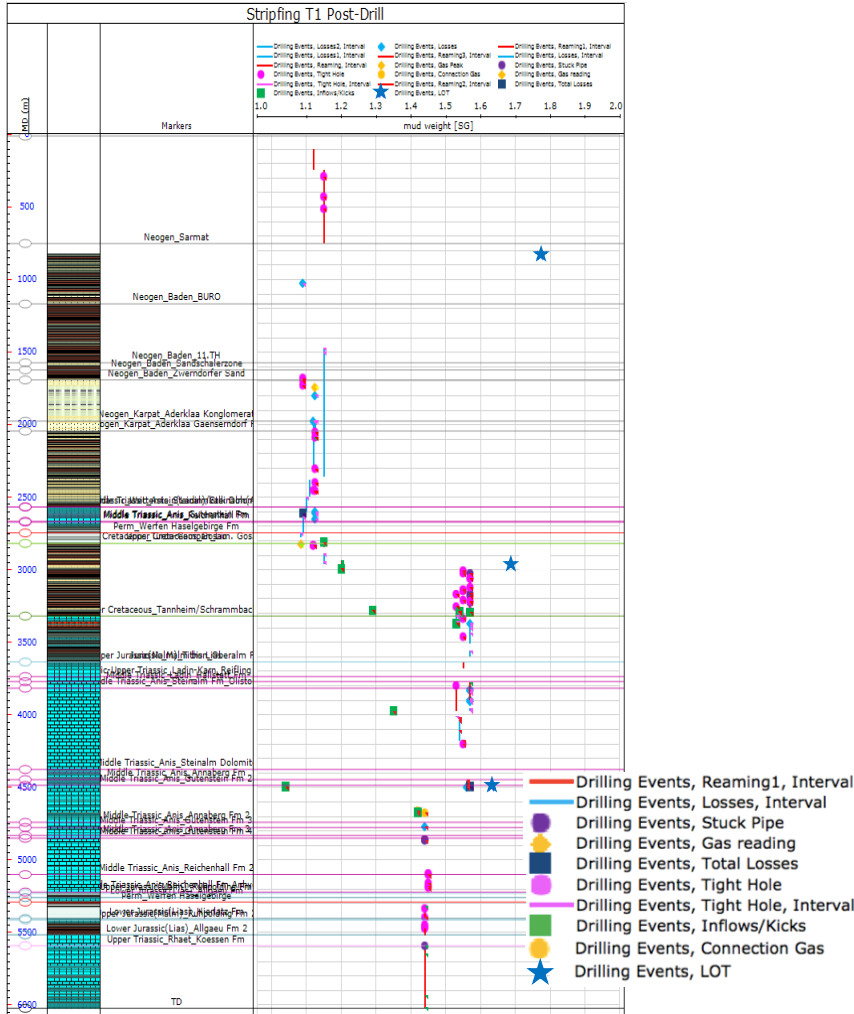


Figure 13: Geomechanical relevant drilling events illustrated in a mud weight vs. depth plot in the JewelSuite™ program, here without the mud weight curves.

One of the first steps that has been carried out during the model update was the determination of the stratigraphy. The exact formation sub-division (Table 5) was done by the responsible geologists and could be adopted. Care had to be taken with the wording, formations which are equal to the forecasted formations must have the same names to make the models comparable for the program as well as for the person analyzing the models. The color coding which is used in Table 5 below is consistent throughout the workflow and will serve as a guidance.



## Post-Drill Geomechanical Model for the Stripfing T1/T1a Well

Erathem	System	Series	Stage		Formation	Base MD
Cenozoic	Neogene	Miocene	Tortonian	Pannonium		
Cenozoic	Neogene	Miocene	Serravallium	Sarmatium		
Cenozoic	Neogene	Miocene	Langhian - Serravallian	Badenium	Buli - Rot - Zone	1166,9
Cenozoic	Neogene	Miocene	Langhian - Serravallian	Badenium	11. TH	1571,3
Cenozoic	Neogene	Miocene	Langhian - Serravallian	Badenium	Sandschalerzone	1620,8
Cenozoic	Neogene	Miocene	Langhian - Serravallian	Badenium	Zwerndorfer Sand	1690,1
Cenozoic	Neogene	Miocene	Burdigalian	Karpatian	Aderklaa Konglomerat	1974,7
Cenozoic	Neogene	Miocene	Burdigalian	Karpatian	Aderklaa Gänserndorf Fm	2043,2
Mesozoic	Triassic	Middle Triassic	Anisian - Ladinian		Wetterstein/Steinalm Fm	2565,51
Mesozoic	Triassic	Middle Triassic	Anisian		Gutenstein Fm	2665
Mesozoic	Triassic	Middle Triassic	Anisian		Reichenhall Fm	2670
Paleozoic	Permian	Upper Permian			Werfen Haselgebirge Fm	2745
Mesozoic	Cretaceous	Upper Cretaceous	Turonian - Campanian		Lim. Gosau Fm	2817,19
Mesozoic	Cretaceous	Lower Cretaceous	Valanginian - Albian		Tannheim/Schrambach Fm	3317,81
Mesozoic	Jurassic - Cretaceous	Upper Jurassic (Malm)	Tithonian		Oberalm Fm	3635
Mesozoic	Triassic	Middle Triassic - Upper Triassic	Ladinian - Carnian		Reifling/Hallstatt Fm	3735
Mesozoic	Triassic	Middle Triassic	Ladinian		Hallstatt Fm	3770
Mesozoic	Triassic	Middle Triassic	Anisian		Steinalm Fm	3815
Mesozoic	Triassic	Middle Triassic	Anisian		Steinalm Dolomite	4375,07
Mesozoic	Triassic	Middle Triassic	Anisian		Annaberg Fm	4445
Mesozoic	Triassic	Middle Triassic	Anisian		Gutenstein Fm	4485
Mesozoic	Triassic	Middle Triassic	Anisian		Annaberg Fm	4740
Mesozoic	Triassic	Middle Triassic	Anisian		Gutenstein Fm	4775
Mesozoic	Triassic	Middle Triassic	Anisian		Annaberg Fm	4830
Mesozoic	Triassic	Middle Triassic	Anisian		Gutenstein Fm	4850
Mesozoic	Triassic	Middle Triassic	Anisian		Reichenhall Fm	5100
Mesozoic	Triassic	Middle Triassic	Anisian		Reichenhall Fm Anhydrite	5220
Mesozoic	Jurassic	Upper Jurassic (Malm)	Oxfordian		Ruhpolding Fm	5231,78
Mesozoic	Jurassic	Lower Jurassic (Lias)	Sinemurian - Toarcian		Allgäu Fm	5258
Paleozoic	Perm				Werfen Haselgebirge Fm	5290
Mesozoic	Jurassic	Lower Jurassic	Sinemurian		Hierlatz Fm	5403,48
Mesozoic	Jurassic	Upper Jurassic (Malm)	Oxfordian		Ruhpolding Fm	5413,56
Mesozoic	Jurassic	Lower Jurassic (Lias)	Sinemurian - Toarcian		Allgäu Fm	5515
Mesozoic	Triassic	Upper Triassic	Rhaetian		Kössen Fm	5590
	TD					6022

**Table 5:** Stratigraphy drilled by the STR T1 well.

## 4.2 Lithology Estimation (Post-Drill)

The basic information for the lithology interpretation have been the GR log as well as the petrophysical interpretation and the cutting analysis done by the responsible petrophysicists and geologists, respectively. The outcome of this lithology estimation can be seen in Figure 14. In this plot, the formations, the GR log (green) and the lithology over the complete wellbore depth are visible for the post- (left) as well as for the pre-drill model (right). Because the forecasted lithology was not met below the Jurassic Malm-Lias formation, the lithology of the pre- and post-drill models are solely matching above the second Middle Triassic occurrence at around 3700m (red framed part of Figure 14). The formations above 3700m MD were found to be nearly identical, located at comparable depths, like it was forecasted for the pre-drill model (see Table 15). The only differences which were discovered are the existence of the Lower Cretaceous Tannheim/Schrambach formation which was not forecasted in the pre-drill model and the

# Lithology Estimation (Post-Drill)

much smaller extend of the Jurassic formations below the Cretaceous Gosau and Tannheim/Schrambach formations. The latter one could arise from the existence of the Middle Triassic sequence which was not expected in the pre-drill model. This Middle Triassic sequence is followed by another Jurassic sequence and appears like encased in Jurassic formations (see Figure 4). Below this second Jurassic occurrence, the Upper Triassic Kössen formation was perforated and it was assumed that the Upper Triassic Hauptdolomit formation would have followed if it would have been possible to drill further than 6022m MD. This Upper Triassic Hauptdolomit formation was the targeted formation for the STR T1 wellbore, like it can be seen in the forecasted lithology below (Figure 14). The occurrence of the not expected Middle Triassic sequence which causes the different stratigraphy is explained in more detail in the geological description at the outset of this thesis (Chapter 2).

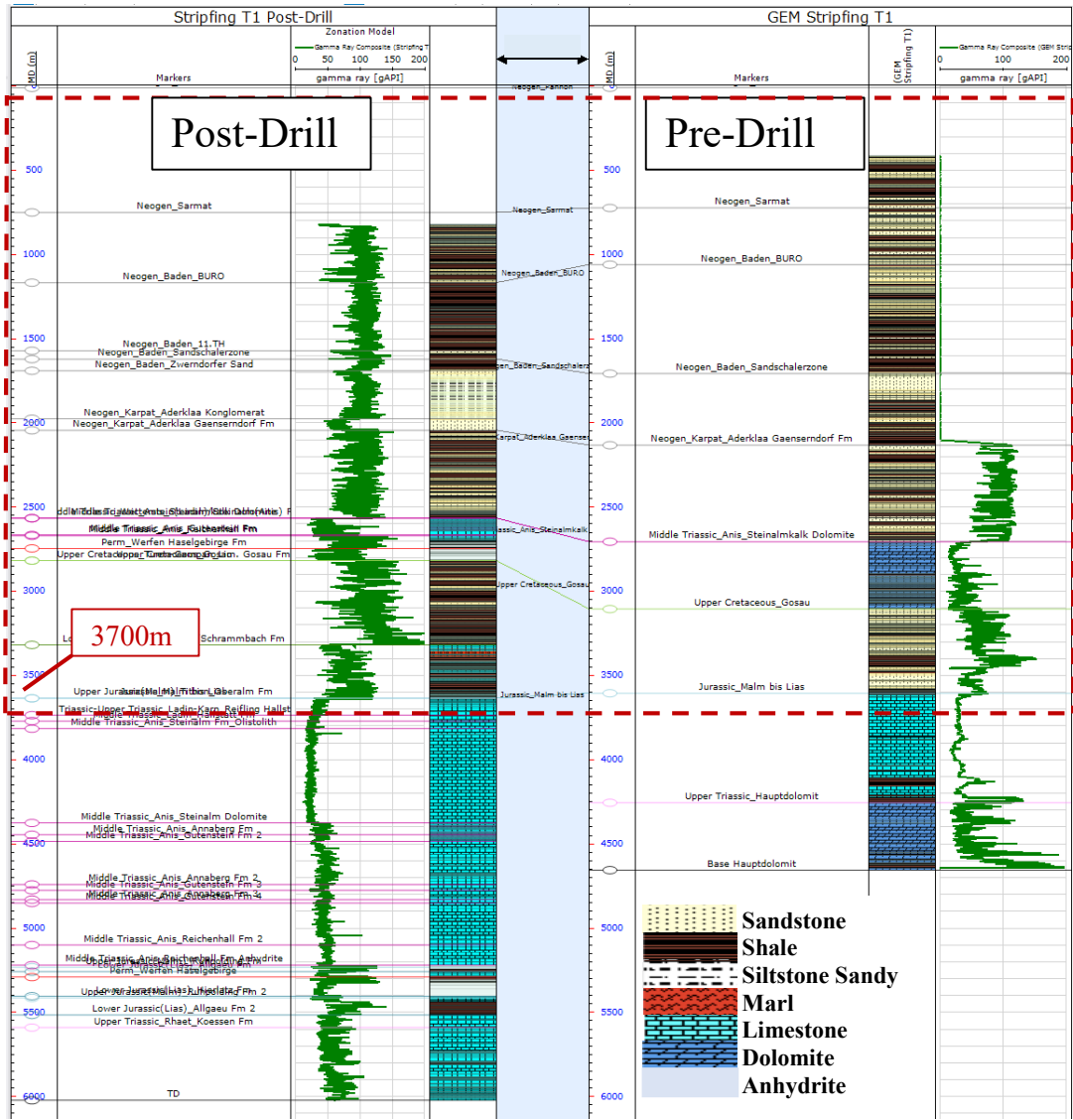


**Figure 14:** Observed stratigraphy, gamma ray and lithology (from left to right) of the STR T1 post-drill model in comparison with the forecasted stratigraphy, lithology and gamma ray (from left to right) of the pre-drill model.

The appropriate determination of the lithology is an essential step of the model building because some of the equations to estimate for example the pseudo density and the different rock properties are rock type dependent. These, on the determined rock type dependent equations and assumptions will be described in more detail subsequently.

### 4.3 Vertical Stress Determination (Post-Drill)

The next step of the workflow is the vertical stress calculation which was done based on the overburden composite log. This log consists of the bulk density composite log from 860m MD to 5170m MD and a trend line from ground level to 860m MD and from 5170m MD to TD. The bulk density composite log on the other hand consists of the ran density log and a pseudo density log calculated from the sonic slowness log. The equations which have been used for these calculations are rock type dependent and are taken from the GEM of the Schönkirchen wellbore, like it has been done for the pre-drill model. In Table 6 below the used equations are listed. The input values for these calculations are delivered, like mentioned above, by the compressional sonic slowness log. This procedure of determining a second density curve is done because the density log is dependent on the borehole condition. If the wellbore is not in gauge, the density tool which is a pad tool shows inappropriate readings and a calculated density from the sonic log should be used instead of the density log, because this measurement is not that strongly affected by the borehole condition. In the picture below (Figure 15) a section of the processed petrophysical log done by the petrophysicist is shown. Here it can be seen that sections which are not in gauge (red areas on the right part of the plot) show too low readings for the density measurement where the sonic slowness logs seem not to be affected.

Lithology	Equation $RHO_{pseudo} [g/cm^3]$
Sandstone	$7.9867 * DTCO^{-0.269}$
Shale/Marl	$9.7032 * DTCO^{-0.305}$
Dolomite	$5.1258 * DTCO^{-0.157}$
Limestone	$5.1258 * DTCO^{-0.157}$

**Table 6:** Empirical equations used to calculate the pseudo density log [ $g/cm^3$ ] from the compressional sonic log [DTCO,  $\mu s/ft$ ].

The equations are borrowed from the Schönkirchen GEM and were already applied for the pre-drill model.

## Vertical Stress Determination (Post-Drill)

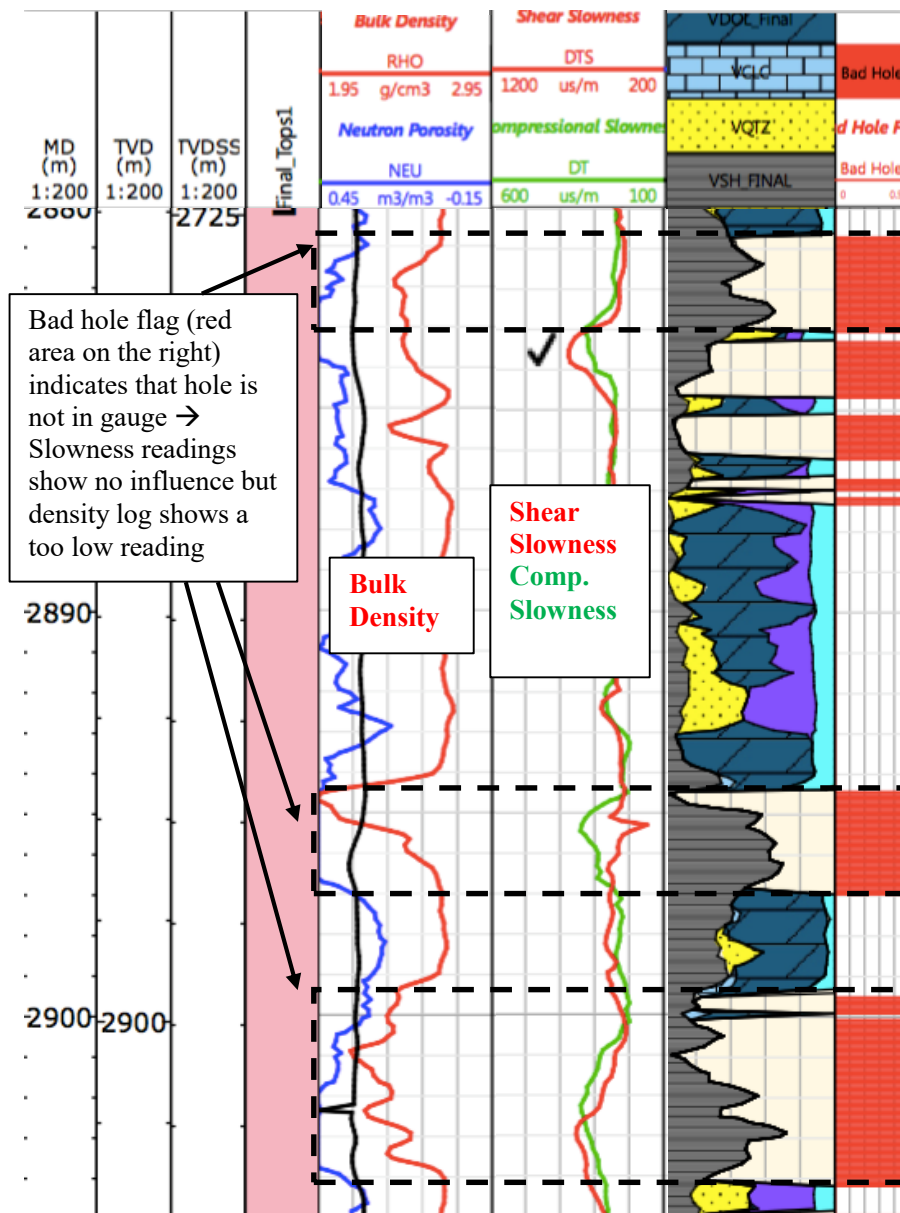


**Figure 15:** Segment of the petrophysical interpretation done with Techlog™, showing the visualization of bad hole sections.

This interpretation was provided by the petrophysical department of OMV.

Figure 16 shows the overburden density curve with the added trend line curve above and below the log measurements. The values of the upper section of the trend line are identical to the pre-drill model and match with the common trend in this region. For the determination of this trend line, the equation which was derived during the pre-drill model workflow was used (Table 7). Based on that overburden composite density curve (right green line) the overburden stress was calculated in stress [MPa] (left purple line) and mud weight [SG] (right purple line) units, using equation ( 1 ).

Lithology	Equation Density Trend Line [g/cm <sup>3</sup> ]
Above Aderklaa Konglomerat	$2.663 - 0.633 * e^{(-0.0006731 * TVD)}$

**Table 7:** Density trend in the Vienna Basin, developed for the STR T1 pre-drill model and borrowed for post-drill model calculation; the unit used for TVD is meters.

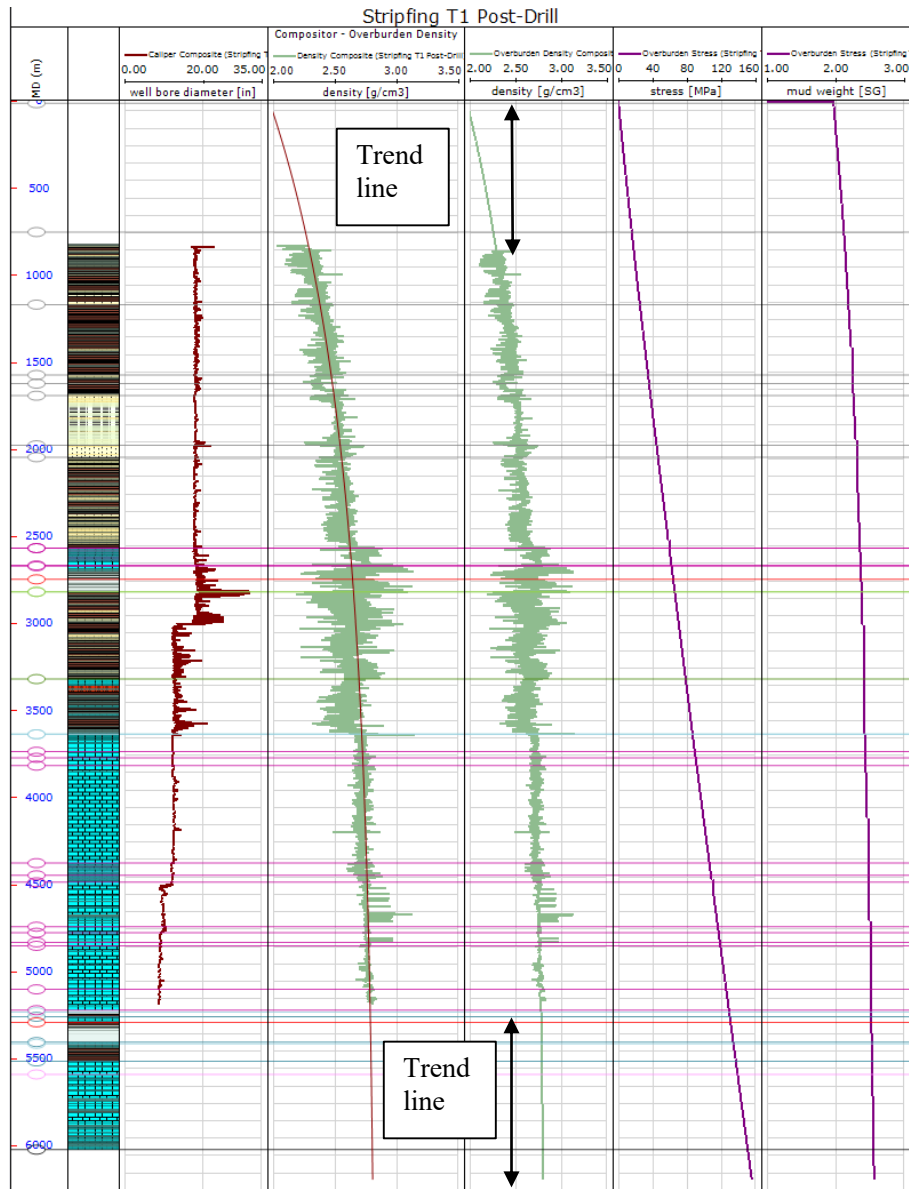


**Figure 16:** Illustration of the overburden density and the resulting overburden stress determined for the post-drill model. The tracks show from left to right: caliper [in], overburden density [g/cm<sup>3</sup>], overburden density [g/cm<sup>3</sup>] with trend line above and below the logged interval, the derived overburden stress in MPa units and the derived overburden stress in SG units. The density in the Vienna Basin Unit varies from 2.00-2.68 g/cm<sup>3</sup>, for the Calcareous Alps Unit from 2.38-2.78 g/cm<sup>3</sup>. The magnitude of the overburden stress increases from 2.00 SG at surface to 2.51 SG at TD.

## 4.4 Pore Pressure Prediction (Post-Drill)

The subsequently conducted workflow step was the pore pressure analysis by applying normal compaction trend (NCT) and Eaton's Method (section 3.4). The input logs for this purpose have been the density composite log for NCT, sonic slowness log for NCT, resistivity log for NCT and sonic velocity log for NCT. The sonic velocity log in this case

## Pore Pressure Prediction (Post-Drill)

is calculated from the sonic slowness log. The affix NCT for all these logs is important to mention because the pore pressure prediction (PPP) method which was used during this workflow was Eaton's Method combined with the usage of normal compaction trend. In comparison to the original logs it can be noticed that all values which are not measured in a shale lithology are missing. The selected NCT method accounts for these missing values because this method is just valid in shale formations. Considering that fact it is obvious that nearly no measurements in the carbonate and dolomite formations below 3700m can be seen on the plot. To calculate pore pressure curves for every previously named log, trend lines had to be fitted to all of them and dedicated pore pressure curves have been calculated for each of the input logs (density, sonic slowness, resistivity and sonic velocity). In Figure 17 the PPP logs are shown next to the lithology analysis. The density, sonic slowness, resistivity and sonic velocity (from left to right) input logs are followed by the pore pressure interpretation. In this interpretation log five different curves are visible, namely the pore pressure interpretation from density, sonic slowness, resistivity and sonic velocity logs (calculated by the program) and the pore pressure interpretation done by the engineer (black curve). This manually adjustable curve was created by the analysis of all helpful information enhancing the PPP. It should be tried to fit the curve to the calculated pore pressure interpretations, but general assumptions, fixed pore pressure values, drilling events and other meaningful input data outrank the prediction by NCT and Eaton's Method. In Figure 17 it can be seen that the PPP by this method shows pressure curves significantly apart from each other and that a prediction which applies only this method will not deliver a satisfying outcome. So, it was tried to align the pore pressure interpretation with the encountered recent drilling experiences and experiences from valuable offset wells. In this manner, it is possible to obtain a general trend for the PPP from the input logs but it is of high importance to adjust the pore pressure to several information collected from drilling and geological data as well as from the pre-drill model or general applicable assumptions for this region. In the case of the STR T1 well following information and assumptions were used to adapt the pore pressure curve as exact as possible to reality:

- Assumption that the pore pressure is hydrostatic until the top of Upper Cretaceous Gosau, supported by the geological experience and data from offset wells
- Kill mud weight (KMW) calculations, used as fixed points in PPP
- Pore pressure ramping up in the Upper Cretaceous Gosau formation, predicted in pre-drill model (turned out to be conclusive with fixed pore pressure points from kill mud weight calculations)
- Loss and gain events used to contain the possible pore pressure values

As drilling was planned to be overbalanced the mud weight was assumed to be slightly above the pore pressure to avoid gains into the borehole. Therefore, it was possible to orient the pore pressure curve to the MW curve during drilling. Encountered losses can be an indication for a too high mud weight but can also indicate fractures (especially in carbonate formations) or other non-drilling related occurrences. Gains of formation fluid observed during drilling, can be caused by a too low mud weight which is an indication to arrange the pore pressure curve above the drilled mud weight.

The pore pressure prediction curve (log on the right side of Figure 17) shows the outcome of this analysis. The pressure is assumed to be hydrostatic to the top of the Gosau formation (Upper Cretaceous) and ramps up within the Gosau formation where the first fixed pore pressure point was calculated as a result of a kick event at the bottom of this

## Post-Drill Geomechanical Model for the Stripfing T1/T1a Well

formation at 3281m MD. The kill mud weight which was calculated for this well control event was 1.52 SG. A second kick occurred shortly after, at 3371m MD in the Tannheim/Schrambach formation (below the Gosau formation, Lower Cretaceous), where a kill mud weight of 1.57 SG was applied to control the kicking well. For this purpose, another very short section of an increase in pore pressure was integrated and the pore pressure stayed at this highest level until the end of this formation. The third well control event which indicated the decrease of the pore pressure, took place at 3973m MD in the Middle Triassic Steinalm formation (carbonate). The inflow occurred after the mud weight was reduced to 1.35 SG because lots of losses were encountered during drilling this carbonate section. After circulating the borehole with this low mud weight a pit gain was observed and the well was killed with 1.52 SG KMW. The MW decrease was assumed to take place in the Jurassic Oberalm formation, on top of the second Middle Triassic sequence starting at 3735m MD. The last fixed pore pressure value obtained from kick events is located at 4496m MD in the middle of this Middle Triassic sequence. The KMW indicated that the pressure at this point equals 1.42 SG which implies another decrease in pore pressure from 1.52 to 1.42 SG. This decline was assumed to take place below the Steinalm formation where the last KMW was calculated and a pressure of 1.52 SG is prevailing.

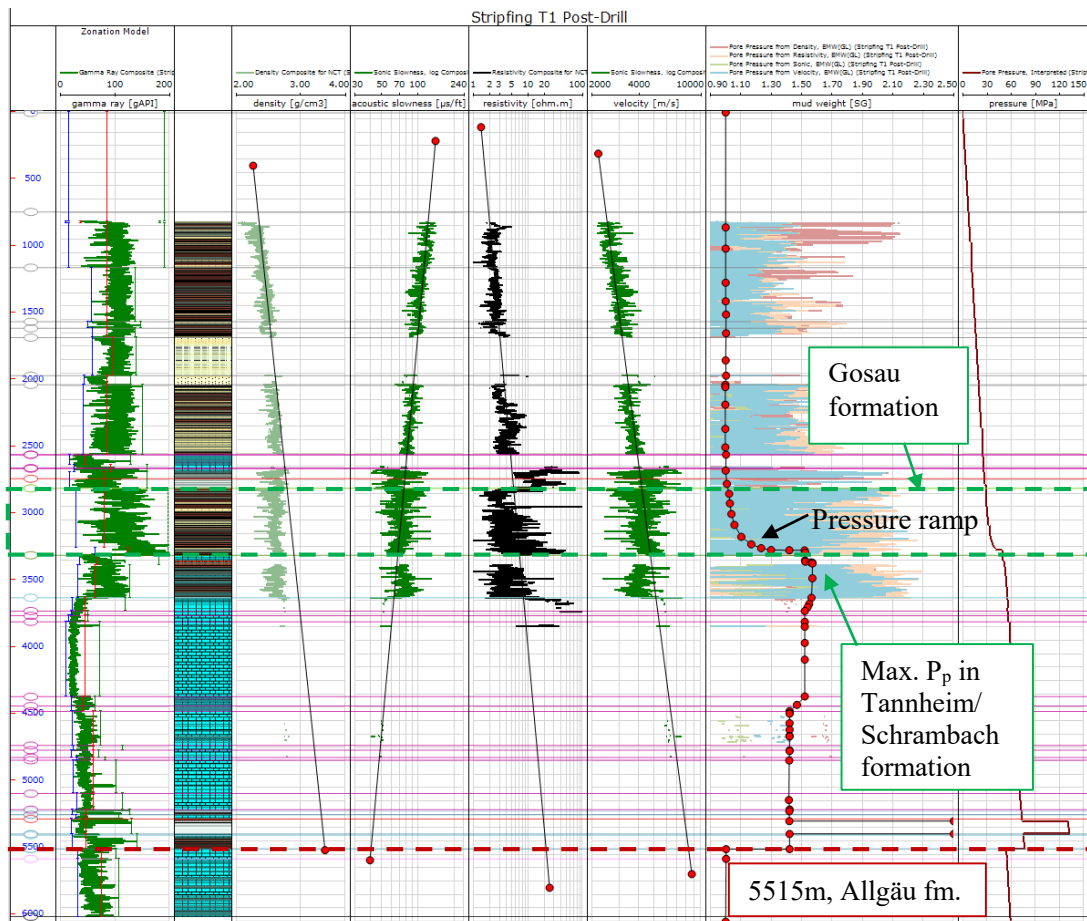


**Figure 17:** Pore pressure workflow view with determined pore pressure curve. The first track shows the gamma ray log with the determined lithology right beside it. Track two to five are showing the pore pressure prediction input logs with applied trend lines, namely density [g/cm<sup>3</sup>], sonic slowness [µs/ft], resistivity [ohm.m] and sonic velocity [m/s] from left to right. The resulting pore pressure predictions can be seen in track six (pastel colors), the manual pore pressure adjustment is visible in the same track



## Pore Pressure Prediction (Post-Drill)

in black, all logs are in SG units. The last track shows the determined pore pressure curve in pressure units [MPa]. The maximum pore pressure was reached in the Lower Cretaceous Tannheim/Schrambach formation with a magnitude of 1.57 SG.

Below this last fixed pressure point no more information was available to contain the pore pressure. Thus, the pressure was assumed to stay constant at the over hydrostatic magnitude at least until the beginning of the Allgäu formation at 5515m MD. The evidence for the statement that the pore pressure cannot decrease to hydrostatic before 5515m MD, was delivered by the Zwerndorf T1 well where the comparable Upper Jurassic Ruhpolding formation (above the Allgäu formation) was drilled and a saltwater inflow occurred at a mud weight of 1.51 SG when entering this formation (see 5.2 for more information).

The lack of information makes it basically impossible to determine the trend of the pore pressure below the Middle Triassic sequence. The short series of Jurassic formations in between the bottom of the Middle Triassic sequence and the Permian Werfen formation originate from residues of the overthrusting of the Tirolic Nappe by the Juvavic Nappe and is assumed to have the same pore pressure as the Middle Triassic formations on top. The Permian Werfen formation itself is described as a predominantly salt containing layer where under the prevalent pressure and temperature conditions the pore pressure aligns with the overburden pressure, which is the reason for the unusual high pore pressure values assumed for the Werfen formation. Below this special case of the salt layer the Jurassic Hierlatz and Ruhpolding formations are following. The pressure in these formations was expected to stay at the same magnitude as the formations above. Nearly the whole Ruhpolding formation consists of shale hence a change in pore pressure would not be noticed during drilling this section. For this reason, the decrease in pore pressure was assumed to be most reasonable directly below this formation like it is shown in Figure 17. However, an over hydrostatic Allgäu formation is possible albeit it is less probable that the pressure is decreasing in the middle of the carbonate formations. In this case, just the Upper Triassic Kössen formation would be hydrostatic. The third option that the pore pressure is not declining to hydrostatic is unlikely because the Kössen formation which was also penetrated in the Gänserndorf Übertief 3 well did not show over hydrostatic pressure. Nevertheless, all of these three versions are possible and due to the fact that no suitable logging run reached this depth, the verification of the conjectures is not feasible.

Another objective of this master thesis was to reveal potential origins of the overpressure starting within the Upper Cretaceous Gosau formation. For this reason, the “centroid buoyancy” workflow which is provided by the JewelSuite™ program was applied to the wellbore model (description and outcome of this workflow step are described in chapter 5.2). The top of this centroid was assumed to be located at 3371m MD, for the bottom of the centroid again three possible depths are feasible like it has been the case for the previous pore pressure prediction. Like it can be seen in Figure 39 the developed pore pressure curve (called final pore pressure) which accounts for the centroid buoyance effect seems like a smoothed version of the predicted pore pressure curve. Because of that the outcomes of the following model building steps are nearly identical and it is appropriate to run the model building workflow with the pore pressure curve from the prediction. However, the calculations and verification were also done for the final pore pressure curve and results almost identical to the ones for the PPP curve were encountered.



## 4.5 Minimum Horizontal Stress Determination (Post-Drill)

After the PPP was finished the least principle stress determination was conducted. For this purpose, the LOT data was interpreted with the quite simple approach of fitting a tangent to the first pressure increase of the pressure vs. volume curve, to see where the pressure plot is deviating from the straight line to determine the leak-off pressure (LOP) value. It is well known that the LOP is not the best choice for minimum horizontal stress estimation. Fracture closure pressure (FCP) or instantaneous shut-in pressure (ISIP) are better measurements for  $S_{hmin}$ . But the available data was just allowing for a LOP estimation because the LOT was terminated after the first deviation of the increasing pressure from the linearity or even after a predetermined pressure has been obtained like it is normally done for formation integrity tests (FITs). An example where a FIT instead of a LOT was conducted can be seen in Figure 22 where the pressure vs. volume data for the STR T1a leak-off test can be seen. The evaluation of the LOP data was done in Excel where the pressure (blue line) and the pump rate (red line) were plotted against the cumulative pumped volume and a tangent was fitted to the pressure plot to graphically assess the LOP value. The analysis of the LOT curves enables the determination of the LOP values for the three different depth sections. The pictures below (Figure 18 - Figure 22) show the LOT evaluation for the  $18\frac{5}{8}$ ,  $13\frac{3}{8}$  and  $9\frac{5}{8}$  casing sections dedicated to the respective depth. The  $13\frac{3}{8}$  LOT was repeated because the obtained pressure was lower than expected. The second curve however shows nearly identical behavior of the pressure vs. cumulative volume curve as it can be seen in Figure 19 and Figure 20. Furthermore, another LOT was performed for the sidetrack of the Stripfing T1 well, called the Stripfing T1a well. Unfortunately, this LOT pressure vs. volume curve cannot be used to extract any information. In Figure 22 it is obviously visible that no leak-off took place and that this curve is not adding value to the evaluation of the minimum principal stress.

An evaluation of the LOT data was also done by the drilling department and values for this analysis could be found in different reports and presentations. In Table 8 below the values which were determined and calculated by the drilling department are shown. The LOP determination by the applied method is a quite subjective one. For the LOTs executed in the 18.625in and 9.625in casing sections the interpretation done for this part of the model building workflow is equal to the one done by the drilling department. For the 13.375in casing section the analysis in this thesis is not conformable with their values. The analysis done for this thesis showed a surface pressure of about 145 bar where the analysis of the drillers showed a pressure of 158 bar. Calculating the EMW this results in 1.69 SG or 1.74 SG, respectively. Another discrepancy is arising when interpreting the LOT of the sidetrack shown in Figure 22. The analysis of the drilling department (Table 8) is showing a value for the surface pressure at leak-off and an EMW value which implies that a leak-off was seen on the plot. From the geomechanical analysis viewpoint no leak-off is visible, the drop of the pressure is clearly a result of the stopping of the pumps and no indication that the formation is leaking-off. Therefore, these values are missing in the geomechanical LOT interpretation and they are not included into the minimum horizontal stress evaluation.

## Minimum Horizontal Stress Determination (Post-Drill)

Casing Size [in]	Depth [m]	Mud Weight [SG]	Surface Pressure at Leak-Off [bar]	Calc. Downhole LOP [SG]
18.625	839	1.08	57	1.77
13.375	2996	1.20	158	1.74
13.375	2996	1.20	158	1.74
9.625	4504	1.4	101	1.63
9.625 (ST)	4496	1.45	72	1.61

**Table 8:** Reported LOTs for the STR T1 well, interpreted by the drilling department. The segments shaded in gray represent the interpretations that differ from the ones done during this thesis.

Casing Size [in]	Depth [m]	Mud Weight [SG]	Surface Pressure at Leak-Off [bar]	Calc. Downhole LOP [SG]
18.625	839	1.08	57	1.77
13.375	2996	1.20	144	1.69
13.375	2996	1.20	145	1.69
9.625	4504	1.4	101	1.63
9.625 (ST)	4496	1.45	-	-

**Table 9:** Reported LOTs for the STR T1 well, interpreted as part of this thesis. The segments shaded in gray represent the interpretations that differ from the ones done by the drilling department.

The determined LOP values are inserted into the program as minimum horizontal stress input values for the calculation of unitless effective stress ratio points. By using the equation defining the Effective Stress Method ( 4 ), unitless effective stress ratio points were determined from this calibration points. The pore pressure ( $P_p$ ) and the overburden stress ( $S_v$ ) which are the other required input values beside the  $S_{hmin}$  value were already calculated in the previous workflow steps. These three unitless ESR points were plotted in a log and used to graphically fit a trend line through to get a continuous curve for the ESR which was afterwards used to determine the minimum horizontal stress. The ESR used to calculate the  $S_{hmin}$  in the post-drill model was found to be 0.5. By applying equation ( 4 ), the minimum horizontal stress for the Stripfing T1 well was calculated from surface to TD in SG as well as MPa units (light green curves in Figure 23) by using the determined ESR, the pore pressure and the overburden stress log. The shape of the minimum horizontal stress curve appears nearly similar to the one of the pore pressure curve and reaches its maximum value at the point of the maximum pore pressure, in the Lower Cretaceous Tannheim/Schrambach formation, holding a magnitude of 2.00 SG.

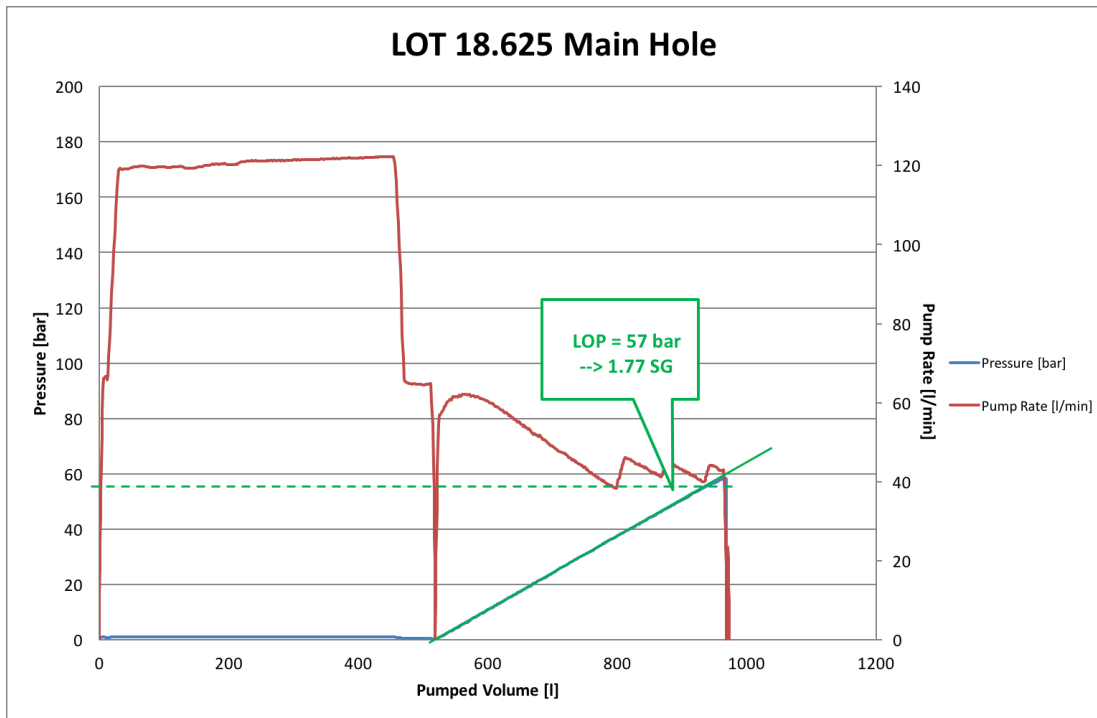


Figure 18: Leak-off test conducted in the 18.625in hole section of the STR T1 well.

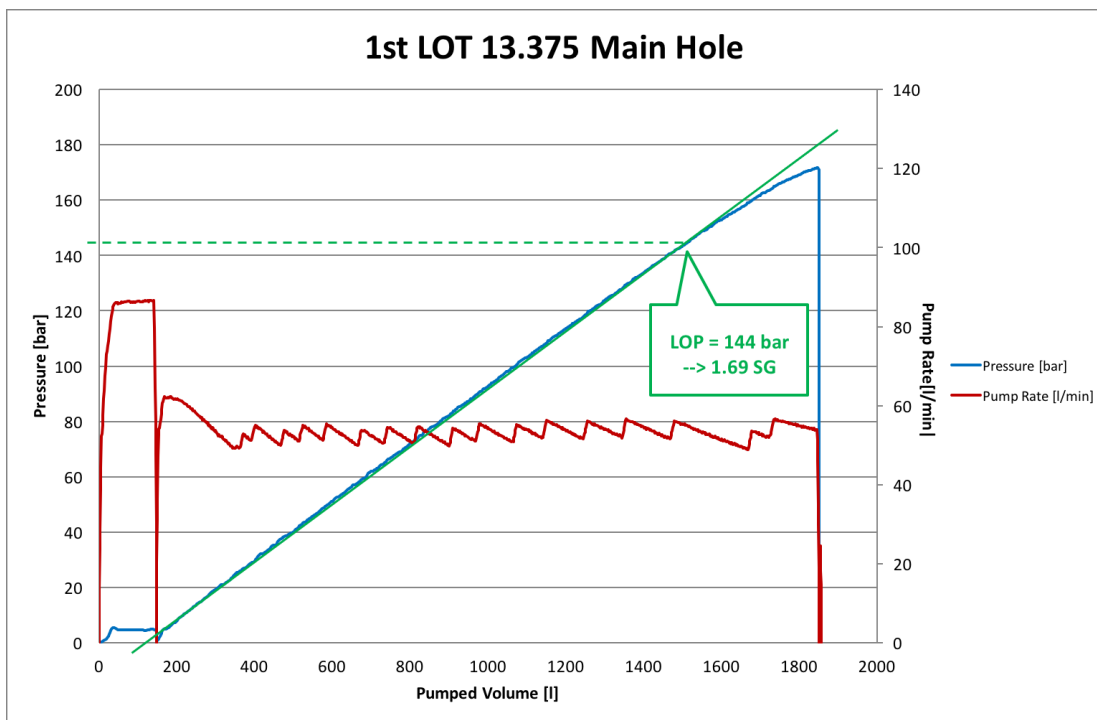


Figure 19: Leak-off test conducted in the 13.375in hole section of the STR T1 well.

Minimum Horizontal Stress Determination (Post-Drill)

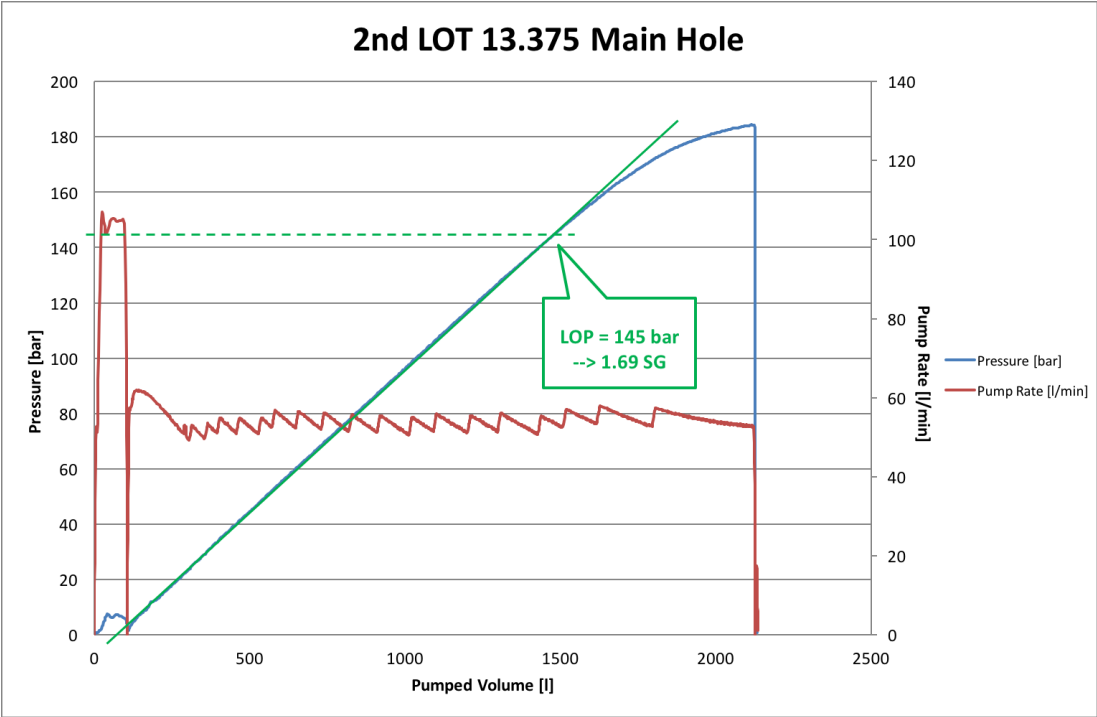


Figure 20: Repeated leak-off test conducted in the 13.375in hole section of the STR T1 well.

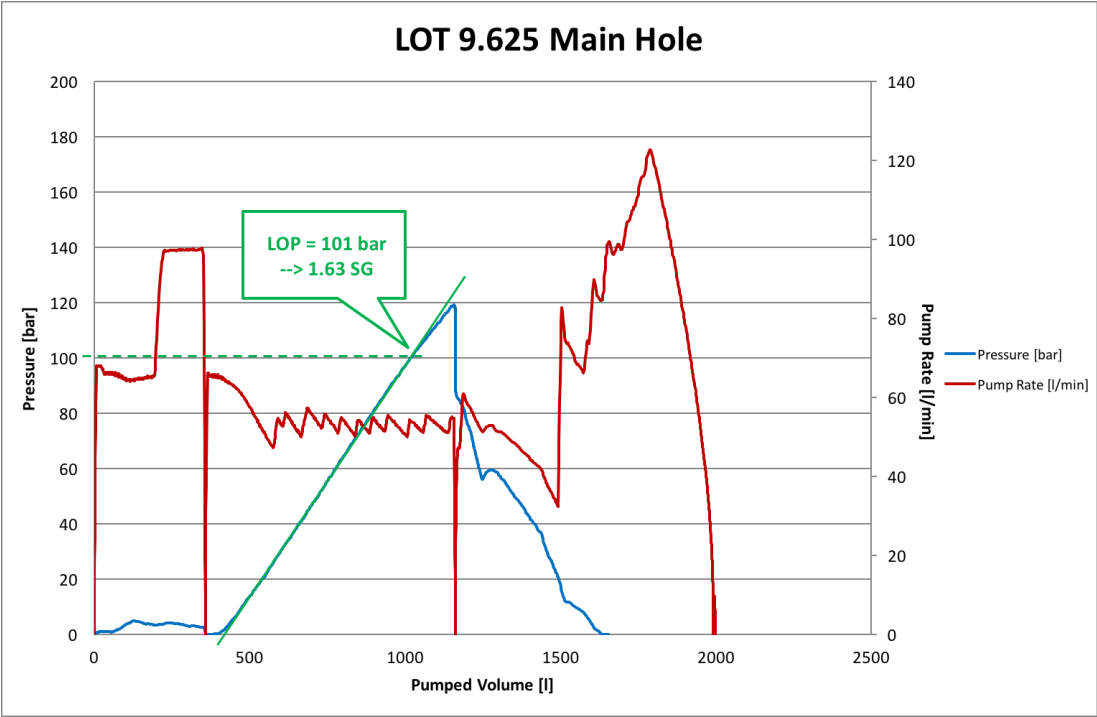


Figure 21: Leak-off test conducted in the 9.625in hole section of the STR T1 well.

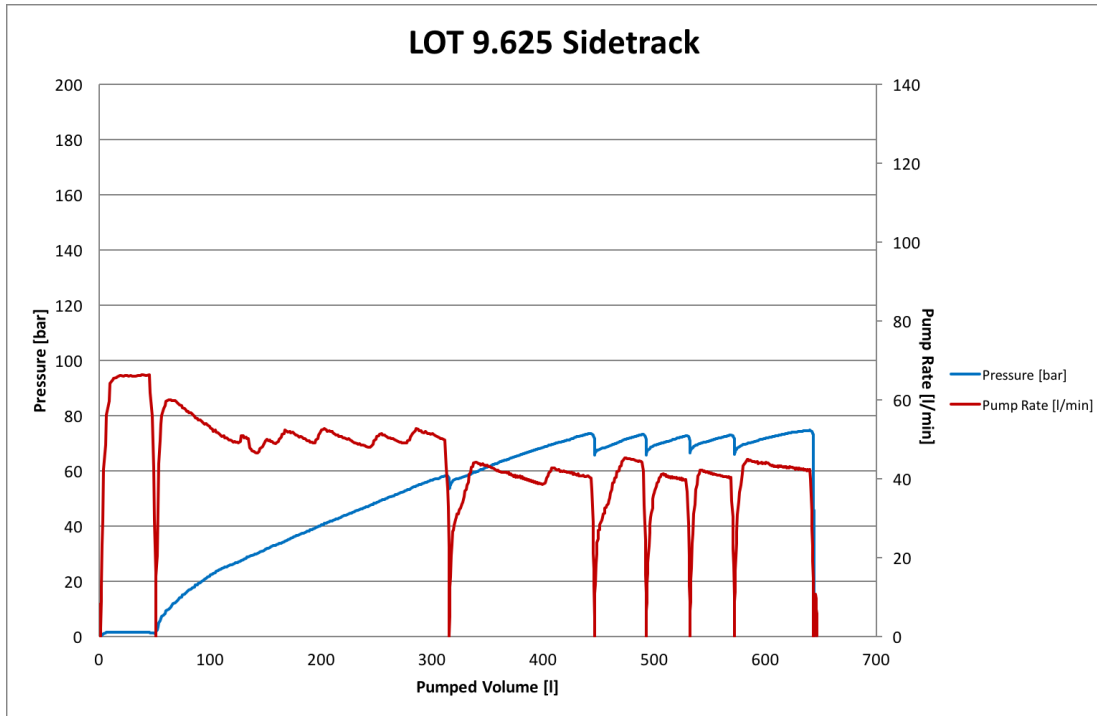


Figure 22: Leak-off test conducted in the 9.625in hole section of the STR T1a well.

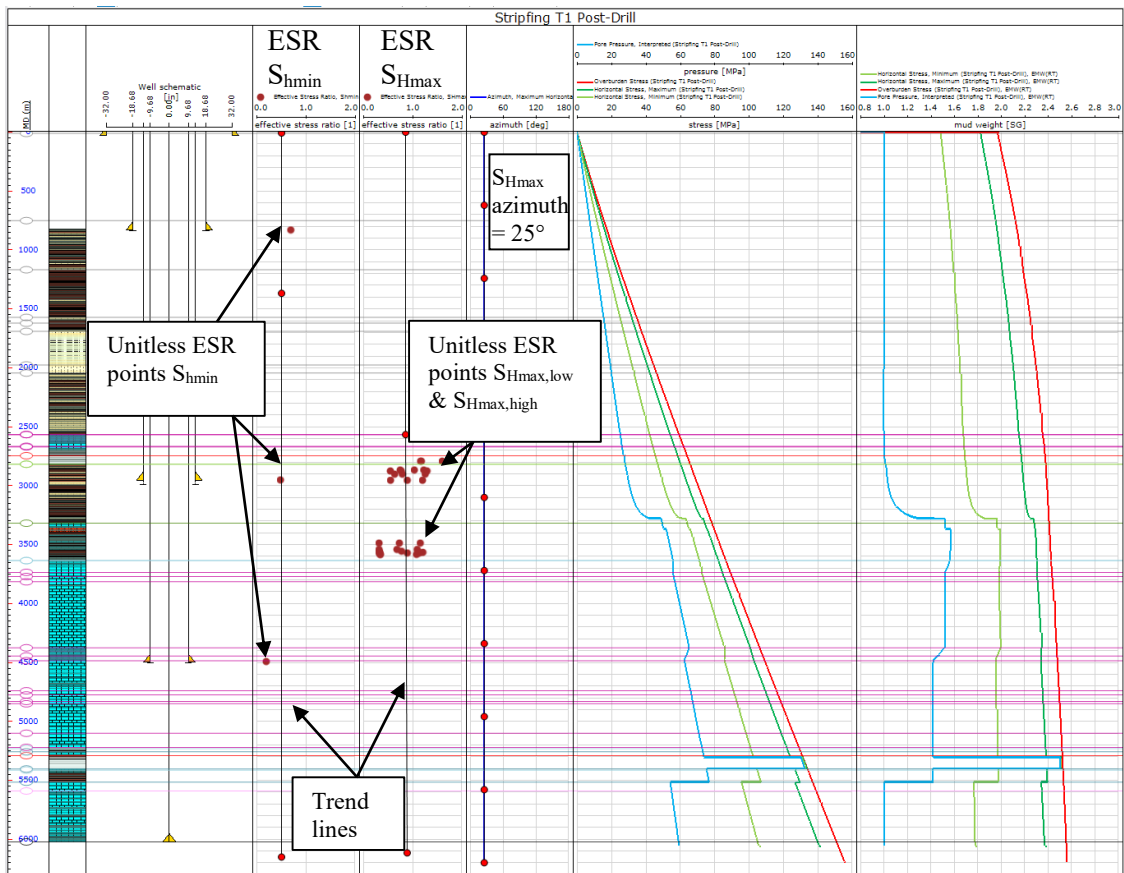


Figure 23: Summary of vertical and horizontal stresses and pore pressure for STR T1. The first and the second track show the ESR points together with the ESR trend line for the minimum and the maximum stress determination, respectively. For the  $S_{hmin}$  determination the LOP points were used to calculate the ESR points, for the  $S_{Hmax}$

## Maximum Horizontal Stress Magnitude and Azimuth Determination, Including Rock Properties Evaluation (Post-Drill)

determination, the stress polygon analysis is the method to determine low and high  $S_{Hmax}$  values for the calculation of the ESR points. The third track shows the  $S_{Hmax}$  azimuth, determined by image log analysis and set to  $25^\circ$  from surface to TD. The fourth and fifth track show pore pressure (blue),  $S_{hmin}$  (light green),  $S_{Hmax}$  (dark green) and  $S_v$  (red) in pressure [MPa] and mud weight [SG] units, respectively. The maximum  $S_{hmin}$  gradient was reached in the Lower Cretaceous Tannheim/Schrambach formation with a magnitude of 2.00 SG.

In Figure 23 the unitless effective stress ratio points with the generated trend lines for minimum horizontal stress are visible to the right of the wellbore schematics. On the right side of the plot the pore pressure (blue), the minimum horizontal stress (light green) calculated from the ESR trend line, the maximum horizontal stress (dark green) and the overburden stress (red) are visible in stress [MPa] (left side) and mud weight [SG] (right side) units. The strong influence of the pore pressure on the horizontal stresses is clearly visible. As the pore pressure starts to rise, below 3300m MD, the stresses start approaching the vertical stress curve and will decrease again when the overpressure starts decreasing back to hydrostatic.

## 4.6 Maximum Horizontal Stress Magnitude and Azimuth Determination, Including Rock Properties Evaluation (Post-Drill)

The maximum horizontal stress curve ( $S_{Hmax}$ ) was also determined by applying the Effective Stress Method. For this purpose, equation ( 5 ) was used to calculate unitless effective stress ratio points like it has been done for the minimum horizontal stress determination. The input values for this procedure require the application of the SFIB™ program to generate different stress polygon plots for several wellbore depths. The workflow how this was done and what input parameters are necessary is described in section 3.8. The prerequisite for this step is an accurate image log examination with precise picked breakouts like it is described in chapter 3.7.1 and the calculation of the rock property logs or the definition of rock property values which are not calculated but approved for the respective lithology (see 3.6). The rock properties which are important for this modeling step are unconfined compressive strength (UCS), internal friction, Young's Modulus, Poisson's Ratio, Biot's Coefficient and sliding friction. Just three of them namely UCS, Young's Modulus and Poisson's Ratio have been calculated from logging results.

Like it has already been discussed in chapter 3.6.5, the Biot's Coefficient is assumed to be 1 for every lithology. Also for the internal friction standard values have been taken like it was done in the pre-drill model to prevent the dependency of the entire rock strength parameters on the sonic log alone (Zheng, Schulze, and Blumenthal 2012). The friction coefficients depend on the rock type and vary from 0.8 for weaker rocks to 1.0 for stronger rocks like it is shown in Table 10.

Lithology	Friction Coefficient
Shale, Marl	0.8
Sandstone, Sandy Siltstone	0.9
Limestone, Dolomite	1

**Table 10:** Friction coefficients for different lithology types, values are borrowed from the pre-drill model.

The last parameter which uses defined standard values is called sliding friction. Like it was already mentioned in section 3.8, the sliding friction was set to 0.6 for every lithology.

For the determination of the dynamic Young’s Modulus the compressional sonic and the shear sonic velocity as well as the density log are needed as input values. The velocities are calculated from the respective sonic slowness logs. In section 3.6.3 the equation for the determination of the dynamic Young’s Modulus can be found ( 6 ). The formula for the calculation of the dynamic Young’s Modulus is not rock type dependent, but the used equations for the determination of the static Young’s Modulus from the dynamic one, are. Due to the fact, that no core measurements have been taken for the STR T1 wellbore, the equations which have been used for these conversions are taken from the pre-drill model. There, published equations by Lacy (1997) were applied to obtain the static Young’s Modulus log. These applied equations can be seen in Table 11. To use these formulas, the unit for dynamic ( $E_{dynamic}$ ) as well as the static Young’s Modulus ( $E_{static}$ ) values must be million psi (Mpsi). However, the in- and output units can be chosen during the model workflow and the conversions will be done by the program. For the geomechanical model of the STR T1 wellbore the Young’s Modulus is plotted in GPa units.

Correlation/Lithology	$E_{static}$ [Mpsi]
Lacy Sand Equation	$0.0293 * E_{dynamic}^2 + 0.4533 * E_{dynamic}$
Lacy Shale Equation	$0.0428 * E_{dynamic}^2 + 0.2334 * E_{dynamic}$
Lacy Limestone/Dolomite Equation	$0.018 * E_{dynamic}^2 + 0.4224 * E_{dynamic}$

**Table 11:** Equations used to calculate the static Young’s Moduli for different lithology types from log-derived dynamic Young’s Moduli. Published equations by Lacy (1997) were used, like it has been done for the pre-drill model, because no rock tests have been conducted to calibrate correlations. The unit for the static and dynamic Young’s Moduli is Mpsi.

The dynamic Poisson’s Ratio can also be calculated from the shear and compressional sonic log. Like it has been discussed in chapter 3.6.4, the dynamic Poisson’s Ratio can be calculated by using equation ( 8 ).  $V_p$  and  $v_s$  are the compressional sonic and shear sonic velocity, respectively, which were calculated from the sonic slowness logs. The evaluation of the dynamic Poisson’s Ratio is not rock type dependent and can be used for every lithology. Like it was already stated in chapter 3.6.4 the static Poisson’s Ratio which is used for calculations during the model workflow can be calculated from the dynamic one. Due to the fact that no core laboratory measurements have been taken and no general correlation for the relationship between dynamic and static Poisson’s Ratio is published, the conversion factor is assumed to be 1.

Maximum Horizontal Stress Magnitude and Azimuth Determination, Including Rock Properties Evaluation (Post-Drill)

The equations for the UCS however are rock type dependent and utilizing the compressional slowness log as input values. Wherever it is possible the log derived results should be calibrated by lab test results. For the Stripfing T1 well no laboratory measurements have been taken which would have allowed such a calibration. Hence the equations for the unconfined compressive strength have been taken from the pre-drill model which on the other hand used equations from the Schönkirchen GEM which have been calibrated to lab test results where possible (Zheng, Schulze, and Blumenthal 2012). The equations used are listed in Table 12 below and are a modification of the equations for the calculation of UCS from compressional sonic measurement developed by Militzer and Stoll (1973) and McNally (1987). For the sandstone/shale formula, the DTC (compressional sonic slowness) values are in  $\mu\text{s}/\text{ft}$  and the resulting UCS values are in psi units. For the dolomite/limestone/anhydrite formulas the compressional sonic velocity in  $\text{km}/\text{s}$  is used as input value and the resulting UCS is in MPa units.

Lithology	Unconfined Compressive Strength (UCS)
Sandstone/Shale/Sandy Siltstone/Marl	$UCS[\text{psi}] = 1.1(8000/DTC[\mu\text{s}/\text{ft}])^{1.82}$
Dolomite	$USC[\text{MPa}] = 2.9623e^{(0.57(v_{DTC}[\text{km}/\text{s}]-0.1))}$
Limestone	$UCS[\text{MPa}] = 2.9623e^{(0.57v_{DTC}[\text{km}/\text{s}])}$
Limestone Strong	$UCS[\text{MPa}] = 1.4 * 2.9623e^{(0.57v_{DTC}[\text{km}/\text{s}])}$
Anhydrite	$UCS[\text{MPa}] = 0.7 * 2.9623e^{(0.57v_{DTC}[\text{km}/\text{s}])}$

**Table 12:** Equations used to derive the UCS for different lithology types from compressional sonic slowness measurements; borrowed from the pre-drill model. These equations were originally derived for the GEM Schönkirchen where these correlations have partly been calibrated.

In addition to the determination of the rock properties, the analysis of the image logs of a wellbore is an essential part of the post-drill model building workflow, not only for the stress direction and the maximum horizontal stress determination but also for the wellbore stability analysis and the verification as one of the last steps of the model building.

Four different image logging runs have been conducted for the STR T1 well, where three of them have been FMI™ logs and one has been a GVR™ log. In the table below (Table 13) it is represented which sections of the borehole have been logged and which method was used.

Logging Run	Logging Method
# 1: 2485 – 2968m MD	FMI™
# 2: 2990 – 3898m MD	GVR™
# 3: 3825 – 4485m MD	FMI™
# 4: 4400 – 5194m MD	FMI™

**Table 13:** Image logging running depth and used method for the STR T1 wellbore.

By using the Imager™ program, the breakouts, drilling induced tensile fractures and drilling enhanced fractures were picked from the image logs according to the procedure

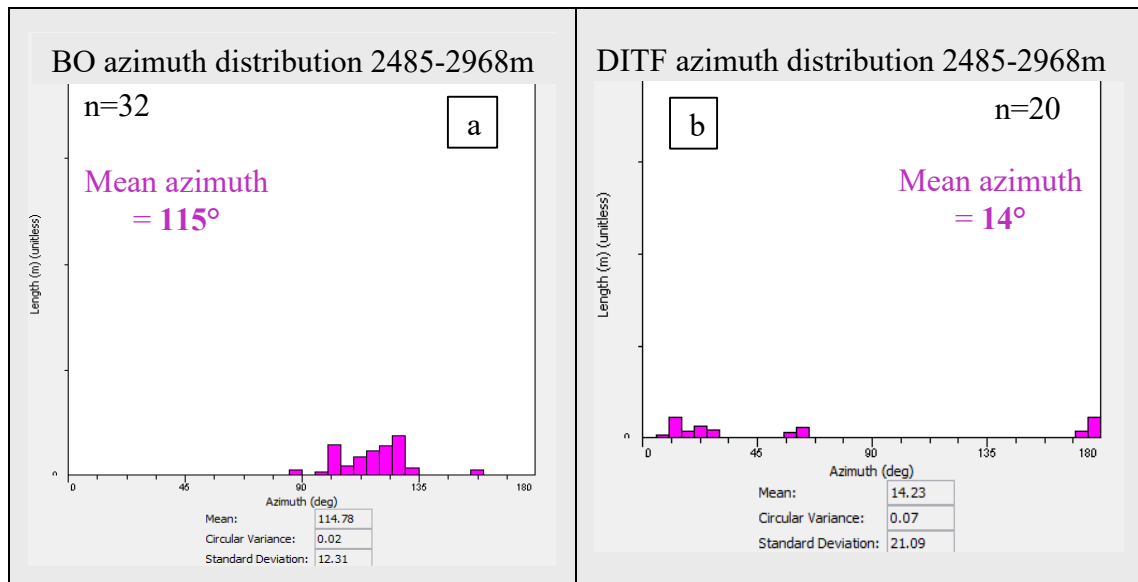


described in chapter 3.7. After sorting out the picked features with lower confidence and the ones which are not assessable as complete feature, the distribution of the azimuths of the breakouts and the drilling induced tensile fractures was plotted and the mean azimuth was calculated by the program. The mean azimuth of the BOs and the DITFs should be 90° apart since the azimuth of the BOs represents the direction of the minimum horizontal stress and the azimuth of the DITFs indicates the azimuth of the maximum horizontal stress direction.

In Figure 24 the distribution for the azimuths of the BOs and DITFs which were picked from the image logs and chosen for stress determination is shown for each image logging run. For the third run from 3825 to 4485m MD no features which are valid for stress and azimuth determination have been picked. On the last run from 4400 to 5194m MD only drilling induced tensile fractures have been picked and could be used for azimuth determination.

For the BO azimuth which determines the minimum horizontal stress direction, both mean values (Figure 24a and Figure 24c) showed a resulting value of 115°, where for the DITFs three slightly different values were calculated. The first run section yielded an outcome of 14° for the mean value, the second section showed 29° as resulting azimuth value and the fourth section showed 24° as an outcome value for the mean azimuth of the drilling induced tensile fractures. 25° was taken as an average value for the azimuth of the maximum horizontal stress which perfectly corresponds with the 115° azimuth of the minimum horizontal stress which always lays perpendicular to the maximum horizontal one.

This magnitude for the  $S_{Hmax}$  azimuth was inserted as a fixed value in the JewelSuite™ program for the whole depth of the wellbore like it can be seen in Figure 23 to the right of the ESRs.



Maximum Horizontal Stress Magnitude and Azimuth Determination, Including Rock Properties Evaluation (Post-Drill)

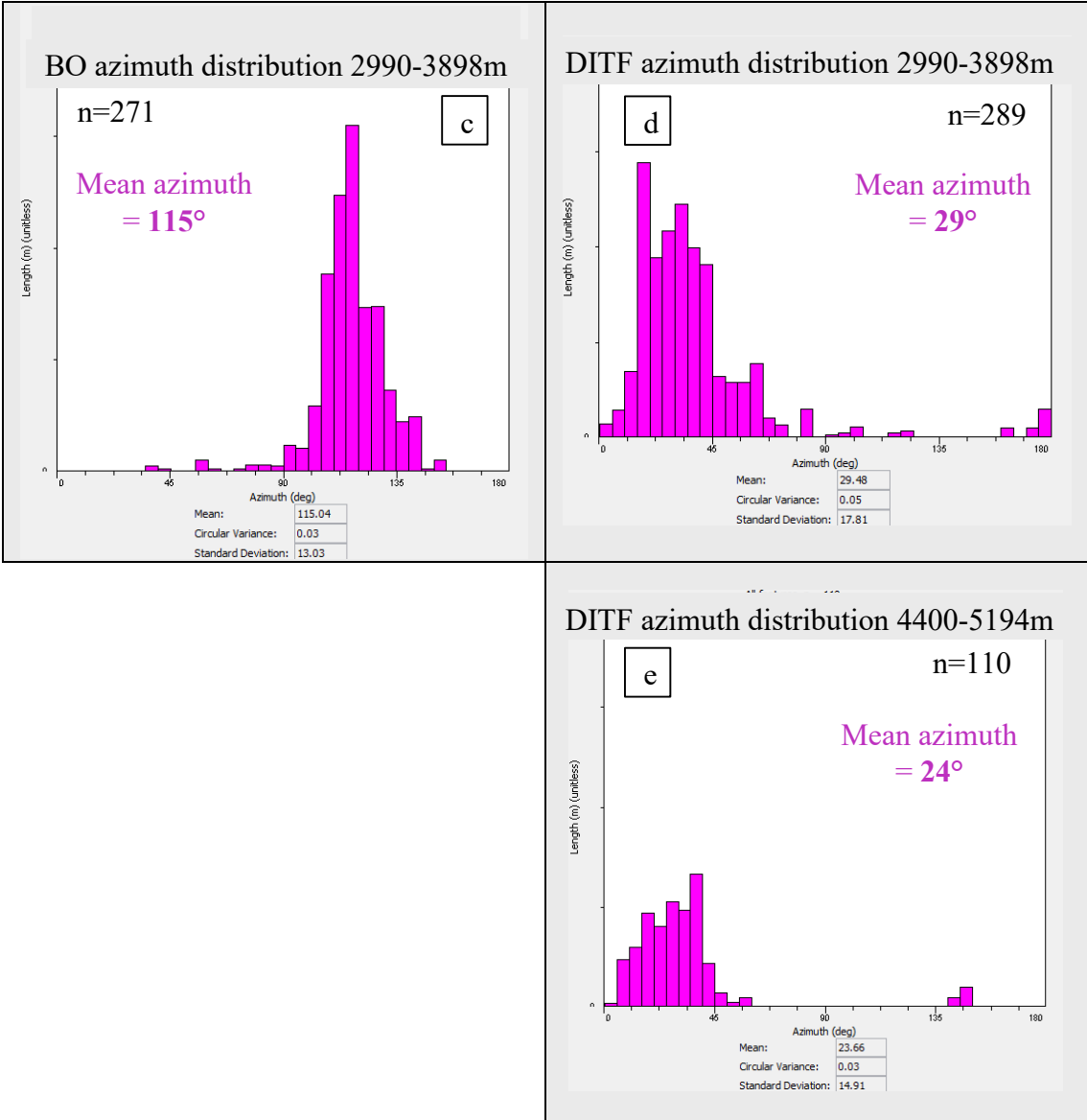
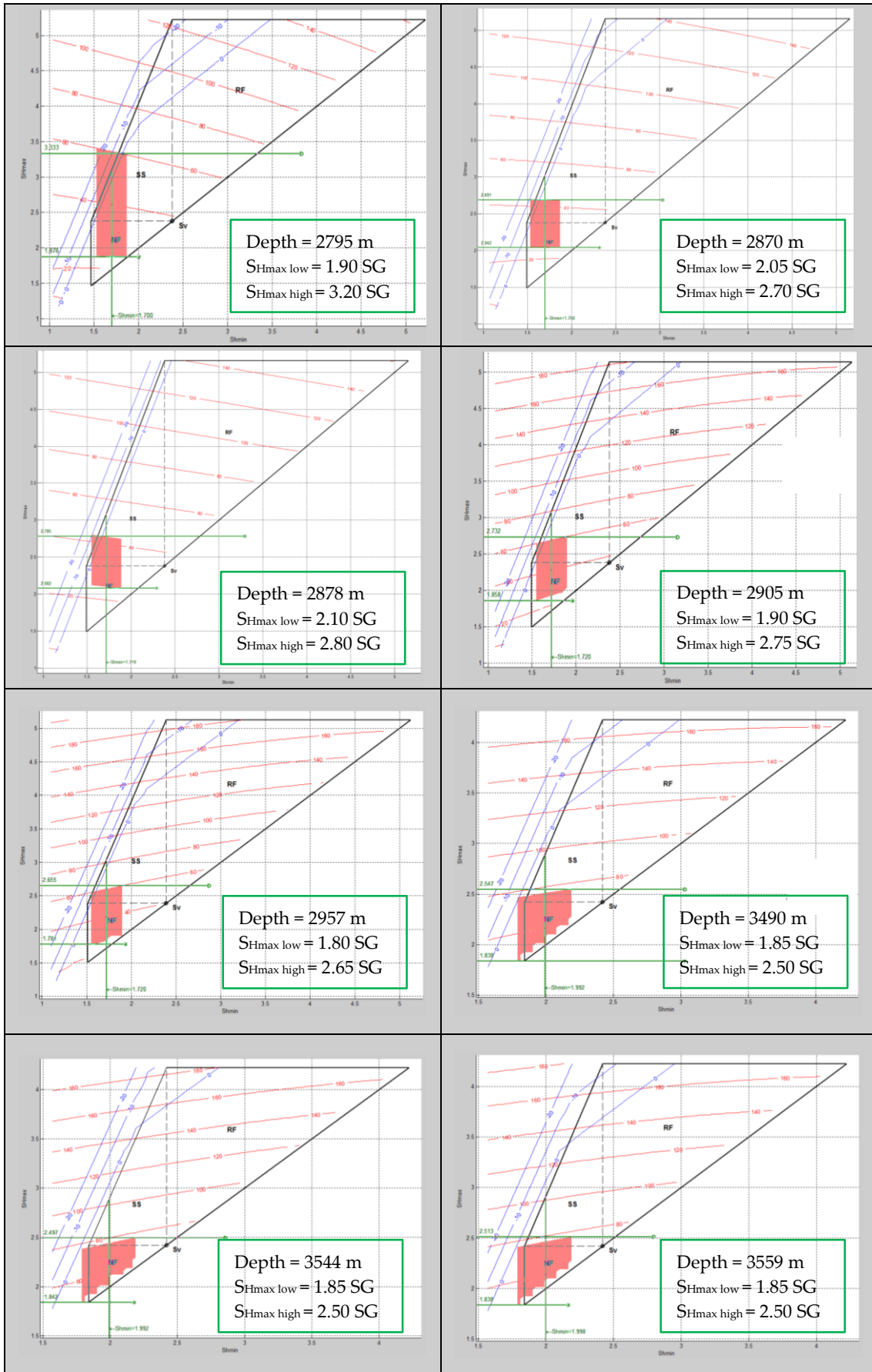


**Figure 24:** Azimuth distribution for drilling induced tensile fractures and breakouts determined by the analysis of picked geomechanical features by using the Imager™ program. The mean azimuths for the different logging sections for the BOs (left side) and the DITFs (right side) show compliant or nearly compliant values, respectively.

The image log analysis however is not just a method to evaluate the maximum horizontal stress azimuth but also the magnitude. The determination of the maximum horizontal stress magnitude cannot be done directly but with the help of stress polygon analyses (see 3.8 for a detailed description of the procedure). For this application, it is again important to precisely select the breakouts which are useful for the stress determination (see 3.7.1). From these picked BOs, single meaningful BOs or significant sections of BOs were chosen, where for the sections with more than one BO, a representative BO which holds the average width was selected. For these breakouts, all essential input parameters for the stress polygon application have been read from the plots generated in the previous workflows, collected in an Excel table and eventually have been inserted in the SFIB™ program. The output of each of these data sets is a dedicated stress polygon where information about the maximum horizontal stress and the stress regime can be attained. Each of the pictures in Figure 25 shows a stress polygon for a single depth generated by

the program using the input values (overburden stress, maximum stress azimuth, pore pressure, mud weight, Biot's Coefficient, azimuth and deviation of the borehole, BO width, internal friction, Poisson's Ratio, sliding friction coefficient and failure criterion) which have been collected from the plots generated during previously executed steps. The list with all the input data as well as wider pictures of all stress polygons can be found in the Appendix (Table 17 and Figure 42 - Figure 52). After the plot has been constructed a range for minimum horizontal stress and unconfined compressive strength must be determined and inserted to get a red square drawn on each plot which reflects the ranges of  $S_{hmin}$  and UCS entered into the program. To identify the ranges of minimum horizontal stress and UCS a closer look on the surrounding of the BO depth is necessary. It is not useful to add and subtract a defined percentage from the read value or to define a distance range around the depth of interest for all BOs where the minimum and the maximum value should be identified. This is because it is possible that the curve for  $S_{hmin}$  and UCS is stable for quite a long distance within a formation or that it is just a very regional occurrence. Hence the distance range can be different for every selected BO and the minimum and maximum values for  $S_{hmin}$  and UCS must be determined to conform the requirements. The red square generated by inserting these ranges confines the maximum horizontal stress values which are possible at the location where these input values are valid. On the x-axis the minimum horizontal stress and on the y-axis the maximum horizontal stress is plotted. The red lines are indicating the UCS values and the blue lines are showing whether the occurrence of tensile fractures is possible (for that reason, the zero tensile stress line must be within the stress polygon). The analysis of the different plots delivered a low and a high maximum horizontal stress value for each depth (see green boxes in Figure 25). This was done by drawing horizontal lines from the highest possible and the lowest possible point of the red square which confines the maximum horizontal stress. The appearance of tensile fractures would enhance the confinement of the maximum horizontal stress. If drilling induced tensile fractures would have been visible next to the breakouts it would have been possible to decrease the range of stress because then it is defined to stay within the polygon, within the red square, and to the left of the zero tension line, indicating the occurrence of tensile fractures (forming under negative hoop stress). For the polygon plots above 3000m MD the zero tension line is outside of the stress polygon which means that a coexistence of drilling induced tensile fractures and breakouts is not possible. For the plots below 3000m MD the existence of DITFs is possible (zero tension line within the polygon) but has not been detected on the image logs.

# Maximum Horizontal Stress Magnitude and Azimuth Determination, Including Rock Properties Evaluation (Post-Drill)



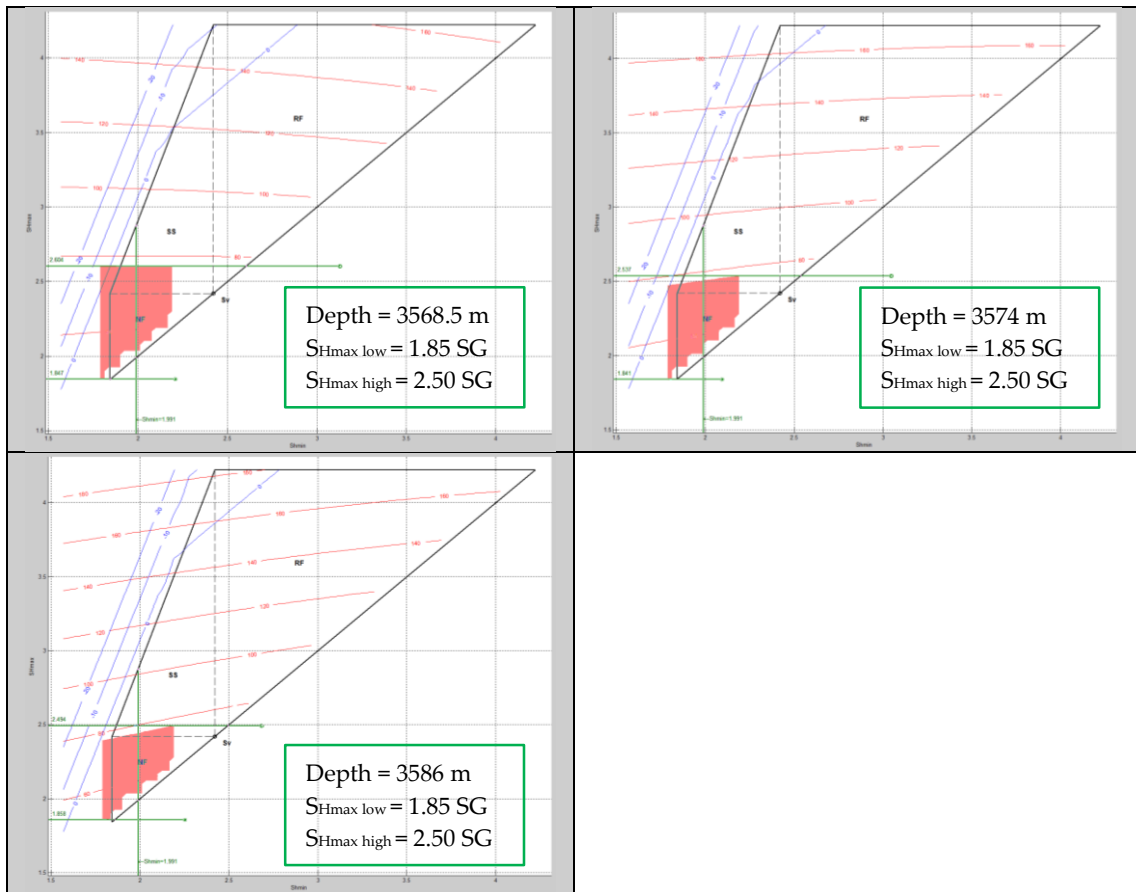


**Figure 25:** Stress polygon plots generated by using the SFIB™ program to determine  $S_{Hmax}$  calibration points for the max. horizontal stress determination workflow. This analysis was conducted for nine different borehole depths which have been chosen to be meaningful for the evaluation of the maximum horizontal stress. The depth values as well as dedicated potential minimum and maximum  $S_{Hmax}$  values are shown in the green-framed boxes.

Due to the fact that no single stress value for a special depth is available like it has been the case for the minimum horizontal stress determination by using LOT values, a low and a high value for the different depths were entered in the program and used for the calculation of the unitless effective stress ratio points which are the reference points for the creation of the ESR trend line. Exactly like in the step before where the minimum horizontal stress was determined, this trend line is used to calculate the maximum horizontal stress in pressure [MPa] and mud weight [SG] units (dark green lines in Figure 23) by applying equation ( 5 ).

Another fact that can be read from the stress polygon plot is the stress regime which is predominant in the region around the analyzed wellbore. In section 3.8 it is described which sections of the stress polygon are representing the respective stress regimes. The different stress polygons of the STR T1 well (Figure 25) show that the main parts of the red squares which determine the confinement of the stresses can be found in the region of normal faulting stress regime, some of them can also partly be found in the section of the polygon which indicates strike-slip stress regime. As the general assumption for the stress regime of the region around the Stripfing T1 well says that a normal faulting stress regime is prevailing this is consistent with the outcome shown by the stress polygon interpretation.

## 4.7 Verification of the Geomechanical Model (Post-Drill)

By determining the stresses and the azimuth of the maximum horizontal stress all input parameters for the wellbore stability analysis are completed and can be selected for this assessment. Figure 29 is showing the selection of input parameters for the wellbore stability analysis, to be specific, pore pressure, overburden stress, minimum and maximum horizontal stress, UCS, static Poisson's Ratio, internal friction coefficient and wellbore inclination. The inclination of the Stripfing T1 wellbore is hardly deviating from zero, hence the STR T1 can be assumed as vertical well from top to bottom. The tensile strength was assumed to be zero throughout the whole wellbore and the failure criterions are consistent with the ones selected in the rock properties step, namely Modified Lade for shales and sandstones and Mohr Coulomb for limestone and dolomite. The breakout limit was set to  $90^\circ$  for vertical wells and  $30^\circ$  for horizontal wells with a linear relationship between them like it is common sense for geomechanical applications, however in this study the wellbore is vertical and the  $90^\circ$  limit is crucial.

The next important step before the observed and the calculated breakouts can be compared is the generation of a special mud weight curve. This curve is constructed to be another input log for the stability analysis. It is not possible to simply take the drilled mud weight or the lowest mud weight the wellbore has experienced, because this may not fit with the mud weight the wellbore has seen before or during image logging. To determine the lowest mud weight which the logged borehole section has experienced before or during image logging is important because the breakouts which are later used for calibration and comparison have been detected on the image log and they have formed at the lowest mud weight the borehole has seen until this logging run. Breakouts which have been formed after this image log runs because the mud weight was reduced are not represented on the images. In case a lower or a higher mud weight is used for the calculation, the breakouts will be over- or underestimated, respectively. Obviously, the breakouts which have formed due to a reduction of the mud weight after the image logging was conducted, are not represented in the model. However, it is possible to simulate the wellbore failure with a different mud weight than the one prevailing at the time where the image log was taken, to for instance assess the overall borehole shape after drilling was finished. But to verify the model the actual MW is of high importance to not falsify the outcome of the verification. For this purpose, it is necessary to have a closer look on the time frame of the image log runs and the lowest mud weight the borehole has experienced since then.

The lowest mud weight is the key mud weight for the stability analysis because the lower the MW the higher the possibility of anticipated breakouts. The breakouts which can be seen on the image log have therefore most likely been formed when the borehole experienced the lowest mud weight prior to the logging run. The caliper log used in the verification step is ideally done at the same mud weight as the image logging to be a good indication for comparison of actual detected and calculated wellbore breakouts.

To depict this an exemplification will be given. The first image run section was logged on the 27<sup>th</sup> of November. On the same day, also the caliper run was executed. The last time that the mud weight has been lowered was the 23<sup>th</sup> of November. From this time schedule which also can be seen in Figure 26 it can be derived that the image log and the

caliper log have seen the same borehole breakouts developed under the lowest mud weight the wellbore has seen prior to the logging runs.

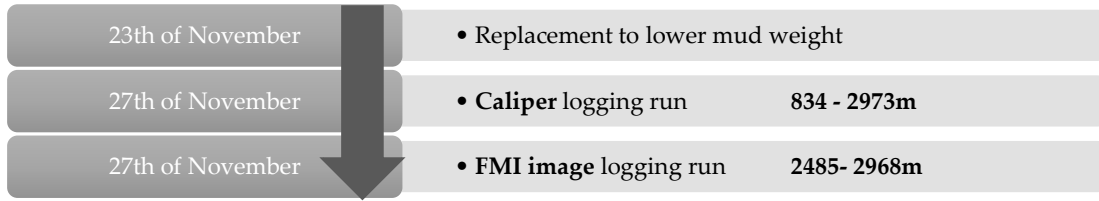


**Figure 26:** Exemplification of the timing of logging running and mud weight alteration.

And exemplification where it is not working to take the lowest mud weight for the whole caliper and image log comparison is shown in Figure 27. The caliper run was executed for the depth interval from 2954 – 4498m MD which includes the depth ranges of two image logging runs, namely the GVR™ logging run and the second FMI™ logging run. After the GVR™ image log was accomplished, the mud weight was lowered which implies that the caliper and also the FMI™ image log experienced a lower mud weight than the GVR™ logging run. Because of that it is not possible to directly compare the breakouts from the GVR™ image run to the caliper run like it was done for the example above and like it can be done for the caliper log and the FMI™ image log in this example. Attention must be paid when verifying the model in the later steps to not misinterpret such sections.

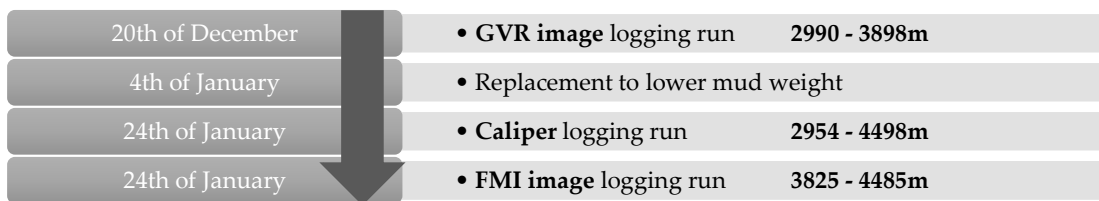


**Figure 27:** Exemplification of the timing of logging running and mud weight alteration.

In the picture below (Figure 28) the mud weight curve (red line) which was composed for the wellbore stability analysis is displayed next to the caliper log (brown line). The distances of the four image logs are also shown in this picture. Like already mentioned, the GVR™ image log has seen a borehole which experienced a different lowest mud weight than the caliper run for this section did. Because the caliper saw a lower mud weight it is possible that more breakouts are visible on the caliper log than on the GVR™ image. For the three FMI™ image logs this is not the case because they found the wellbore in the same condition as the caliper does.

## Verification of the Geomechanical Model (Post-Drill)

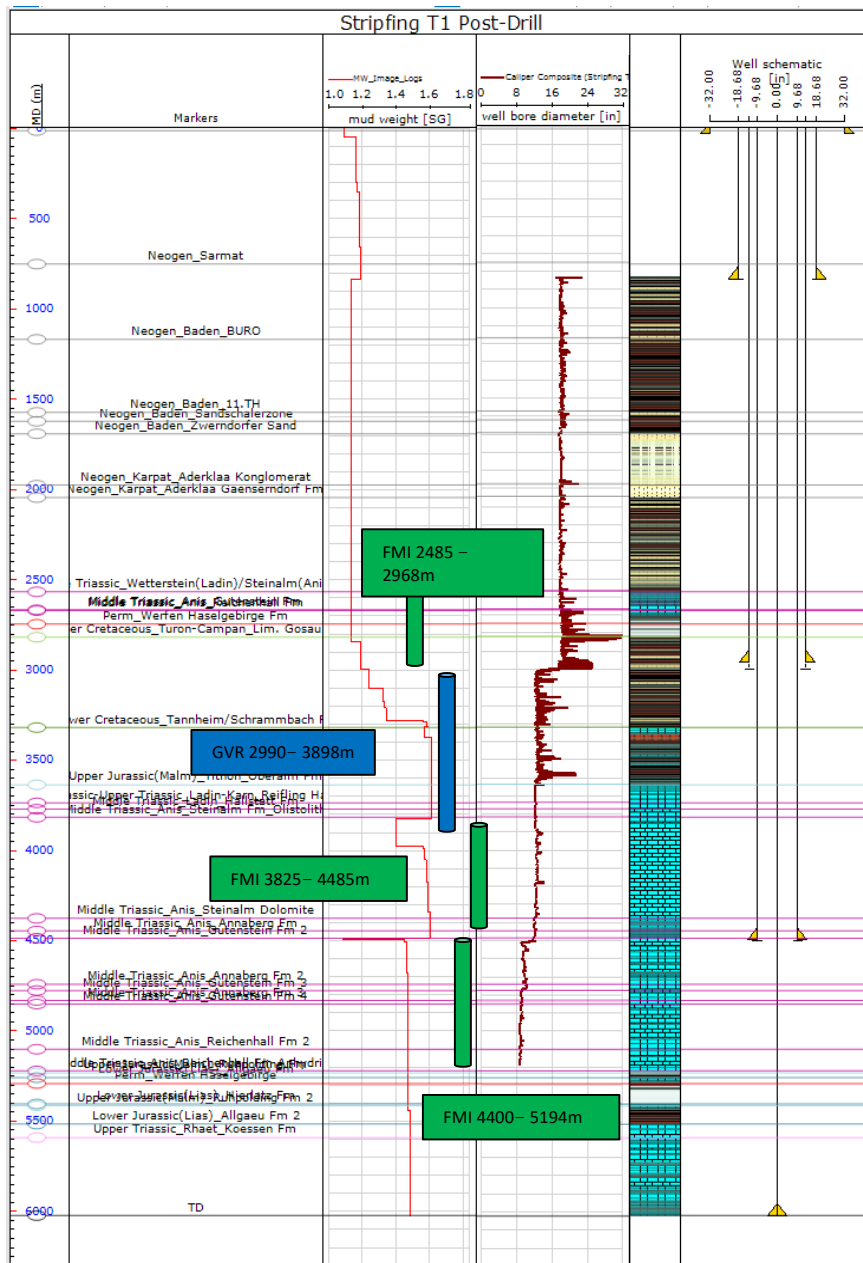


**Figure 28:** Illustration of the lowest mud weight the borehole has experienced before or during logging and which therefore serves as input MW for the BO prediction. The conducted logging runs are added to the MW log (first track). The second track shows the caliper log for the STR T1 well next to the drilled lithology (right side).

After all input parameters for the wellbore stability analysis have been determined (Figure 29), the breakouts which have been picked were exported from the Imager™ program and imported into JewelSuite™ to visualize them on a plot. In Figure 30 the observed breakouts are displayed as blue dots (b) on a scale of 0 – 180°, representing the BO width. The blue asterisks (c) show the breakouts which have been used for stress modeling on the same scale. For the wellbore stability evaluation however it is more useful to do the calculation on the basis of observed breakouts, because these BOs, even if it is not possible to detect their boundaries, are existing and most likely even bigger in size in real than seen on the logs. Log (a) in blue shows the calculated borehole BO width on a scale of 0 – 180°, the blue vertical line at 90° indicates the BO limit for vertical wells. It can be



## Post-Drill Geomechanical Model for the Stripfing T1/T1a Well

seen that the detected BOs fit very good with the calculated BOs and the caliper log (brown line). The breakouts which have been calculated above 2500m MD are not represented on the log as blue dots or asterisks simply because the image logging did not start until 2500m.

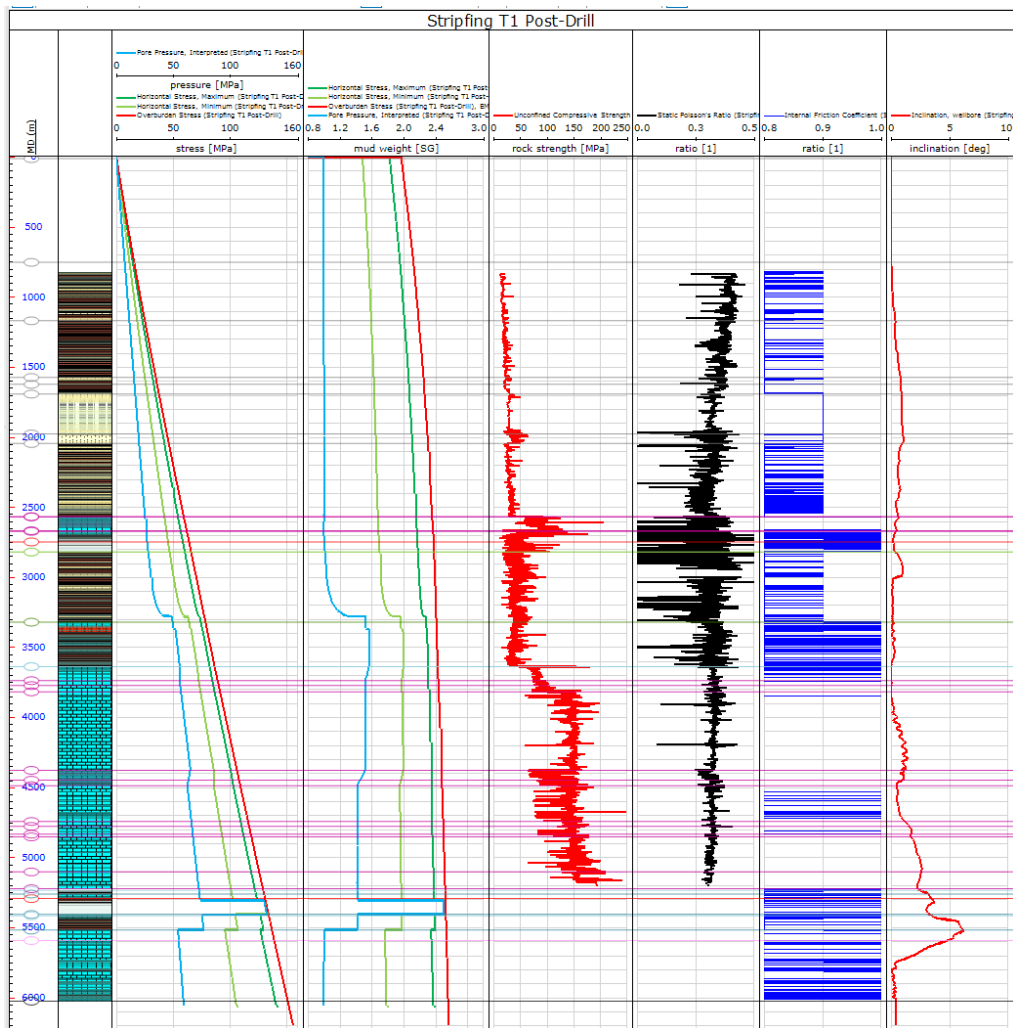


**Figure 29:** Visualization of the input parameters of the wellbore stability calculation. The pore pressure and the stresses (first track [MPa], second track [SG]), as well as rock properties, namely UCS (third track [MPa]), static Poisson's Ratio (fourth track) and internal friction (fifth track) and the wellbore inclination (rightmost track, [deg]) are necessary input parameters for the stability calculation. Additionally, the tensile strength (set to zero), the Biot's Coefficient (set to one) and the failure criterion (similar to the ones used for the  $S_{Hmax}$  determination) have to be determined during this workflow step. The inclination of the borehole together with the specified values for the critical BO widths (vertical and horizontal) are important to calculate the compressional wellbore failure.

## Verification of the Geomechanical Model (Post-Drill)

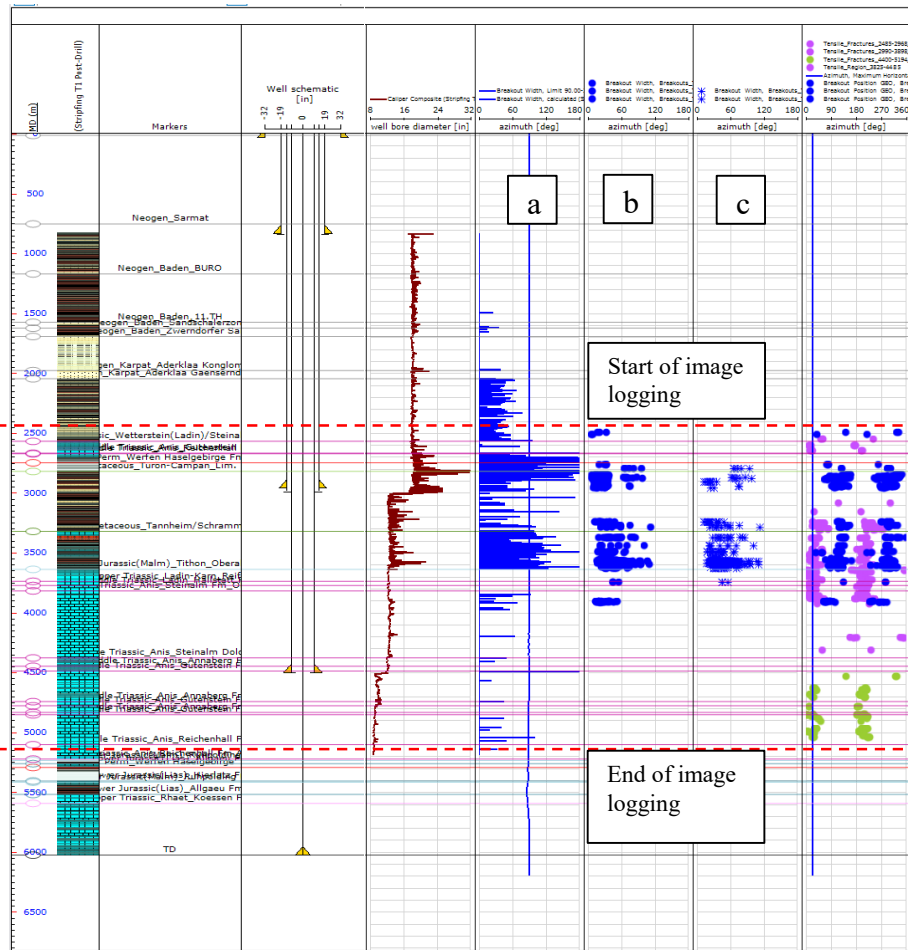


**Figure 30:** Illustration showing the caliper log [in] next to the calculated BO width (a) to compare the measured wellbore failure (BO) with the calculated one.

Track b and c are showing the BO width of all picked BOs and BOs used for  $S_{Hmax}$  magnitude and azimuth determination, respectively. The rightmost track illustrates the picked BOs (blue) and DITFs (purple and green) azimuths next to the  $S_{Hmax}$  azimuth (blue line). Track a, b and c are represented on a 0 - 180° scale, where the rightmost track shows a 0 - 360° scale.

In Figure 30 it can be seen, that the breakouts which have been detected by the caliper logging show a very good conformity with the breakouts which have been calculated by the program. By the use of input parameters like pore pressure, stresses, stress direction, rock properties and lowest mud weight, this failure along the wellbore trajectory was calculated and represents the computed failure along the depth of the wellbore where input logs are available. By comparing the calculated failure with the failure seen on the caliper and the image logs the model can be verified. For this purpose, it is useful to identify regions where significant failures have been detected on the caliper logging runs and assess whether these failures are also visible on the calculated failure log and whether the width of the failures show a good match. If these failures are not matching to a satisfying extend, the pore pressure or the UCS equations must be adapted. Due to the fact that the rock strength is the most uncertain parameter it was decided to change this input value first. For this model, it was tried to keep the proven equations for the UCS determination which have already been used in the pre-drill model and to reach a good match without severe changes. For the purpose of adding sequences of different strength,

it is necessary to insert a new zonation at the depth where the UCS should be changed. Therefore, a copy of the existing rock was produced where all rock properties were kept constant, except the equation for the UCS. In Table 12 the used formulas for the UCS calculations, which are exclusively taken from the pre-drill model, can be seen. Eventually just a short section of a stronger limestone had to be added within the second Middle Triassic sequence (at 3850m MD) which was realized by using the limestone formula multiplied by 1.4. Additionally, an equation to describe the anhydrite section, which was not predicted in the pre-drill model, had to be added. However, for this very short sequence of anhydrite lithology (approximately 50m) starting at 2745m MD, no additional formula was introduced but the limestone/dolomite equation with a rock strength reducing factor of 0.7 was used. This was done because it was not worth the additional effort to find an appropriate published equation for an anhydrite lithology suitable for this geological region for such a short section of lithology. Furthermore, the Permian Werfen formations consist of a mixture of different rock types like anhydrite, claystone and halite (most likely dissolved in water based mud) for the first occurrence and additional limestone for the second occurrence at 5500m MD. For the second occurrence of Permian anhydrite at a depth below 5500m MD, no logging data would have been available anymore to get input data for the UCS determination, albeit it is not proven whether this formation has a stable matrix providing a rock strength or whether the matrix is used to be salt which is not providing a noticeable rock strength at this pressure and temperature conditions.

On the other hand, considerable compressional failures which can be seen on the calculated failure curve should be as well compared to the caliper log. If these failures cannot be detected on the caliper curve, it is likely that the rock strength is underestimated in this region or that the pore pressure which was predicted is too high and by this, breakouts have been calculated which are not existing in reality. Like it was done before, the adaption of the parameters will be necessary to align the calculated and the detected wellbore failure.

In the case of the STR T1 geomechanical model, the comparison of the failures showed a very good match which required just minor changes to represent a sufficient model. This convincing match of the observed and calculated breakouts could be achieved by a good interpretation of the pore pressure and stresses and the unconfined compressive strength. Pore pressure and UCS values have been adapted to reach an as good as required conformity. Overall, the verification of the built model was satisfying.

## 4.8 Evaluation of Data Received from Sidetrack Drilling Occurrence

Another potential source of information to enhance the quality of the STR T1 post-drill model was the sidetrack well, which has been drilled after the stuck pipe event occurred at a depth of 6022m MD and it could not be managed to drill ahead. The procedure to build the model for the sidetrack of the STR T1 well was equivalent to the one for the main hole. GR, sonic and shear slowness logs have been available for the sidetrack section hence all feasible workflow steps were accomplished according to the main hole procedure. In Figure 31 it is visible that the overlapping lithology of the sidetrack (left) and the main hole (right) are nearly identical. This makes it possible to reason that findings which are potentially gained from the sidetrack evaluation will also be valid for the model of the main hole and that it is possible to utilize several input information and findings,

## Evaluation of Data Received from Sidetrack Drilling Occurrence

like density logs, pore pressure and stresses ( $S_v$ ,  $S_{hmin}$ ,  $S_{Hmax}$ ) which originate from the STR T1 wellbore to accomplish the STR T1a model workflow steps. Assumptions and equations for the calculations and determinations of the rock properties were as well taken from the STR T1 post-drill model. It was reported that a leak-off test was performed at a depth of 4496m MD. The plot of the pressure vs. volume readings of the LOT performed in the sidetrack section can be seen in Figure 22. Like already stated in chapter 4.5 which describes the minimum horizontal stress determination of the main hole, the pressure drops which can be detected on the plot are results of the repeated stopping of the pumps, without a leak-off taken place. Hence no useful information for another minimum horizontal stress calibration point can be received from this test. Also, a further confirmation of the maximum horizontal stress and the stress azimuth was not possible with the data collected for the sidetrack well, because the for this analysis necessary image logging was not conducted for this section.

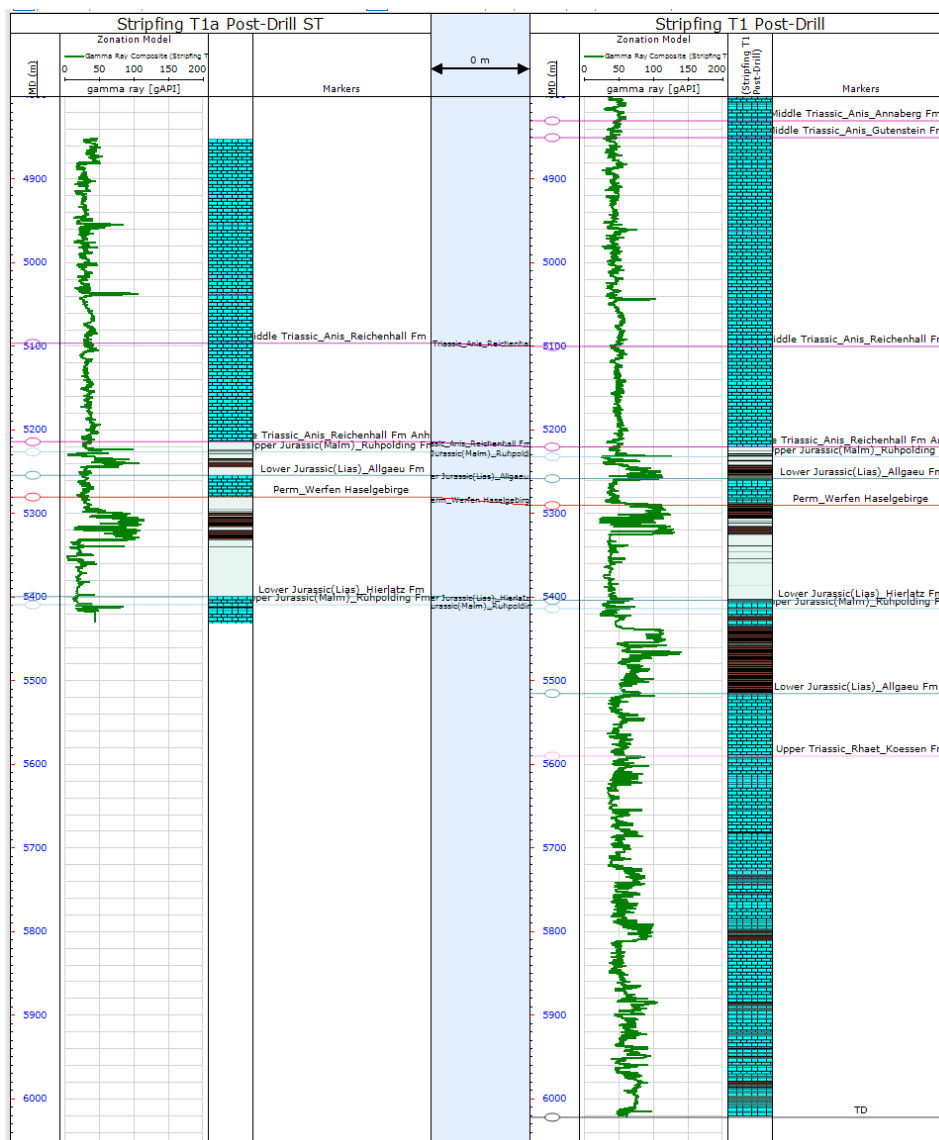


**Figure 31:** Comparison of the sidetrack (left) and the main hole (right) lithology.

The last step of the model workflow for the sidetrack wellbore, namely the verification, was done with the help of the caliper logging data. Due to the fact that no image logging was conducted, the caliper log together with the drilling experience were the only source

## Post-Drill Geomechanical Model for the Stripfing T1/T1a Well

of information to verify the STR T1a model. The caliper log showed an in-gauge hole which could be expected in this Middle Triassic carbonate formations because this was also visible on the image and caliper logs of the main hole in this depth range of the wellbore. Equivalent to the main hole, the caliper log was terminated above 5200m MD, so no further verification of the calculated breakouts was feasible below this depth. The drilling experience (Figure 32) showed tight holes and stuck pipe in the anhydrite section, where the stuck pipe was later the reason to terminate the drilling operation. Frequent reaming was required during this section due to the attempt to free the drill string. However, no extraordinary drilling events occurred which would deliver any additional information to enhance the accuracy of the model.

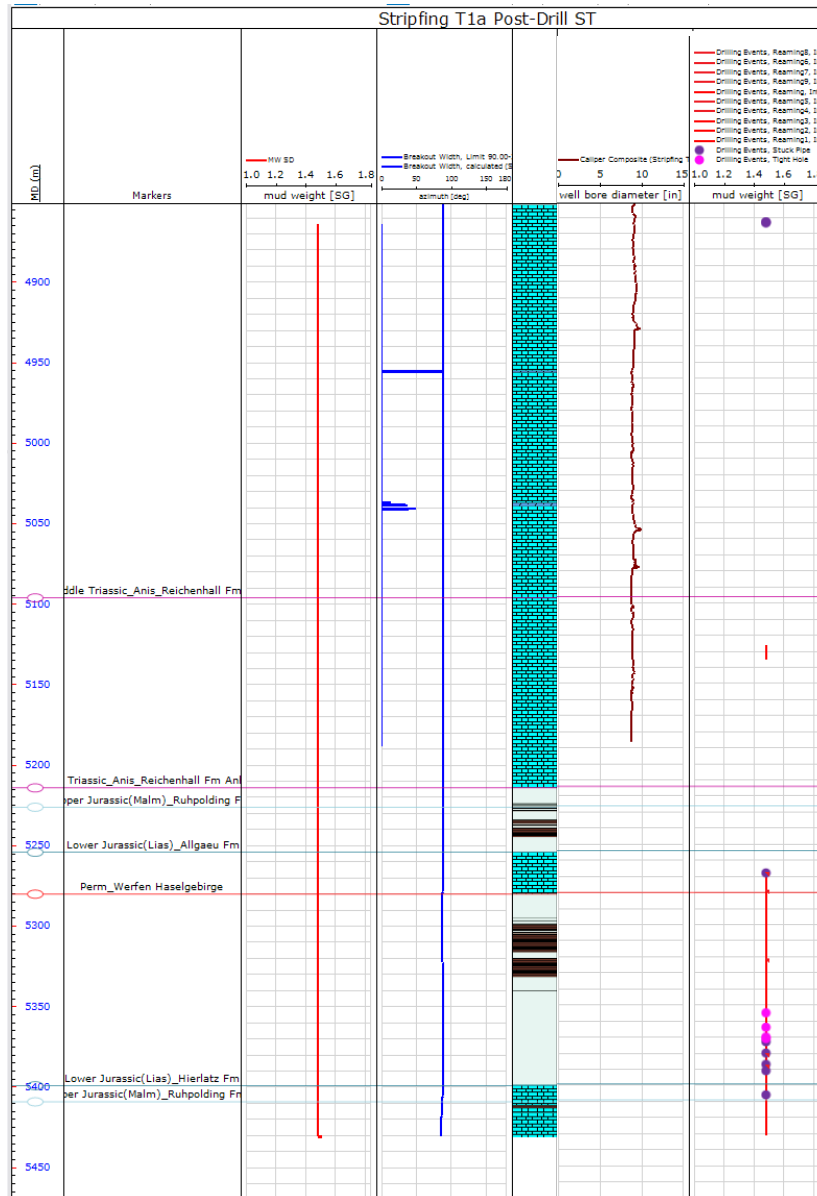


**Figure 32:** Illustration showing mud weight [SG], calculated BO width and BO width limit (0 - 180° scale), caliper log [in] and drilling events (from left to right) for the sidetrack of the STR T1.

## Evaluation of Data Received from Sidetrack Drilling Occurrence

Since the logging of the sidetrack was terminated at the same depth as the one for the main hole, it was tried to collect information about the formations below 5200m MD from other offset wells of the STR T1 wellbore. For this reason, it was of high importance to make sure that the offset wells drilled the same formations at a comparable depth and that no geological feature, like an impermeable fault, separates the formations leading to different properties which would make the comparison invalid. For this purpose, it is advisable to consult a geologist who is familiar with the geological setting of the different wellbores.

The analysis of the formations drilled by the offset wells showed that the Tallesbrunn S1, the Tallesbrunn T1, the Zwerndorf T1 and the Gänserndorf Übertief 3/3a wells perforated parts of the Jurassic formations (TAL S1, TAL T1 and ZW T1) as well as the Upper Triassic Kössen formation (GUET 3/3a) which were found in the STR T1/T1a well below 5200 m MD, at a comparable depth. Compressional slowness, resistivity and spontaneous potential logs were available for these wells, except the Gänserndorf Übertief 3, and were planned to be integrated into the model and depth stretched to the STR T1/T1a formations. The formations which could have been useful to enhance the model have been Upper, Middle and Lower Jurassic which were partly drilled by the three named offset wells. Due to the lack of logging data for the Upper Triassic Kössen formation, no data for the verification of the last section of the Stripfing wellbore could be gained.

The quality check and analysis of the digitalized logging data unfortunately did not show the required outcome. Some of the data was sorted out after the QC because of not replicable data, the remaining logs were inserted into the model and depth stretched to the Jurassic formations of the STR T1 well, but a verification enhancing result could not be found.

The fact that the evaluation of the sidetrack as well as the attempt to include depth stretched offset well logs for the sections where logging information was missing did not add value to the verification of the model, reflects the statement of the beginning - building a model means collecting lots of information and data from different departments and trying to extract the relevant information to construct a consistent model which verifies in the end and at the same time taking the quality and the meaningfulness of the data into consideration to not include inappropriate data which would falsify the analysis.

# Chapter 5 Discussion

## 5.1 Comparison of Pre- and Post-Drill Model

The objectives of this thesis, stated at the outset of this work, include the update of the geomechanical pre-drill model for the Stripfing T1 wellbore. This pre-drill model has not been done in-house but was developed by colleagues from Baker Hughes. All information about the pre-drill model which has been used during the completion of this thesis was taken from the model report (Zheng, Schulze, and Blumenthal 2012) or from the model itself. An update of a pre-existing model is of high importance because the assumptions which have been made during the pre-drill model workflow and the equations which have been used can be confirmed, improved or replaced to develop a conclusive model which verifies after all workflow steps have been conducted. The improvement of such a model enhances the determination of the pore pressure, stress magnitudes and stress direction. This can be done by directly optimizing the parameters (e.g. enhancing the pore pressure prediction by measurements of the pore pressure) or by optimizing input values for the determination of the parameters (e.g. enhancing the correlation of logging results to UCS by laboratory core measurements and by this decreasing the uncertainty of this important input parameter for maximum horizontal stress determination). If the assumptions and equations of the pre- and post-drill model are kept equal like it has been the case for this model update, the conclusiveness of the used assumptions and calculations can be proven with input parameters originating from real drilling and logging results. For this purpose, the updated model is built according to the pre-drill model and the verification of the post-drill model is done by the comparison of the predicted and real wellbore failure. If the compressional wellbore failures match to a reasonable extend, the model can be supposed to be conclusive.

In this section, the comparison of the pre- and post-drill model is shown, including the comparison of the input data, utilized methods to determine model parameters and the outcomes of the workflow steps. Differences of calculated or determined parameters arising from new input data or input data of higher quality are pointed out and the methods which could be used because of the higher extend of input data are named. In the following explanation, the order of the compared parameters equals the order of the parameters determined from the consecutive workflow steps to build a geomechanical model. This facilitates the understanding of the determined successive parameters which are often dependent on the previously calculated ones.

### 5.1.1 Data Acquisition and Quality Check (Comparison)

Figure 5 can be helpful to get a quick overview of the model building workflow steps. Like it can be seen in this flowchart, the model building starts with data acquisition and quality check of the data. This first step is the basis for all geomechanical models and no fundamental differences should be present for this workflow steps. All available data should be screened, quality checked, analyzed, processed and imported into the program. The only difference which arises during this step and as well emerges during the other workflow steps is the amount and the quality of the delivered data. Keeping in mind that a pre-drill model represents a synthetic wellbore with information taken from several offset wells, it is obvious that the pre-drill model accesses a huge amount of data but just

## Comparison of Pre- and Post-Drill Model

a selected proportion of this data is valid for the specific wellbore. Until the measurements of the drilled wellbore are available there is no evidence that the depth stretched logging values of the pre-drill model are representing the prevailing conditions. The post-drill model accesses logging measurements for the dedicated wellbore of state-of-the-art quality which mostly deliver data of better quality and quantity representing the wellbore surrounding.

For the Stripfing T1 pre-drill model data from seven offset wells, namely Tallesbrunn 40, Tallesbrunn S1, Zwerndorf T1, Strasshof T5, Tallesbrunn T1, Tallesbrunn 6 and Stripfing 1, has been used. The first four wells act as key offset wells, whereas the Perchtoldsdorf 1 wellbore was used to represent the Aderklaa/Gänserndorf formation and the Strasshof T5 wellbore represented the Hauptdolomit which has not been reached by any other of the offset wells. For the workflow steps where no data was available, the GEM Schönkirchen was used as reference since it shows similar geological characteristics in the Vienna Basin.

### 5.1.2 Lithology Estimation (Comparison)

Building the lithology plot for a pre-drill model requires offset well data of wellbores which drilled through the expected formations to generate a gamma ray log along a synthetic wellbore. These formations are showing an average thickness determined from the offset well stratigraphy information and adding up to a fictive true depth of this synthetic wellbore.

For the post-drill model, the gamma ray log is available representing the prevailing lithology of the borehole. By the use of the GR log, the petrophysical interpretation and the cutting analysis of the geologists, the lithology curve was built according to the workflow described in section 3.2. The lithology plots for the pre- and post-drill model of the STR T1 well can be seen in Figure 14 and Figure 33. The first notable difference is the much greater depth of the post-drill model with a TVD of 6020m in comparison to 4655m for the pre-drill model. Comparing the two lithology models it can be seen, that the lithology is nearly identical to the forecasted one (pre-drill model) until the Jurassic Malm-Lias formation, at approximately 3650m MD, and differ significantly below. In the stratigraphic table of the pre-drill model (Table 15) it is visible that the expected sequence of formations starts with the Neogene formations (Vienna Basin unit), followed by Middle Triassic, Upper Cretaceous, Jurassic and Upper Triassic formations which form the Calcareous Alps unit. The Vienna Basin unit of the post-drill model showed nearly the same depths and comparable lithology and formation subdivisions. However, below the top of the Jurassic Malm-Lias formation the stratigraphy differs noticeably from the forecasted one. The reason for this is a unique geological incident which could not be determined clearly. Like it has already been discussed in Chapter 2, a salient structure was visible on the seismic image and several options to explain this structure have been worked out. At the present time, two possible explanations for this special stratigraphy are existing, namely the occurrence of the Middle Triassic body as a result of the overthrusting of the Tirolic nappe by the Juvavic nappe (body represents individual nappe or thrust sheet) or resulting from an olistolith slipping into an inverted Jurassic basin (Strauss 2015 and Knoop 2015). Having a closer look on the stratigraphy of the post-drill model, it is visible that the Middle Triassic sequence starting directly below the Upper Jurassic formation at approximately 3750m MD, is followed by another Upper and Lower Jurassic sequence, which allows to draw the conclusion that the Middle Triassic sequence



is a special local occurrence within the prevailing regional stratigraphy which appears similar to the one described in the pre-drill model. Another evidence for that is the presence of the Upper Triassic Kössen formation which was the last formation that has been drilled in the STR T1 project. It is believed that below this Upper Triassic Kössen formation the Upper Triassic Hauptdolomit will follow like it was predicted in the pre-drill model. In summary it can be said, that the difference in stratigraphy and lithology below 3650m MD originates from a not expected sequence of formations which was assumed to be unusual in this geological region.

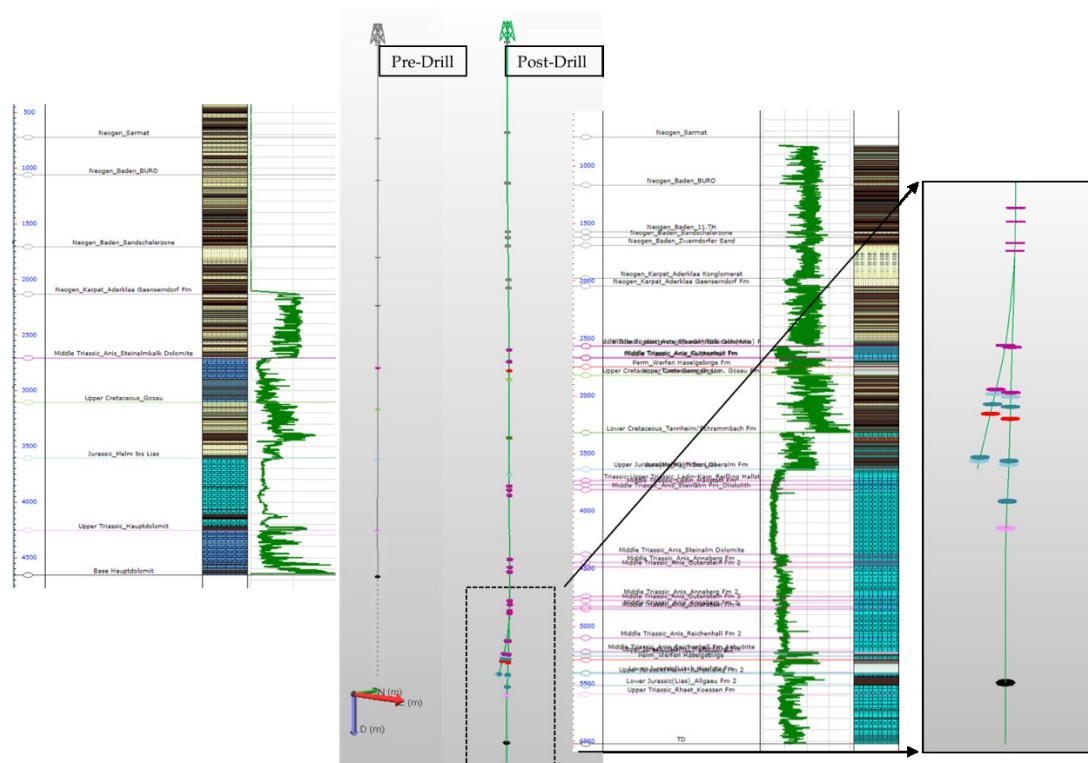


**Figure 33:** Comparison of the pre- (left) and post-drill (right) model stratigraphy, lithology and gamma ray log.

### 5.1.3 Vertical Stress Determination (Comparison)

The workflow how the vertical stress for geomechanical models can be determined was already described in chapter 3.3. This method works equally for pre- and post-drill models. For the pre-drill model, density data for some of the offset wells and compressional sonic data for most of them was available. This compressional sonic data was used to calculate the pseudo density curves by applying formation dependent equations from the Schönkirchen GEM. Above the Aderklaa Konglomerat a trend line was used to represent the density in these shallow formations. From all this information, a composite overburden density curve was built and used as input log for the overburden stress determination. The procedure applied to determine the overburden stress for the post-drill model was equal to the one for the pre-drill model. Density, pseudo density from compressional sonic and a trend line curve have been used to calculate the overburden stress. The formation dependent equations and the derived equation for the trend line curve have been borrowed from the pre-drill model and therefore also depend on the Schönkirchen GEM.

## Comparison of Pre- and Post-Drill Model

In Figure 34 the overburden density (green) and the resulting vertical stress (red and purple) for the pre- and post-drill model are illustrated. The density across the Vienna Basin unit of the pre-drill model varies between 2.00-2.47 g/cm<sup>3</sup>. The density at surface in the post-drill model equals the one for the pre-drill model, namely 2.00 g/cm<sup>3</sup>, however the maximum density across the Vienna Basin unit is about 10% higher and shows a value of 2.68 g/cm<sup>3</sup>. Across the Calcareous Alps unit, the densities for pre-and post-drill model are quite similar and show values between 2.35-2.82 g/cm<sup>3</sup> and 2.38-2.78 g/cm<sup>3</sup>, respectively. The magnitude of the overburden stress gradient for both models increase from 2.00 SG at surface to 2.51 SG at true depth.

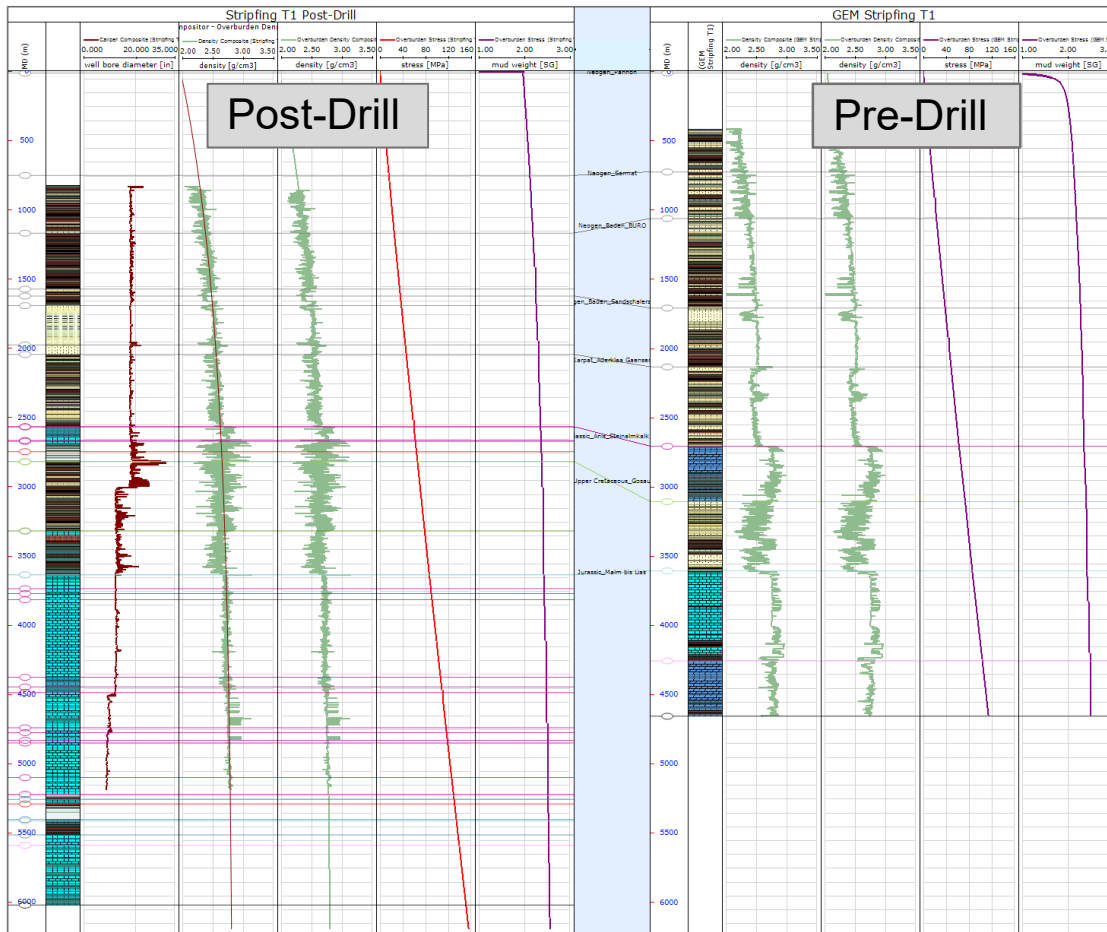


**Figure 34:** Comparison of overburden density (green) and resulting overburden stress (red and purple; in MPa on the left and SG on the right) for pre- and post-drill model.

### 5.1.4 Pore Pressure Prediction (Comparison)

The next step of the model workflow as well as for the comparison of the both models is the pore pressure prediction. In this step, the procedure differs a little more than it has been the case for the overburden stress determination, because the method how the pore pressure is determined for the post-drill model requires logging data which has not been available for the pre-drill model offset wells.

The pore pressure determination of the pre-drill model was accomplished by building pore pressure models for the key offset wells and modeling the pressure for the STR T1 wellbore by the help of the assumptions made from the pore pressure models of these wells. The offset well pore pressure models were created from reservoir pressure

measurements (OHT, CHT) and drilling events which constrain the pore pressure. In Figure 35 the different reference points for the constraint of the pre-drill pore pressure can be seen. The prominent pressure increase in the Cretaceous Gosau and Jurassic Malm-Lias formation is evidenced by the reported influxes experienced in the ZWE T1 and the connection gas occurrences in the TAL S1 wellbore.

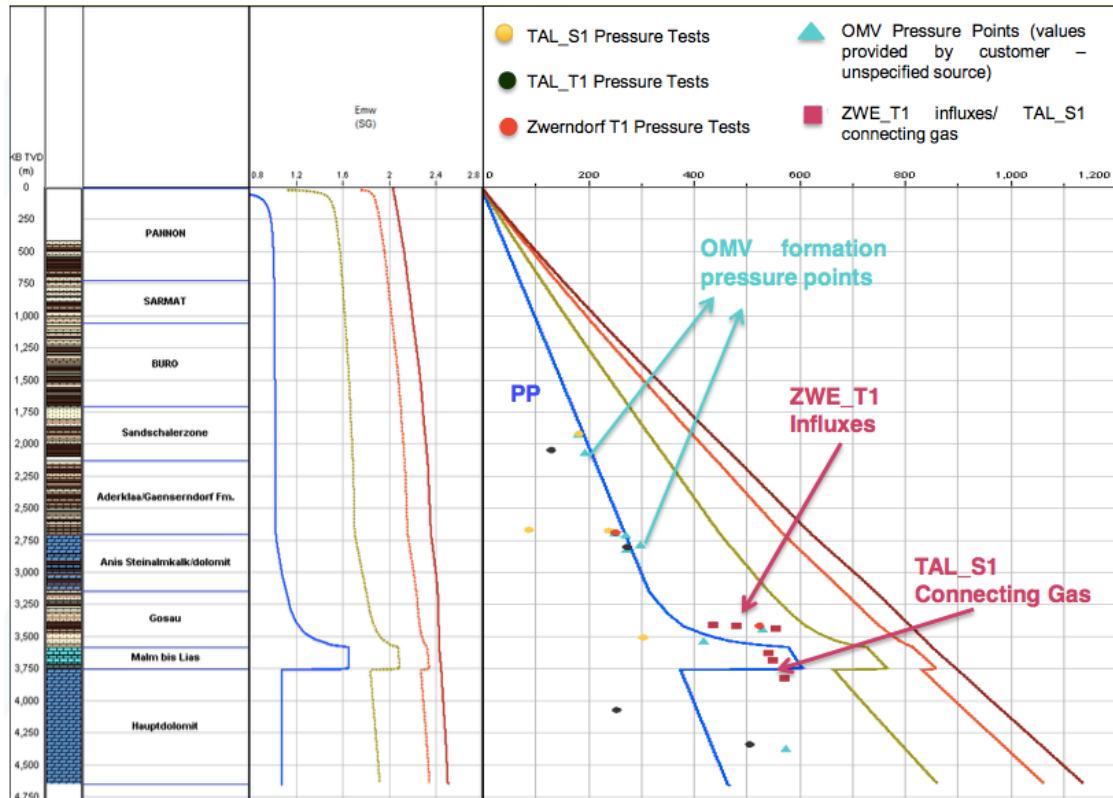


**Figure 35:** Summary of events and measurements used to constrain the pore pressure of the pre-drill model.

This plot is taken from the pre-drill model report (Zheng, Schulze, and Blumenthal 2012).

For the generation of the post-drill pore pressure curve, these sources of information (pressure measurements, drilling events) are also of great importance and should be used if available. In the case of the STR T1 wellbore, pressure measurements were not conducted as of this writing. However other sources of information were available to constrain the pore pressure, like drilling events, kill mud weight calculations and general assumptions in the well explored region of the Vienna Basin. For the geomechanical model of the already drilled well, logging measurements were conducted and the resulting data was used to apply the pore pressure prediction by Eaton's Method and normal compaction trend (see 3.4 and 4.4). However, the drilling events, drilling MW, KMWs and general assumptions were a more reliable source of information, because the PPP from Eaton's Method and NCT shows widespread calculated pore pressure curves for the different input logs, namely density, resistivity and sonic (see Figure 17).

Figure 36 below shows the comparison of the pre- and post-drill pore pressure curves. Both models show a hydrostatic pore pressure until the top of the Upper Cretaceous Gosau formation and a pressure build-up within this formation. The highest pore pressure was forecasted in the Jurassic Malm-Lias formation with 1.65 SG but was discovered in the Lower Cretaceous Tannheim/Schrambach formation (on top of the Jurassic sequence)

## Comparison of Pre- and Post-Drill Model

with a calculated pressure below the forecasted one, at a value of 1.57 SG (KMW calculation). The pressure trend for the pre-drill model shows a pressure drop right below the Jurassic Malm-Lias formation and assumes the pore pressure to be hydrostatic in the Triassic Hauptdolomit like it was indicated by the offset wellbore Strasshof T5. For the post-drill model the pressure drop was determined to take place stepwise. The evidence for that are different pressure points evaluated from well control events which are indicating that the pressure is dropping back first to 1.52 SG in the Upper Jurassic Oberalm formation, secondly to 1.42 SG across the Middle Triassic Steinalm Dolomite-Annaberg formation and finally to hydrostatic most likely in the Lower Jurassic Allgäu formation (see 4.4).

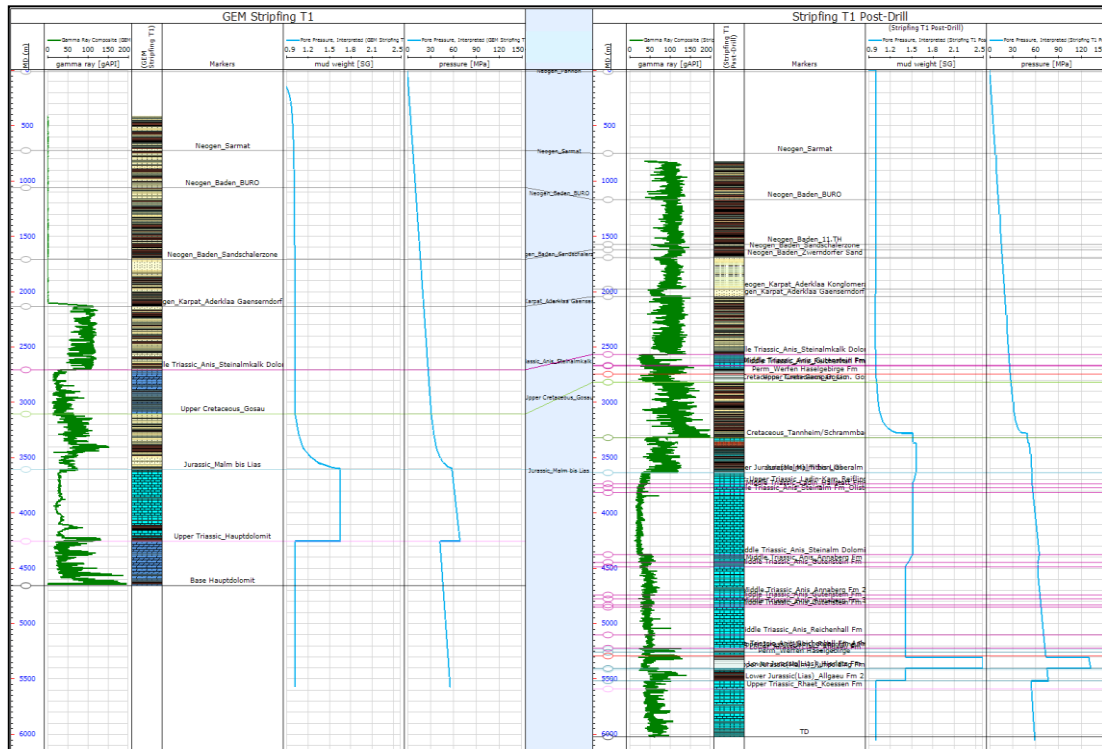


**Figure 36:** Comparison of the pre- and post-drill model pore pressure determination. The left part of the picture illustrates the pre- and the right part the post-drill model. The gamma ray logs can be seen in green to the left of the lithology. The pore pressure curves are shown in blue, where the left track is in SG units and the right track in MPa units.

### 5.1.5 Minimum Horizontal Stress Determination (Comparison)

For the minimum horizontal stress evaluation, results from LOTs, XLOTs and hydraulic fracturing tests are used to determine calibration points for the  $S_{hmin}$  calculation using the Effective Stress Method. This is applicable for the pre- as well as the post-drill model workflow.

For both models, LOTs for the minimum horizontal stress determination were available. The pre-drill model however is depended on LOT data from offset wells. In the case of the pre-drill model for the STR T1 wellbore, three LOTs have been reported, but neither pressure vs. volume data nor a fracture closure pressure analysis was available. In addition to this missing data, the LOTs have been conducted at very shallow depth, hence the

reliability is reasonably shortened. These facts are the reason why it was decided to take the effective stress ratio of the Schönkirchen GEM instead of basing the minimum horizontal stress determination on unreliable data.

For the post-drill model, three LOTs were conducted in the main well and another one was performed in the sidetrack of the wellbore, approximately at the same depth as the deepest one of the main hole tests. Pressure vs. volume data was available for this recently drilled well, even though the conduct of the fracture pressure analyses was not possible simply because the LOTs have been terminated too early. The LOT data was analyzed (see 3.5 and 4.5) to receive calibration data for the Effective Stress Method. In Figure 37 the ESR calibration points (for the post-drill model only), the ESR trend lines as well as the determined pore pressure (blue), minimum (light green) and maximum (dark green) horizontal stresses and the overburden stress (red) are visible. As stated above, for the pre-drill model the ESRs of the Schönkirchen GEM have been used to calculate the  $S_{Hmin}$  and  $S_{Hmax}$ . For the post-drill model the ESR points were calculated from the LOP values and an ESR trend line was applied. The ESR for the pre-drill model holds a constant value of 0.51 from surface to the base of the Gänserndorf formation (at approximately 2700m MD) and from there on increases to 0.59 at TD. For the post-drill model the analysis yields an ESR of 0.5 from surface to TD without any evidence that the ESR should increase with depth. The first LOP and therefore the first ESR point seems to high (reduced reliability at shallow depth) and the third one seems to low (reduced reliability of LOT conducted in fractured carbonate). The LOT of the sidetrack well could not deliver any data to enhance the analysis because it was also conducted in fractured carbonate and did not even reach the LOP.

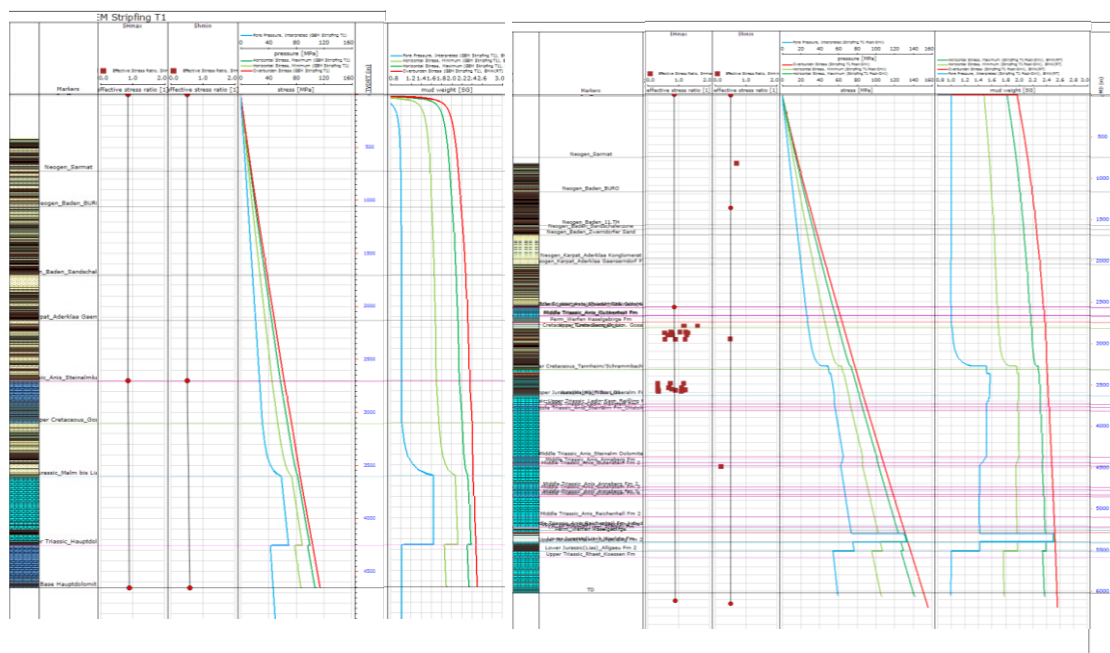


**Figure 37:** Comparison of the maximum and minimum ESR points with trend lines and resulting max. and min. horizontal stresses for pre- (left) and post-drill (right) model. The first tracks show the max. ESR points with applied trend line, the second tracks the minimum ones with trend line, respectively. The stress plots show pore pressure (blue),  $S_{Hmin}$  (light green),  $S_{Hmax}$  (dark green) and  $S_v$  (red) in MPa (left) and SG (right) units, respectively.



The trend of the calculated minimum horizontal stress can be seen in Figure 37 above. The highest  $S_{hmin}$  gradients can be detected at the same depth interval where the highest pore pressures occur and reach magnitudes of 2.09 SG for the pre- and 2.00 SG for the post-drill model. The decrease of the minimum horizontal stress takes place at the top of the Upper Triassic Hauptdolomit to 1.92 SG for the pre-drill model and stepwise to 1.98 SG (Upper Jurassic Oberalm fm.), 1.95 SG (Middle Triassic Steinalm Dolomite-Annaberg fm.) and finally to 1.78 SG (Lower Jurassic Allgäu fm.) for the post-drill model, similarly to the pore pressure drops for both models.

### 5.1.6 Rock Properties Evaluation (Comparison)

Rock properties including Poisson's Ratio, Young's Modulus, coefficient of internal friction, rock strength and Biot's Coefficient are generally predicted by utilizing logging data and laboratory tests which are used to calibrate these log-derived properties.

The assumptions and equations to calculate the rock properties are the same for the pre- and post-drill model. Neither for the pre- nor for the post-drill model lab tests have been available. This lack of calibration results in the use of partly calibrated correlations from the Schönkirchen GEM to calculate the rock strength from compressional sonic logs. The second rock strength parameter, namely the coefficient of internal friction, was not calculated from sonic logs but rock dependent constants were used like already mentioned in the previous chapters (e.g. 3.6.2). The elastic parameters (Young's Modulus and Poisson's Ratio) were determined from compressional, shear and density logs. All of these logs were available for the post-drill model. For the pre-drill model however, the shear sonic log was calculated from the compressional sonic log (equations see Table 16). The determination of the static Young's Modulus and Poisson's Ratio from the dynamic ones which were determined from logging data was done by applying published equations from Lacy (1997) for the Young's Modulus (Table 11) and by assuming the static Poisson's Ratio to equal the dynamic one because no published equations were available and no laboratory measurements which would allow for a calibration have been conducted. The last parameter among the rock properties is called the Biot's Coefficient, which is assumed to be one for all lithology types of the pre- as well as the post-drill model. A summary of all rock property logs for the pre- and the post-drill model can be found in the Appendix (Figure 53).

### 5.1.7 Maximum Horizontal Stress Azimuth Determination (Comparison)

The method to determine the stress direction of the post-drill model depends on the analysis of image logging data together with the appropriate caliper logging data. Due to the lack of image and oriented caliper logging data for the offset wells of the pre-drill model the procedure which has been applied for the post-drill model could not be deployed for the forecasting model. For the offset well Tallesbrunn 40, image logging runs have been conducted and analyzed by Fronterra. However, no stress induced wellbore failure was detected and a reinterpretation was impossible due to bad quality of the logging data. Hence the maximum horizontal stress direction was assumed from previous studies and GEMs (Perchtoldsdorf, Schönkirchen and Erdpress) and was defined to be  $165^\circ \pm 20^\circ$ . For the post-drill model the image analysis (see 3.7) showed wellbore breakouts and drilling induced tensile fractures of high confidence which enabled the determination of the maximum horizontal stress direction with a satisfying accuracy and

yields a value of 25°. This magnitude deviates slightly from the forecasted one, but the orientation stays nearly the same, namely almost exactly north-south.

## 5.1.8 Maximum Horizontal Stress Determination (Comparison)

The determination of the maximum horizontal stress requires the identification of horizontal stress calibration points which are used as input values for the Effective Stress Method (like it has been the case for  $S_{\text{hmin}}$  determination). For the post-drill model this calibration points could be gathered by stress polygon analyses, where again the image analysis is an important prerequisite. In chapter 3.8 and 4.6 the stress polygon analyses and the input parameters for this workflow are described in detail.

Due to the fact that no image analysis was possible for the pre-drill model, again the ESR of the Schönkirchen GEM was used to calculate the horizontal stress. This ESR trend line, which can be seen in Figure 37, has a magnitude of 0.85 from surface to the base of the Gänserndorf formation at approximately 2700m MD and increases to 0.89 at true depth. For the post-drill model the ESR trend line which was applied to the ESR points showed a magnitude of 0.86 from surface to TD and was not assumed to increase (similarly to the ESR of the minimum horizontal stress). The calculation of the magnitude of the maximum horizontal stress showed a  $S_{\text{Hmax}}$  value of 1.92 SG at 500m, increasing to 2.34 SG at TD for the pre-drill model forecast. The resulting values of the post-drill model are very close to the forecasted ones and increase from 1.91 SG at 500m to 2.37 SG at TD. Both models show a minor drop back of the  $S_{\text{Hmax}}$  gradient where the overpressure decreases to hydrostatic pressure.

## 5.1.9 Verification of the Geomechanical Model (Comparison)

By completing the determination of the pore pressure, the stresses and the stress direction, the geomechanical model is built and the wellbore stability analysis can be conducted to verify the model. This workflow step is done by comparing the predicted wellbore failure to the observed wellbore failure considering the geomechanical model, the well path and the mud weight. The procedure how this mud weight should be determined is explained in chapter 3.10. The usage of the correct mud weight is of high importance because mud weights during caliper and image logging which are not compatible with each other or with the MW used as input value for the failure calculation, can result in misinterpretation of the failure. This practice allows for a better comparison of the present wellbore failure, detected on the image and the caliper logs, with the calculated failure.

Another method to verify a geomechanical model is the comparison of predicted wellbore failure to reported drilling experiences for wellbores where no image logging was conducted or as addition to the comparison of predicted and observed wellbore failure. For the pre-drill model offset wells, like mentioned several times before, no image logging data was available which could have been used to detect the wellbore failure of these wells. This implies that a verification for this model is just possible by comparing the predicted wellbore failure with the reported drilling experience. For this reason, the pre-drill model is applied for the key offset wells (TAL 40, TAL S1, ZWE T1 and STRA T5) and the reported drilling experiences are used to verify the models. For the post-drill

model much more information, like image logs, oriented caliper logs and detailed daily drilling report are available which make the verification much easier and more precise. In Figure 11-Figure 13 and Figure 30 the summary of the drilling events identified from the DDRs and the calculated and observed wellbore failures of the STR T1 post-drill model, respectively, are represented. From this verification, it can be concluded that the post-drill model with the assumptions and calculations adopted from the pre-drill model, and updated with data gathered during drilling and logging, is a conclusive and approved model which can be used in the future to predict pressures and stresses as well as drilling parameters and troublesome geological formations and furthermore delivers helpful information for other disciplines like completion and production.

### 5.1.10 Recommendations – Fulfilled or still suggested

At the outset of this chapter it was mentioned, that the information about the pre-drill model was taken from the report prepared by the persons in charge from the Baker Hughes company. In this report, recommendations have been suggested which should be carried out to enhance the quality of the model. After creating the post-drill model, it was possible to remove some of the items from the list, but some of them could still not be fulfilled and remain as important recommendations for future updates of the geomechanical model with newly gained data from drilled wells or laboratory tests. The list below shows the recommendations made after the pre-drill model was built and indicates whether they have been implemented (✓) or whether they are still unaccomplished (✗) and remain as advices for further applications. Although some of the recommendations have been fulfilled during drilling the STR T1 wellbore and analyzing the gathered data, all of these tasks remain as objectives for subsequent drilling operations to further improve the model by integrating data from wells drilled in the future.

- ✓ • Test and update the model with data from newly drilled wells
  - Constrain the minimum horizontal stress by running LOT, XLOT, frac tests
    - ✓ ○ Record pressure vs. volume data in small time steps
    - ✗ ○ Conduct an extended LOT to determine FCPs
- ✗ • Conduct UCS measurements in laboratory
  - To develop a better correlation between logs and rock strength
  - To calibrate static elastic properties (Young's Modulus, Poisson's Ratio) to dynamic ones
  - To better constrain the  $S_{Hmax}$  magnitude
- ✓ • Log compressional and shear sonic together with density
  - To improve the relationship of compressional sonic and density log for pseudo-density estimation
  - For better understanding of elastic moduli
- ✗ • Conduct pressure measurements to improve pore pressure profile especially in overpressured regions
- ✓ • Complete image and multi-arm caliper logs for  $S_{Hmax}$  magnitude and direction evaluation
- ✓ • Summarize the drilling experience of the newly drilled well to test the model

Having a closer look on the listed information above, it can be seen, that several of the recommendation have been accomplished. The enhancement of the quality of the model is mostly reached by the collection of new data gained by conducting log measurements



and leak-off tests and by analyzing the drilling experience of the drilled wellbore. The list below shows the model parameters of the STR T1 well which showed an improvement of quality after the recommendations have been fulfilled.

- Vertical stress and dynamic parameters calculated from density and sonic logs
- Pore pressure constrained by drilling experience
- Minimum horizontal stress determined by LOT analyses
- Maximum horizontal stress direction determined from image log analyses
- Maximum horizontal stress constrained by stress polygon analyses

However, a greater enhancement of the quality of the model could have been reached if the planning team would have drawn from further resources. These further resources for the STR T1 wellbore include pore pressure measurements to improve the pressure prediction especially in overpressured regions, rock laboratory measurements to better define the rock strength and determine relationships for the conversion of dynamic to static rock properties and the conduct of extended leak-off tests to evaluate the fracture closure pressure as a more precise measurement for the minimum horizontal stress determination. Furthermore, the more precise defined rock strength would enhance the quality of the maximum horizontal stress because so far, the UCS is the most uncertain input parameter for the determination of the maximum horizontal stress.

## 5.2 Evaluation of Potential Reasons for the Overpressure Occurrence Encountered During Drilling the STR T1/T1a Wellbore

In the course of this thesis it was mentioned already several times, that a significant part of the drilled formations is holding an overpressure with a maximum magnitude of 1.57 SG. The occurrence of this over hydrostatic pressure was forecasted and did not appear unexpected. However, the reason for the overpressure is unresolved so far. To identify a feasible reason for the over hydrostatic pressure predicted and discovered for the STR T1 well, a brief overview of overpressure generation mechanisms is given below. On the basis of this overview, the possible mechanisms for the elevated pressure should be ascertained. Figure 38 shows an overview plot of the different causes of overpressures referring to a paper published by Grauls (1999) and a thesis published by Atashbari (2016). This structure should be the basis for the determination of the overpressure, where it should be tried to find the overpressure mechanism by successively striking out the improbable ones.

## Evaluation of Potential Reasons for the Overpressure Occurrence Encountered During Drilling the STR T1/T1a Wellbore

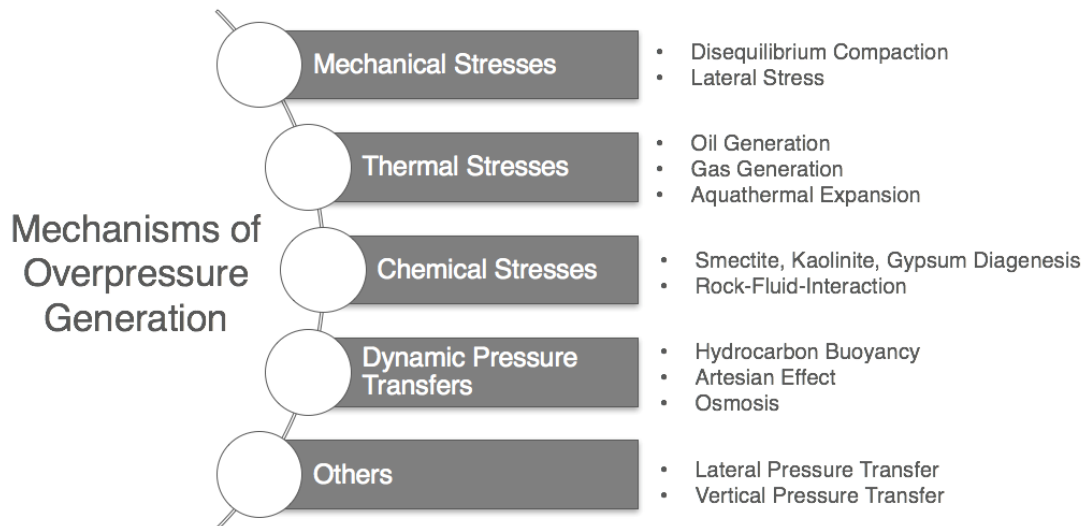


**Figure 38:** Mechanisms of overpressure generation, cf. Grauls 1999 and Atashbari 2016.

Before starting with this evaluation, it is important to recap the pore pressure situation, and more specifically the overpressure situation of the STR T1 wellbore (see e.g. Figure 36). The pressure build-up starts at the base of the Upper Cretaceous Gosau formation and is assumed to look like a pressure ramp. A second minor pressure increase takes place in the Lower Cretaceous Tannheim/Schrambach formation directly below the Gosau formation and represents the highest pore pressure gradient of the entire wellbore depth. Below this maximum pore pressure point, the pressure gradient decreases over the entire length of the Lower Cretaceous Tannheim/Schrambach, the Upper Jurassic and the complete not expected Middle Triassic carbonate and dolomite formations. Below these sequence of formations, the pressure gradient decreases to hydrostatic most likely below the top of the Lower Jurassic Allgäu formation. Augmenting this pore pressure description with the post-drill concept of the stratigraphy of the STR T1 wellbore, developed by the responsible geologists (Table 5), it can be assumed that the sequence of Middle Triassic formations is sealed by the overlying Lower Cretaceous Tannheim/Schrambach and the underlying Jurassic formations. The fact that the major part of the overpressure holding formations (except for the Upper Cretaceous Gosau formation) shows a carbonate or dolomite lithology complicates the prediction of the pressure. Like explained in chapter 3.4, the PPP with NCT is a valid tool for shale intervals, but is not the correct approach for the use in carbonate formations. Using velocity data to find anomalies in the porosity and by this predicting the pore pressure is the traditional PPP method used for shales, but cannot predict the pore pressure of a carbonate section on a basin-scale because the porosity of the carbonates is not only controlled by stress but varies also as a result of other processes like fracturing, dissolution, diagenesis or varying depositional environment (Green, Edwards, and O'Connor 2016). In the paper published by Green, Edwards, and O'Connor (2016), an interesting approach is described, stating that different porosity types in carbonates leading to different overpressure scenarios. In more detail this means, carbonates with sufficient interconnected porosity form good reservoirs which show the same overpressure from the base to the top of a sequence or can also lead to an increased pressure at the crest due to pressure transfer from down-dip. The other porosity type represents carbonates with tight porosity which form good seals and often act as pressure

transition zones or define pressure ramps with elevated pressure gradients (Green, Edwards, and O'Connor 2016).

Recollecting the shape of the pressure curve, this different porosity types can be identified on the pressure plot. The major part of the Lower Cretaceous Tannheim/Schrambach, the Upper Jurassic and the complete Middle Triassic sequence represent the carbonate with sufficient interconnected porosity where the pressure increases towards the crest of this section. The section above this one (upper part of the Lower Cretaceous Tannheim/Schrambach and lower part of the Upper Cretaceous Gosau formation) however could represent a carbonate section with tight porosity which would form a pressure transition zone for the overpressure of the sequences below. Like explained before, these section shows a ramping up pressure and the lithology is described as a mixture of carbonates, marls and shales which would also correspond to the description of the tight carbonates in the paper of Green, Edwards, and O'Connor (2016).

Coming back to the overview of the different overpressure mechanisms (Figure 38), a short description of the different sources of overpressure will help to eliminate not adequate processes of enhanced pressure for the case of the STR T1 well.

*Mechanical Stresses* as the reason for overpressure generation are separated in vertical stress related (NF stress regime) due to disequilibrium compaction and lateral stress related (SS and RF stress regime) where the overpressure is caused by stress imposed on a sediment body in areas of thrusting or faulting (compressional tectonics). Both processes can be excluded from the list of possible solutions for the enhanced pressure detected during drilling the STR T1 well. Vertical and lateral mechanical stresses are potential sources of overpressure in clastic rocks, where overpressure is generated as result of extended load on sufficiently sealed pore volume by overburden stress during burial (fluid cannot be expelled fast enough) or where the enhanced pressure is caused by the reduction in porosity and permeability due to lateral compaction. The reduction of the porosity in carbonate formations however, cannot be modeled by mechanical compaction but is mostly governed by chemical compaction (Croizé 2010). For overpressured carbonates, like they were found in the STR T1 wellbore, these processes do not play a major role, even if for example compressional tectonics are common processes which occurred in the region of the Northern Calcareous Alps.

*Thermal Stresses*, in Figure 38 subdivided into oil generation, gas generation and aquathermal expansion, outlines another group of overpressure mechanisms which can be excluded from the list of possible sources. Hydrocarbon shows for the STR T1 well are assumed to be too minor to generate a sufficiently high overpressure by kerogen or oil cracking. Aquathermal expansion, even if the prerequisites are fulfilled (fluid in sediments is buried and heated and a sealing is existing), is not representing a high overpressure magnitude creating mechanism (Swarbrick, Osborne, and Yardley 2004).

*Chemical Stresses*, or in detail smectite, kaolinite and gypsum diagenesis and rock fluid interactions can lead to volumetric increase of free water or a pore space reduction, respectively which leads to a generation of overpressure in sand-shale dominated environments (Swarbrick, Osborne, and Yardley 2004). Diagenesis as well as rock fluid interaction can alter the pore space of carbonates as well, leading to an enhancement (recrystallization, solution enlargement, dissolution and replacement) and/or a reduction (recrystallization, replacement and cementation) of the porosity (Green, Edwards, and

## Evaluation of Potential Reasons for the Overpressure Occurrence Encountered During Drilling the STR T1/T1a Wellbore

O'Connor 2016). The complexity of chemical stresses as mechanism for overpressure generation makes an assessment of the influence of this process on the overpressure of the STR T1 well very difficult and cannot be evaluated.

*Hydrocarbon Buoyancy* describes an overpressure mechanism due to the difference in densities between water and hydrocarbons (HC). The pressure gradients of the HCs show a steeper slope and yield a fluid pressure greater than the hydrostatic one which would be obtained at the same depth without HC accumulation. Due to insufficient hydrocarbon occurrence, this mechanism can also be excluded.

Other processes of overpressure generation like enhanced pressure due to *hydraulic head/artesian effect* (overpressure due to hydraulic continuity to subsurface where the water level is located at a higher elevation) and *osmosis* (pressure increase due to osmotic flow to equalize naturally occurring salinity differences) can be excluded because it is unlikely that there is a hydrodynamic connection to an outcrop at surface and because for the STR T1 case it is not plausible that such a high salinity difference and a very good membrane efficiency is prevailing leading to high overpressure occurrence, respectively.

*Dynamical Pressure Transfers* combine lateral (Darcy flow in tilted reservoir units) and vertical (flow through pathways formed by open faults or hydrofracturing) hydraulic flow of hydrocarbons leading to overpressure at the highest structural closure and within fault or fracture networks, respectively (Grauls 1999). The explanation by Grauls (1999) can be completed by the assumption that pressure transfer is also valid for sections which do not represent reservoir units and where no HCs but pore water is in place to generate overpressure. In case an overpressured compartment is connected with a shallower one with hydrostatic pressure or less overpressure, a vertical pressure transfer can occur until equilibrium pressure is reached, where the transfer of the pressure depends on the permeability of the pathways (e.g. faults and fractures) and the timing (Grauls and Cassagnol 1993). Lateral pressure transfer on the other hand occurs within interconnected porous rock, where a surrounding seal is required. The pressure diffuses along the tilted aquifer with high permeability until a pressure gradient parallel to the hydrostatic one is reached (Traugott and Heppard 1997). The outcome of this kind of pressure transfer is an enhanced pore pressure at the top of the structure. The lateral pressure transfer, also known as centroid buoyancy concept shows different pressure gradients for the surrounding sealing (shale) and the permeable compartment which are in equilibrium at the centroid point (Atashbari 2016). Above this centroid point, the pressure in the permeable compartment is higher than the pressure of the surrounding shale, whereas the pressure below the centroid point is lower than the one which can be found in the sealing formation. The pressure gradient of the permeable system develops parallel to the hydrostatic pressure gradient (pressure decreases at hydrostatic rate with decreasing depth) because the fluids are in communication and equilibrate (Atashbari 2016). The gradient of the surrounding seal however develops parallel to the overpressure gradient (pressure decreases at overburden rate with decreasing depth). In case hydrocarbons are present within the overpressured compartment, the pressure difference at the top of the structure will be even higher. Traugott (1997) additionally stated that it is possible to lose circulation into the seal when the mud pumps are turned on and get inflow from the wellbore with pumps are turned off, in case the drilled well intersects the structure exactly at the top.

Concluding it can be said, that it is possible that the pore pressure of shale is much different from the pore pressure of the nearby permeable compartment due to the impermeability of the shale and the overpressure redistribution in the porous and permeable adjacent compartment along a gradient parallel to the hydrostatic one. To predict such an overpressure, even in non-shale units with large vertical amplitudes, the centroid buoyancy concept can be used (Traugott and Heppard, n.d.).

The reason why the concept of dynamic pressure transfers, especially lateral pressure transfer, is explained in more detail is the consideration of the possibility that the enhanced pore pressure of the STR T1 wellbore originates from lateral pressure transfer.

The JewelSuite™ program allows for the interpretation of the centroid buoyancy effect by an optional workflow step, called “centroid buoyancy”, where the centroid effect as well as the buoyancy effect can be calculated. For this purpose, the top and base of the assumed structure, the top and the base of the wellbore intersecting the structure, the fluid types, densities and the height of the fluid columns have to be inserted into the program to generate a pore pressure curve which accounts for the centroid buoyancy effect. In the case of the Stripfing T1 well it was assumed that the wellbore intersects the structure exactly at the top and the base and therefore the depth values for top of structure and top of intersect as well as base of structure and base of intersect are the same. The values assumed for the top and base of the structure and intersect of the STR T1 wellbore are 3371m MD (top) and 5515m MD (base). 3371m MD was estimated as top of the structure because it shows the highest pore pressure and by this indicating the top of the overpressured compartment. The base was assumed to be equal to the top of the Allgäu formation where the pressure most likely drops back to hydrostatic. The pore fluid is assumed to be water with a density of 1.03 g/cm<sup>3</sup>, however if hydrocarbons would be present, also HC fluid columns and densities can be added. Additionally, a calibration point for the centroid pore pressure must be added (EMW and depth). In this case the calibration point at 3371m MD with a density of 1.57 SG calculated as kill mud weight for a well control event during drilling, was inserted. These input values are used by the program to calculate a pore pressure curve within the specified depth range accounting for the centroid effect. In Figure 39 the determined centroid pore pressure curve (dark blue) is shown next to the predicted pore pressure curve (light blue) generated during the PPP workflow (see chapter 4.4). Comparing both pressure curves, it can be seen that the centroid pore pressure curve within the overpressured compartment (3371 – 5515m MD) follows nearly the same trend as the predicted pore pressure curve and appears like a smoother version of the already predicted pore pressure. In other words it can be said, that the modeled pore pressure in the overpressured section which was assessed by the help of the KMW calculations shows an almost identical pressure curve like the one calculated by the centroid effect workflow, which makes the lateral pressure transfer a plausible overpressure generation mechanism in the case of the STR T1 wellbore. At this point it is convenient to revisit the statement of Green, Edwards, and O’Connor (2016) mentioned at the outset of this section. They explained in their paper that two different overpressure scenarios are existing for carbonates, depending on their porosity. Carbonates with interconnected porosity will form compartments with equally enhanced pressure from bottom to top or compartments where the overpressure increases from bottom to top like it is the case for the STR T1 wellbore, where the lateral pressure transfer leads to an increased pressure gradient at the top of the structure. The second porosity type represents the very low porosity carbonates which form seals and act as pressure transition zones. These often define pressure ramps with elevated pressure gradients. This

## Evaluation of Potential Reasons for the Overpressure Occurrence Encountered During Drilling the STR T1/T1a Wellbore

description may be an explanation for the overpressured formations above the determined centroid structure, namely the overpressured part of the Upper Cretaceous Gosau formation and the overpressured Lower Cretaceous Tannheim/Schrambach formation above the centroid. The lithology of this depth section is mainly a mixture of shale, marl and carbonate which is consistent with the description of the tight porosity carbonate formations which are able to form sealing formations as transition zones between overpressured structures and normally pressured formations on top, showing a ramping up structure like it can be seen in the STR T1 pressure prediction. Additionally to the pressure trend information, the drilling experience showed immediately consecutive gains and losses in the depth range of the pressure ramp to the top of the overpressured structure which could be the result of the convincing argument of Traugott (1997), who mentioned that it is possible to lose circulation into the seal with turned on mud pumps and get inflows from the formation when the pumps are turned off, in case the wellbore intersects the porous structure exactly at the top.

In summary it can be said, that the overpressure trend within the mostly Middle Triassic sequence could be a consequence of lateral pressure transfer, leading to maximum pressure values at the top of the structure. Above the centroid structure, the pressure transition zone is formed by the upper part of the Lower Cretaceous Tannheim/Schrambach and the lower part of the Upper Cretaceous Gosau formation which generate a pressure ramp with an elevated pressure gradient. The reason for losses and gains within the sealing sequence, which occur immediately after each other could be the intersection of the centroid structure by the wellbore exactly at the top of this structure.

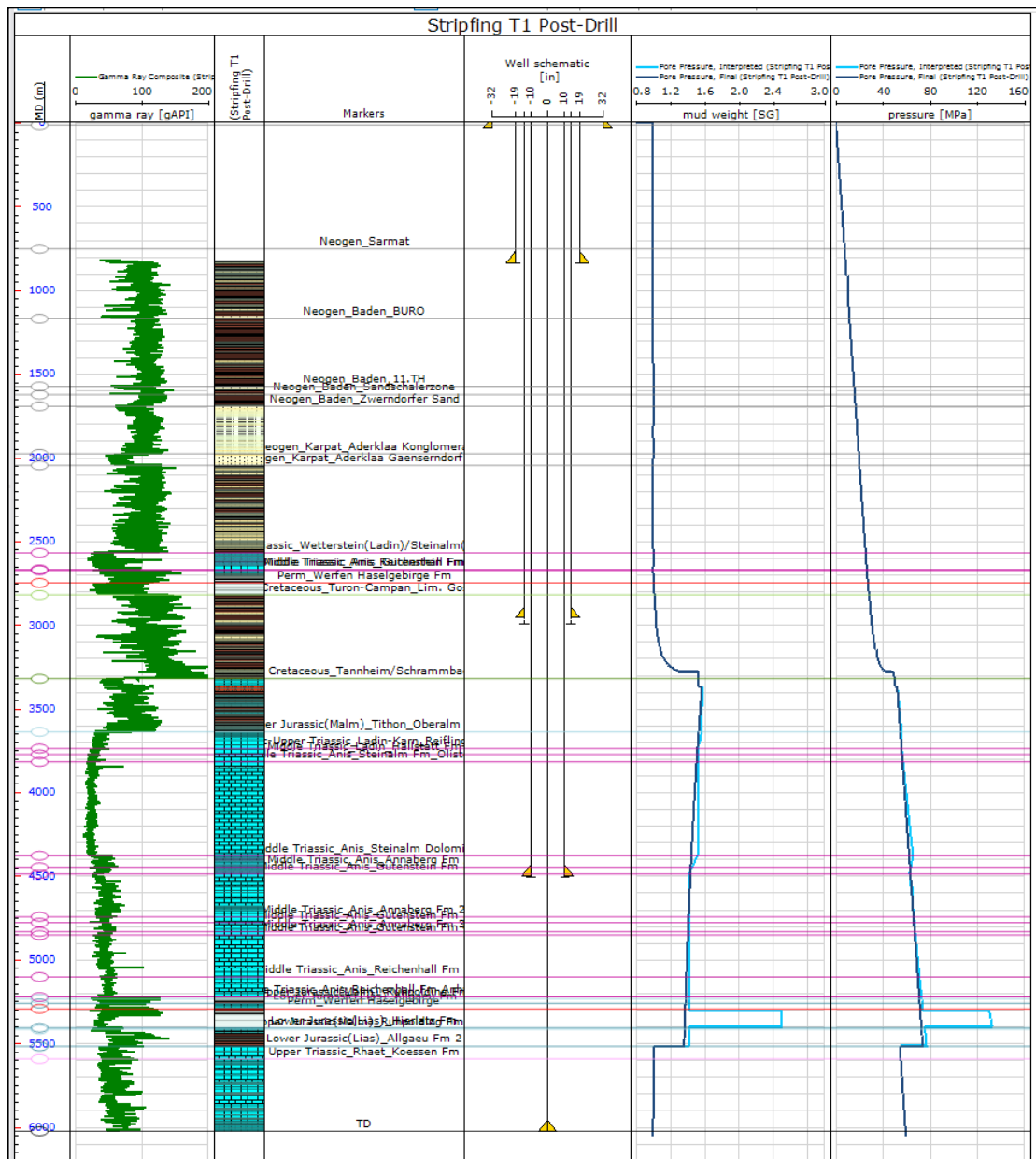


**Figure 39:** Illustration of the pore pressure determined from NCT and Eaton’s Method, using two different approaches to determine the trend in the overpressured section. The light blue pore pressure curve shows the version where the KMWs are used to adjust the pore pressure of the overpressured zone, compared to the pore pressure where the centroid effect is applied to predict the pressure of the overpressured zone (dark blue) from 3371-5515m MD.

## Evaluation of Potential Reasons for the Overpressure Occurrence Encountered During Drilling the STR T1/T1a Wellbore

The explanation how the overpressure of the STR T1 wellbore can show such high values at relatively low depth could be delivered by the explication above. However, the question where the pressure, charging the centroid structure, comes from is still unanswered. Considering the concept of the centroid effect, implying that a tilted porous structure is enclosed within an overpressured sealing formation, allowing the generation of a highly overpressured structure by lateral pressure transfer, raises the question: Which formation surrounding the centroid structure of the STR T1 wellbore is able to represent a sealing, overpressured formation leading to centroid pressures lower than the pressures of the surrounding seal below the centroid point and vice versa above the centroid point. A closer look on the post-drill concept of the stratigraphy (Table 5) and the lithology (e.g. Figure 14) of the STR T1 wellbore indicates whether such a formation is present. As discussed above, the sealing formation from above is represented by the Cretaceous formations on top of the overpressured structure. Below the centroid structure it can be seen, that the Upper Jurassic Ruhpolding formation shows a shale lithology of approximately 100 m height at the bottom of the formation superimposed by a carbonate lithology of smaller extent. The argumentation that this Upper Jurassic Ruhpolding formation is holding an overpressure rather than being hydrostatically pressured is delivered by a drilling event in the Zwerndorf T1 offset well. This wellbore also drilled through the Upper Jurassic Ruhpolding formation, albeit the formation was found at much shallower depth, at approximately 3400m MD. The drilling reports of this offset wellbore offered the opportunity to apply the centroid workflow to this overpressured Ruhpolding formation to undergird the centroid theory as origin of the overpressure occurrence. The information which could be found in the report clarified that there has been a saltwater inflow into the wellbore at 3440m MD (Ruhpolding fm.) while the drilling mud weight yielded a value of 1.51 SG. The well was killed with a mud weight of 1.68 SG to control the saltwater inflow. In case the Ruhpolding formation seen in the STR T1 and the ZW T1 wellbore is continuous, the centroid effect could be an evidence that this formation cannot be hydrostatically pressured. The information which has been used to apply the centroid workflow to the Ruhpolding formation included, like for the centroid workflow before, top and base of structure and intersect, calibration point data and fluid column height and density. As top of the structure and intersect, the top of the Ruhpolding formation in the ZW T1 wellbore (3288m MD) was used. The base of the structure and intersect has been at 5515m MD like for the SR T1 well. The pore fluid was assumed to be water with a density of 1.03 g/cm<sup>3</sup>. The depth of the saltwater inflow has been taken as calibration point, whereas different densities between 1.51 SG (drilling MW) and 1.68 SG (weighted MW) have been tried. In Figure 40 the outcome of this analysis can be seen. The centroid pressure gradient line for the calibration point with the highest density of 1.68 SG (right purple line) shows a too high pressure gradient compared to the one of the STR T1 well (blue). For a density of 1.55 SG at 3440m MD wellbore depth, an adequate centroid pressure gradient was calculated which matches with the one determined for the STR T1 well. This implies that it is possible that the high overpressure seen at relatively shallow depth in the ZW T1 wellbore is caused by a centroid effect and that the theory of the overpressure in the STR T1 well can be supported by this assumption.

The initial source of the overpressure, namely the sealing shale surrounding the porous structure could be the lower part of the Upper Jurassic Ruhpolding formation which shows a 100m thick shale package, together with the sealing Cretaceous formations above the centroid, like stated before. Why however the pressure tight formations around the porous structure are holding an overpressure cannot be assessed in this thesis.



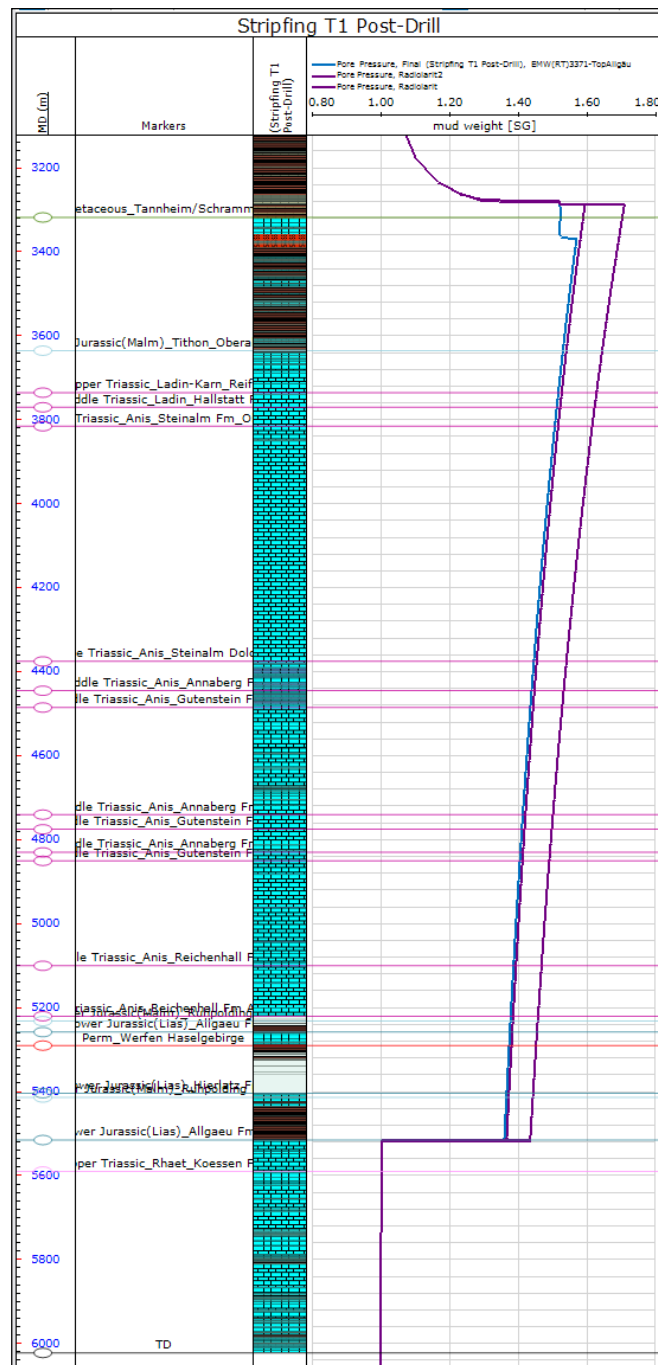


**Figure 40:** Application of the centroid buoyancy workflow to evaluate the overpressure in the Ruhpolding formation of the Zwerndorf T1 wellbore.

The picture shows the overpressured section of the STR T1 well, where the blue curve shows the determined centroid pressure for the STR T1 and the purple curves show the centroid pressures that would result for the input data of the ZW T1 for the top section together with input data of the STR T1 for the base section. The left purple line shows the outcome for a pressure (or MW) of 1.55 SG, the right one shows the resulting curve for a pressure (or MW) of 1.68 SG prevailing in the Ruhpolding formation of the ZW T1 at 3440m MD. The curve calculated for a pressure of 1.55 SG corresponds to the pressure curve of the STR T1 well and would results in the same pressure value at the base of the overpressured section.

## 5.3 Estimation of Leak-Off Test Results as a Method for Minimum Horizontal Stress Determination

The execution and analysis of a leak-off test is a common practice to determine the least principal stress ( $S_3$ ) by a direct measurement of this lowest one of the earth in-situ stresses. The best methods which can be used for the direct measurement of the least principal stress are methods where hydraulic fractures (HFs) at depth are initiated and propagated into undisturbed rock, which makes a  $S_3$  determination feasible. The in-situ stresses in the earth control the orientation and the propagation direction of the hydraulic fractures whereas the stress concentration around the wellbore affects the initiation of these fractures. The HFs open in the direction of the least principal stress (because this is the least energy configuration) and propagate perpendicular to  $S_3$ , in the fracture plane generated by the intermediate ( $S_2$ ) and the highest principal stress ( $S_1$ ). Hydraulic fracturing tests, leak-off tests (LOTs) and extended leak-off tests (XLOTs) are typical tests for the least principal stress determination by a direct measurement at the defined wellbore depth.

Despite that hydraulic fracturing is the more precise method for  $S_3$  determination, the most commonly used ones to evaluate the minimum in-situ stress for a wellbore region are the accomplishment and analysis of LOTs or XLOTs. There is the general opinion that LOTs and XLOTs are similar to the hydraulic fracturing tests and can therefore be used to measure the minimum in-situ stress magnitude. But due to the operational procedure the correctness of the outcome can be shortened. Enever et al. (1996) listed some important statements demonstrating the drawbacks of LOTs and XLOTs compared to HF:

- LOTs/XLOTs are “barefoot” tests which are performed without downhole packers, therefore no defined sealed-off zone is present like it is during HF.
- For long open-hole sections, pre-existing fractures can influence the leak-off test data, because these pre-existing fractures will be re-opened instead of generating new fractures.
- Problems can occur when pressurizing large fluid volumes to pressurize the bottom hole section of a deep well.
- Instead of recording the initiation of a new fracture in the intact rock, artifacts like mud compressibility, casing expansion and leakage of the casing cement can be seen on the pressure plot.

Nevertheless, the conduct of LOTs during drilling is a standard procedure not only to determine the minimum horizontal stress but for example also to test cement integrity or to determine the maximum drilling mud density and because of that became the most common method applied during drilling.

The measurements of the least principal stress, in literature often described as minimum horizontal stress (which is correct for normal and strike-slip faulting regimes, but not for reverse faulting regimes), are indispensable input values for the minimum horizontal stress determination during the geomechanical modeling workflow and moreover the

minimum horizontal stress serves as important input parameter for further modeling steps including maximum horizontal stress determination and wellbore stability analysis. Leak-off tests and extended leak-off tests are executed according to the same procedure, albeit the XLOT is an improved version of the LOT. During the XLOT the complete first pressurization cycle is performed according to schedule or the pressurization cycle is even repeated (could be up to four times). Such repetitions of the tests are done to remedy the tensile strength of the rock and the stress concentration around the borehole which must be overcome during the first LOT cycle.

The following description explains the characteristic of a general XLOT, which pressure values can be extracted for the evaluation of the minimum horizontal stress and where the advantages of such a test, compared to a LOT, are. The procedure of LOTs and XLOTs is a frequently discussed topic in the oil and gas industry, hence the description is tried to be kept as brief as possible to be able to point out the important information for the stress determination.

The typical idealized pressure vs. volume curve for a XLOT can be seen in Figure 41 below. For a better understanding, the used acronyms are briefly explained in Table 14, right below the pressure vs. volume plot.

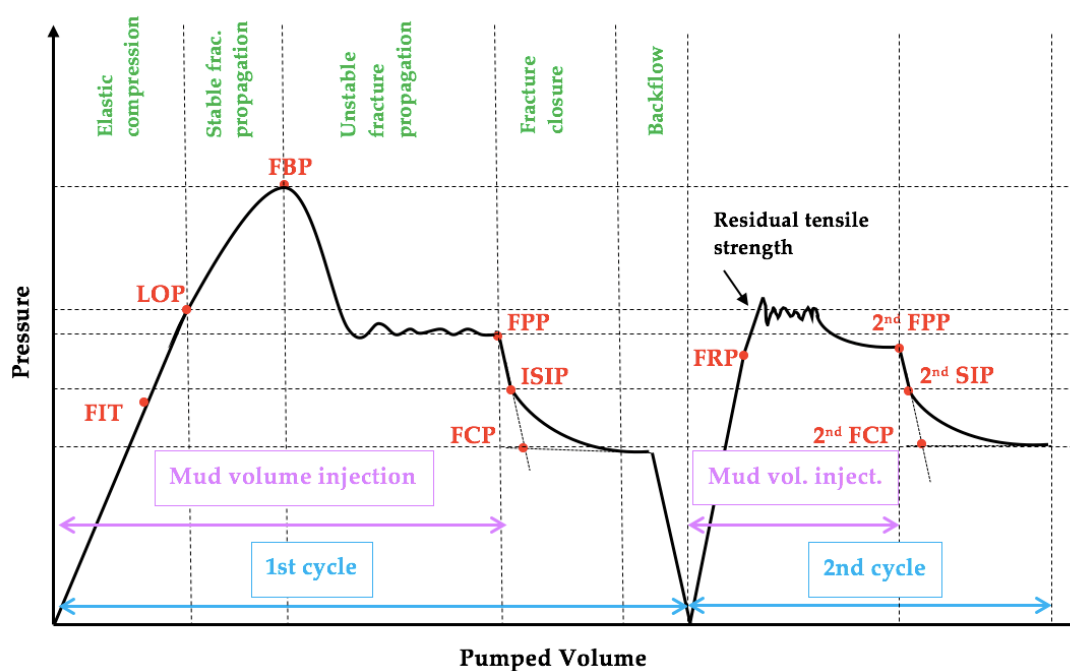


**Figure 41:** Idealized pressure versus volume plot of an extended leak-off test, cf. White, Traugott, and Swarbrick (2002) and von Eberstein et al. (2004).

## Estimation of Leak-Off Test Results as a Method for Minimum Horizontal Stress Determination

<b>FIT</b>	Formation Integrity Test Pressure	Pre-defined pressure which is applied to check whether formation can hold the pressure; no leak-off
<b>LOP</b>	Leak-Off Pressure	Pressure where the fluids starts to flow into the formation (pressure vs. volume curve deviates from linearity)
<b>FBP</b>	Formation Breakdown Pressure	Pressure which is required to initiate a fracture in an intact rock, maximum pressure recorded during LOT
<b>FPP</b>	Fracture Propagation Pressure	Pressure at which the fracture is propagating away from the wellbore
<b>ISIP</b>	Instantaneous Shut-In Pressure	Pressure measurement at point of initial pressure decline after pumps were turned off
<b>FCP</b>	Fracture Closure Pressure	Pressure where fracture has closed after the pumps were stopped (= pressure which is needed to open a fracture, after the fracture has already propagated)
<b>FRP</b>	Fracture Re-Opening Pressure	Pressure at fracture re-opening, therefore no additional tensile strength must be overcome

**Table 14:** Summary of the pressure values which can be obtained from the pressure vs. volume plot analysis of an extended leak-off test.

LOTs as well as XLOTs are pumping pressure tests which are carried out immediately after the casing was set, cemented in place and the shoe track, usually 3m of new formation, was drilled out. There are several reasons why a LOT is performed, like cement integrity testing and mud density determination for the next wellbore section (maximum pressure which can be applied to the borehole without mud loss occurrence). Furthermore, like stated at the outset, by now it is common practice to collect LOT and XLOT data to estimate the magnitude of the least principal in-situ stress.

The casing shoe, which is always the weakest part of the next wellbore section is pressurized by the drilling fluids which is pumped through the drill pipe to the shoe, while

the well is shut-in. The pressure which is present at the casing shoe during this process can be determined by adding the pressure of the static mud column to the obtained surface pressure or directly by downhole pressure measurements.

The drilling fluid is pumped into the borehole to gradually increase the pressure. During this procedure, the fluid undergoes a volumetric compression while the casing string and the surrounding rock experience an elastic expansion. The pressure in the borehole increases linearly with the pumped volume until the leak-off pressure (LOP) is reached (this can be recognized because the pressure vs. volume curve deviates from the linear trend). The size and orientation of the fracture, as well as the magnitude of the LOP depend on the in-situ stresses in the earth. Whereas the magnitude and orientation of the three principal stresses of the in-situ stress field are determined by the tectonic regime, the rock properties, the depth and the pore pressure (Nolen-Hoeksema 2017). Moreover, the existence of pre-existing fractures will have an influence on the magnitude of the least principal stress (Li, Lorwongngam, and Roegiers 2009).

For most of the simple LOTs the procedure is terminated at the point where the leak-off pressure is reached. If the testing procedure however is terminated even before the LOP is reached, a formation integrity test (FIT) was conducted. In this case, the pressure was not sufficient to exceed the least principal stress or to initiate a fracture into the wellbore wall. The pressure value determined from the FIT, also called a limit test, is not delivering useful information for the  $S_3$  evaluation. During such tests, the wellbore is pressurized to a pre-designed pressure magnitude to test whether the shoe and the formation can hold this pressure. There is no aim to break the formation during a FIT and therefore the stress determination cannot be based on a formation integrity test.

For an extended LOT pumping is continued after the leak-off took place. Several further pressure values can be determined from this pressure vs. volume curve for an improved stress estimation. The next prominent pressure point which is approached during an extended leak-off test is the formation breakdown pressure (FBP). At this point the pressure reaches its maximum value during the XLOT procedure. At the peak pressure, a fracture is initiated in the surrounding rock of the well and pumping is continued to propagate the fracture away from the well into undisturbed rock. This propagation of the fracture is described as unstable propagation. Immediately after the FBP was reached, the pressure starts decreasing because the fluid flow from the wellbore into the formation occurs faster than the fluid can be supplied by the pump (Zoback 2010).

After a certain amount of time and continuous pumping at a constant rate, the pressure starts to approach to a constant level. This pressure at which the fracture is propagating away from the wellbore is called the fracture propagation pressure (FPP). The FPP is very close to the least principal stress, hence the FPP magnitude should also be close to the one of the LOP, if near-wellbore resistance is absent, meaning that the flow rate and the viscosity are low enough (e.g. Hickman and Zoback 1983). This correlation between FPP and LOP is the reason why LOTs are often terminated after the leak-off was determined, instead of performing a complete LOT cycle.

After reaching this point the pumps are turned off and the pressure starts to decrease, first with a linear relationship and afterwards the pressure decline starts to flatten. This transition point between linear and not linear decline equals the instantaneous shut-in pressure (ISIP). The ISIP is an even better measurement for the least principal stress than the FPP, because the viscous friction pressure losses vanish after the immediate stop of fluid flow into the well (Haimson and Fairhurst 1967). On the perspective of many scientists the fracture closure pressure (FCP) which can be determined by the use of two

## Estimation of Leak-Off Test Results as a Method for Minimum Horizontal Stress Determination

intersecting tangents or the square root of time method is the most important pressure value which can be obtained by the analysis of the XLOT. This pressure point is the result of the closure of the newly initiated fracture. At this point the remaining fluid pressure and the stress in the formation are in mechanical equilibrium (Lin et al. 2008). The pressure value is simply determined by drawing two intersecting tangents into the pressure vs. volume curve like it is shown in Figure 41 or by plotting the pressure as a function of the square root of time and detecting the point where the curve is deviating from its linear behavior. Zoback (2010) argued that LOP, FPP and ISIP have nearly the same magnitude, when the test is carefully conducted at constant and low flow rates (approximately 200 liter/min) and with a low viscosity fluid such as water or thin oil. If the fluid however is a viscous fluid, the FPP increases due to friction pressure losses and the fracture closure pressure (FCP) would be a better measurement for the least principal stress than the FPP or the ISIP. According to Nolen-Hoeksema (2017), the difference between the FPP and the FCP is called the “net pressure” which consists of the frictional pressure drop and the resistance of the fracture tip to propagation. If the pressure measurements during this test are continuously conducted, a reliable information about the least principal stress magnitude can be gained.

To improve or reinforce the identification of the FCP and the ISIP, a second, third or even a fourth cycle is advisable (the more cycles are chosen the more stable the determined values get). Due to the fact that the fractures have already formed during the first cycle, a re-opening pressure (FRP) can be diagnosed which is approximately in the same pressure range as the FPP for the first cycle. Moreover, the FPP, SIP and FCP of the following cycles are approaching to a steady value, respectively.

It is not just an assumption within the geomechanical department of the OMV that the FCP is the best measurement for the minimum principal stress estimation. Owing to difficulties to determine this FCP value, mainly because the testing is terminated before reaching this pressure point, in practice the LOP measurement is also taken as reference for the  $S_3$  value in case the FCP could not be determined.

The execution and analysis of LOTs seem to be a straightforward procedure. Unfortunately, this is just valid on paper. Not satisfyingly conducted leak-off tests, not consistent LOT procedures and data analyses can be the reason for inconsistent pressure and stress results. Two main questions arise when analyzing LOT data to receive least principal stress values, namely:

*Did the formation show a leak-off, or has a FIT been conducted instead of a LOT?*

In case the leak-off pressure of the formation was reached, the first pressure incline shows a deviation from the linearity while continuously pumping fluid into the wellbore. The pressure value at this point can then be used as a measurement for  $S_3$ , if not, the pressure measurement cannot be taken for least principal stress estimation.

*If an extended leak-off test was conducted, which reliable pressure values are provided?*

If a stable fracture propagation could be obtained, the shut-in pressure or the fracture closure pressure (dependent on the viscosity of the used fluid) will be a good measurement for the least principal stress because the fracture propagation away from the wellbore is clearly visible. If not, the LOP should be the appropriate value of choice.

Even though the least principal stress determination by the application of LOTs is a common practice within OMV, there are several alternative methods to evaluate the magnitude of  $S_3$ . Step rate tests, mini frac tests and micro frac tests are possible other options for the determination of the least principal stress. However, a more detailed description of other methods for stress determination is not part of this thesis. According to Zoback (2010), further information can be found in literature where various techniques for least principal stress determination were reviewed, like: Zoback and Haimson (1982), Baumgärtner and Zoback (1989), Rummel and Hansen (1989), Hayashi and Haimson (1991) and Guo, Morgenstern, and Scott (1993).

If leak-off tests are projected in the well planning phase it should be recommended to perform an extended leak-off test because the additional work and expense is marginal in comparison to the increase in reliability of the values for the stress estimation. Executing a LOT instead of a XLOT has several deficiencies like:

- The possibility that the first cycle which is terminated shortly after the potential LOP has been detected, is not an indication for the far-field stress. The fracture is induced into the plastic zone close to the borehole wall and is not propagating into undisturbed rock where a measurement of the far-field stress should be conducted (Addis et al. 1998).
- The influence of the rock tensile strength on the first cycle of the LOT affects the leak-off pressure measurement but can be remedied by conducting further cycles because at the re-opening of the fracture, no tensile strength of the rock has to be overcome anymore.
- The question whether a single logged pressure value can be valid as input parameter for the stress estimation because it can be problematic to perform a reliable minimum principal stress estimation from a pressure value with noticeable degree of uncertainty serving as minimum horizontal stress calibration point. Furthermore, the execution of multiple XLOT cycles (at least three) delivers more reliable results for the FPP, SIP and FCP because with rerunning cycles they are approaching to a steady value.

Applying the previously described information about LOTs and XLOTs to the minimum horizontal stress determination of the STR T1 wellbore, some of the difficulties and limitations stated above can be found during this workflow step. In Figure 18-Figure 22 the pressure vs. volume plots of the different LOTs of the Stripfing T1 well, including the sidetrack, are visible. Like already mentioned in section 4.5, the minimum horizontal stress determination of the STR T1 well was based on information of three LOTs for the main and one LOT for the sidetrack well. Due to the fact that no XLOT was conducted, the LOPs represent the values which have been used as  $S_{hmin}$  calibration points. For the sidetrack well, the pressure vs. volume curve did not show an indication of a leak-off, which indicates that a FIT instead of a LOT was conducted. Like explained at the outset of this chapter, a FIT cannot be used to determine the least principal stress and because of that no information enhancing the  $S_{hmin}$  determination could be extracted from this test. The determination of the leak-off points from the pressure vs. volume plots of the LOTs of the main well, was done by applying a tangent to the linear pressure increase of the pressure vs. volume tracks. The LOPs were directly read from the plots, at the point where the pressure curve deviates from the applied tangent. The fact that the interpretation of the drilling engineers and the interpretation done during this thesis varies for two of the

## Estimation of Leak-Off Test Results as a Method for Minimum Horizontal Stress Determination

tests (second LOT of the main well and the LOT of the sidetrack, see 4.5), illustrates that the application of the LOP analysis is not the most accurate method which can be used for the least principal stress determination. Hence, the extent and quality of the test procedure and the collected pressure information define the achievable data and can limit the quality of the outcome.

Apart from the fact that the analysis of the leak-off tests done by various engineers can lead to different results, the conduct of the tests in formations with different lithology types can also lead to a misinterpretation of the outcomes. For the STR T1 wellbore, the first and the second LOT have been conducted in a formation with shale/sandstone lithology, the third LOT however was done in a carbonate formation. Due to the fact that the first LOT shows a high LOP of 1.77 SG at 839m MD, it can be assumed that this test was conducted within a formation which is more elastic and harder to fracture, most likely an almost pure shale. The high LOP value can also be confirmed by the cutting analysis of the geologists where the formation is described as soft, plastic and sticky clay. Another evidence for a more elastically deforming shale is delivered by the high Poisson's Ratio (approximately 0.4) and the low Young's Modulus at the depth range where the LOT took place. The second LOT, conducted at 2996m MD (Upper Cretaceous Gosau), showed a lower LOP value of 1.69 SG. Keeping in mind, that the Gosau formation consists of a mixture of conglomerate, sandstone, marl and shale, the lower LOP value seems not unrealistic. The cutting analysis showed moderately hard, calcareous claystone, siltstone and sandstone which is in accordance with the decrease in Poisson's Ratio (approximately 0.3) and the increase in Young's Modulus (approximately 20 GPa), indicating a lesser elastic, stiffer rock which fractures easier. The last LOT reported for the STR T1 wellbore was performed at 4504m MD in a Middle Triassic carbonate formation (Gutenstein fm.). This LOT showed an even smaller pressure value than both of the other tests, namely 1.63 SG. The fact that the test was done in a carbonate/dolomite formation makes it difficult to compare the result of this test to the results of the tests conducted in shale and sandstone (or a mixture of both) formations. Fully comparable results could normally just be delivered from LOTs performed within the same lithology type, normally shale. However, in reality it is nearly not feasible to accomplish the LOTs of a wellbore solely in shale formations. A possible explanation for the smaller pressure values within the carbonate formation at increased depth would be the increase in Young's Modulus (approximately 50 GPa) representing the increased stiffness of the rock and the high probability that the carbonate is fractured (partial and total losses have been reported, see Figure 11) and that a pre-existing fracture has opened instead of a new fracture has been initiated.

The resulting unitless effective stress ratio points, calculated from the  $S_{hmin}$  calibration points (LOP values) also showing a decrease over depth. Nevertheless, the ESR trend line which was applied to the ESR points was kept constant from surface to TD. This was done, because the first LOT was assumed to show a too high value and the third LOT was assumed to show a too low value. This presumption was also based on the ESR data from the pre-drill model which is based on several offset well measurements. The increase in ESR, determined for the pre-drill model, however was not realized for the post-drill model because no evidence for such an increase was present.

In summary it can be stated, that the minimum horizontal stress determination by the help of the conduct and analysis of LOTs is a widely used method within the petroleum industry. The results achieved by this application should not be applied without assessing



the applicability and accuracy of the data, though. Like mentioned above, the execution of an extended instead of a simple leak-off test will help to determine more reliable pressure values for the  $S_{hmin}$  determination and can be recommended for future leak-off test procedures. Another issue which could be found during analyzing the leak-off test values and calculating the minimum horizontal stress by the use of the Effective Stress Method is the difficulty of comparing test data from different lithology types. It was possible to find potential explanations for the decrease in leak-off pressure values with depth by having a closer look on the sedimentary rock type. However, the minimum horizontal stress determination was to some extent based on assumption of the pre-drill model which was in accordance with the second LOT, because it was assumed that the shallow test and the test in the carbonate formation do not deliver representative values. To overcome this problem, it could be helpful to try other  $S_{hmin}$  determination methods like for example the Eaton equation (Eaton 1969), where the Poisson's Ratio is an additional input parameter accounting for different lithology types. Basing the minimum horizontal stress determination on the LOT data of a single well seems doubtful from this point of view, especially for the case where the LOTs were conducted in formations with different lithology types. As it is usually the case, an increased number of LOTs or XLOTs gathered from several wellbores in the specific region will enhance the quality of the analysis and helps to identify uncertain pressure values which therefore should be excluded from the minimum horizontal stress evaluation



# Chapter 6 Conclusion

Like for every other for-profit corporation, it is of high importance for the oil and gas industry to conduct and accomplish as many operations as possible within the limits of the operations financial resources. However, it should be kept in mind that the safety of the activities is the most significant objective to consider. In the drilling engineering context, an enhancement in safety and cost-effectiveness can be determined by the utilization of geomechanical models. By the application of such predictive models, pore pressure, in-situ earth stresses and rock properties can be forecasted and the uncertainties of the drilling procedure can be reduced. Eventually the application of geomechanical models reduces the risks during drilling and by this improves the safety of the drilling process, reduces non-productive time and diminishes the expenditures.

This thesis covers the methodology of the generation of such a geomechanical model in general and for the specific case of the Stripfing T1/T1a wellbore, drilled in 2014 as an OMV exploration well in the central Vienna Basin. Based on this (post-drill) geomechanical model which was intended to be an update of the already built pre-drill model, which was used during the well planning phase to improve the decision making and the drilling operation itself, the importance of updating already created models with data from recently drilled wells, is represented. Due to the occurrence of a significantly overpressured section along the well path, an additional objective covered in this thesis arose, namely the determination of a possible explanation for the elevated pressure which has been forecasted before and approved during drilling.

The accomplishment of this thesis allows to draw conclusions concerning the model building in general as well as concerning the specific case of the STR T1 wellbore. Generally applicable recommendations for the creation of geomechanical models can be easily summarized. The better the quantity and quality of information (logging data, pressure tests, fractures tests, daily reports, etc.) the better the outcome will be. This is based on more advantageous analyzing methods which can be applied if certain data is available and more reliable results if the amount of calibration data is enhanced. Nevertheless, the increase in available data results in an increased effort to screen and assess this data before it can be utilized for the model building.

With respect to the post-drill geomechanical model of the STR T1 wellbore, it can be stated that the comparison to the pre-drill model showed a good conformity, which however is not visible immediately. The reason for that is the stratigraphy of the wellbore which was not expected to look like discovered. Incorporating this change in stratigraphy into the analysis visualizes the good quality of the forecasting model which, updated with newly gained data, but applying the original assumptions and equations, verifies satisfyingly with the drilling events and compressive wellbore failures.

Here it is to say that the improved availability of data influences the determination of the pore pressure, the minimum and maximum horizontal stress magnitude and direction and the verification of the model, the most. The application of a pore pressure predication, LOT analyses, image logging interpretations and stress polygon analyses could be conducted due to the recently gathered data and enhanced the quality of the model, compared to the pre-drill one.

Nevertheless, the generated post-drill model, or rather nearly every geomechanical model which describes the pore pressure, rock properties and stresses of the wellbore vicinity,

## Conclusion

offers room for improvement and every new information should be included into the model to enhance the accuracy. For the model built during accomplishing this thesis, however some recommendations are of higher relevance because these tasks were never before realized for any of the offset wells and the STR T1 well itself. These recommendations include the conduct of extended leak-off tests whereby the analysis of the least principal stress would be enhanced by the more precise determination of the pressure where the fractures, initiated into the formation, open, as well as the laboratory measurements of important rock properties to enhance the correlations between logs and UCS and the calibration of dynamic to static elastic properties and by this allowing a better constraint of the maximum horizontal stress and an improved wellbore failure prediction. Moreover, the conduct of pressure measurements, especially in the overpressured formations, would improve the current pore pressure prediction.

Cutting analysis as method to determine the causes of wellbore failures was not conducted during this thesis and could contain additional information to enhance the model. Some other subjects belonging to the specific model of the STR T1 wellbore are not addressed in this thesis and offer interesting topics for further research, namely the influence of chemical stresses as an overpressure mechanism leading to the enhanced pressure found during drilling the STR T1 as well as several offset wells and the determination of the origin of the overpressure in the surrounding of the carbonate sequence which was assumed to seal off the porous and permeable centroid, where the pressure transfer led to an elevated pressure gradient at the top of the structure, and holding an overpressure itself which was the prerequisite for the application of the centroid concept. A more general subject for future research could be the evaluation of different methods to determine the least principal stress. Here, a more precise evaluation of the advantages and disadvantages of different methods to determine fracture pressures and the associated analyses for the minimum horizontal stress determination could be beneficial to force decisions towards more advanced and maybe more expensive methods which however deliver more exact and reliable results and because of that would be the favored methods after the execution of a cost-benefit analysis. Another useful comparison from the viewpoint of horizontal stress determination could be the assessment of different approaches to calculate the minimum and maximum horizontal stress (e.g. Effective Stress Method, Stress Contrast Method), here especially the LOT/XLOT (or more general fracturing test) data analysis for testing conducted in different lithology types to calculate or calibrate the minimum horizontal stress from or to fracturing test calibration points. To ascertain how strong the minimum horizontal stress calculation is influenced by the changing lithology of the tested formations and which one of the methods is affected least by these changes would simplify the selection of the stress determination method.

Important topics beyond the objectives of this thesis, but related to the topic of post-drill model building are the methodology of the model building for deviated wellbores and further fields of application for geomechanical models, which are both not discussed in this thesis but provide a good starting point for other researches.

# Appendix

Erathem	System	Series	Stage		Formation	Base MD
Cenozoic	Neogen	Miocene	Tortonian	Pannonium		9
Cenozoic	Neogen	Miocene	Serravallium	Sarmatium		723,6
Cenozoic	Neogen	Miocene	Langhian - Serravallian	Badenium	Buli - Rot - Zone	1060
Cenozoic	Neogen	Miocene	Langhian - Serravallian	Badenium	Sandschalerzone	1707
Cenozoic	Neogen	Miocene	Burdigalian	Karpatian	Aderklaa Gänserndorf Fm.	2132
Mesozoic	Triassic	Middle Triassic	Anisian		Steinalm Fm./Steinalm Dolomite	2705
Mesozoic	Cretaceous	Upper Cretaceous	Turonian - Campanian		Lim. Gosau Fm.	3105
Mesozoic	Jurassic	Upper Jurassic (Malm)				
Mesozoic	Jurassic	Lower Jurassic (Lias)				3605
Mesozoic	Triassic	Upper Triassic	Norian		Hauptdolomit	4255

**Table 15:** Stratigraphy forecasted for the STR T1 wellbore (pre-drill model).

Lithology	Equation $v_s$ (pseudo) [km/s]
Sandstone	$2.4462 * \ln(v_p) - 1.1947$
Shale/Marl	$2.5099 * \ln(v_p) - 1.2981$
Limestone/Dolomite	$3.1048 * \ln(v_p) - 2.2567$

**Table 16:** Equations used to derive pseudo shear sonic [km/s] from compressional sonic [km/s] for the pre-drill model workflow.

Depth	$S_v$	Azimuth SH	BO Width	Borehole Azimuth	Borehole Deviation	Delta Pressure	Mud Weight	Pore Pressure	Poisson's Ratio	Internal friction	UCS low	UCS high	$S_h$ low	$S_h$ high	Lithology
m	SG	°	°	°	°	SG	SG	SG			MPa	MPa	SG	SG	
2795	2.38	25	72.4	320.5	0.225	0.05	1.09	1.04	0.384	0.8	23	60	1.53	1.87	Shale
2870	2.38	25	63.5	309.5	0.77	0.08	1.15	1.07	0.316	0.8	24	43	1.53	1.87	Shale
2878	2.38	25	69	310	0.81	0.08	1.15	1.07	0.066	0.8	24	43	1.55	1.89	Shale
2905	2.38	25	24.5	308.5	0.97	0.07	1.15	1.08	0.334	0.8	25	60	1.55	1.9	Shale
2957	2.39	25	23.8	324.5	0.98	0.05	1.15	1.1	0.335	0.8	25	60	1.55	1.9	Shale
3490	2.42	25	40.5	341.1	0.2	-0.21	1.36	1.57	0.345	0.8	49	77	1.79	2.19	Shale
3544	2.42	25	27.4	357	0.29	-0.21	1.36	1.57	0.3	0.8	50	77	1.79	2.19	Shale
3559	2.42	25	35.8	347	0.26	-0.21	1.36	1.57	0.334	0.8	50	77	1.79	2.19	Shale
3568.5	2.42	25	59.6	359	0.23	-0.21	1.36	1.57	0.319	0.8	50	77	1.79	2.19	Shale
3574	2.42	25	46.5	5	0.22	-0.21	1.36	1.57	0.275	0.8	50	77	1.79	2.19	Shale
3586	2.42	25	33.4	16	0.2	-0.21	1.36	1.57	0.295	0.8	51	77	1.79	2.19	Shale

**Table 17:** Input values for the stress polygon analysis conducted to determine the maximum horizontal stress for the STR T1 wellbore.

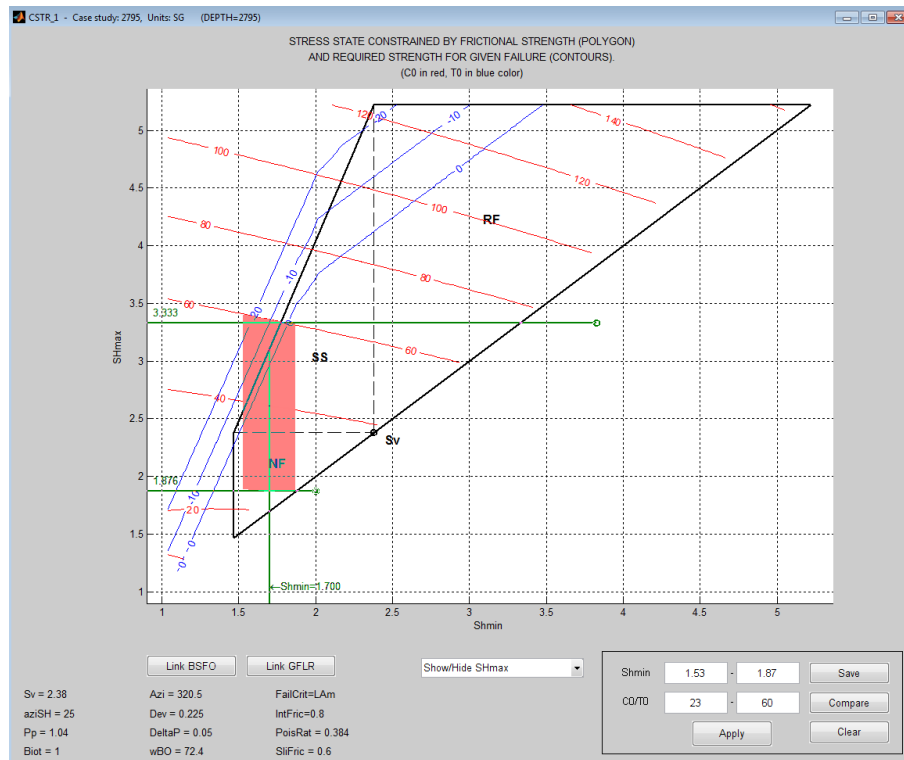


Figure 42: Stress polygon plot for prevailing conditions at 2795m MD.

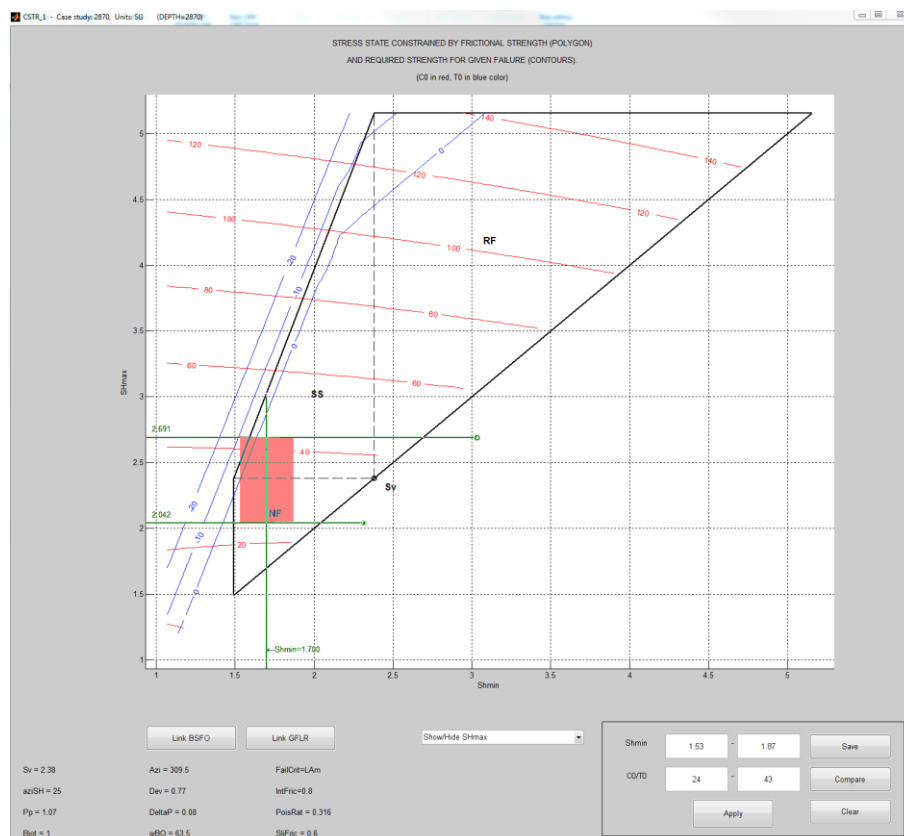


Figure 43: Stress polygon plot for prevailing conditions at 2870m MD.

# Appendix

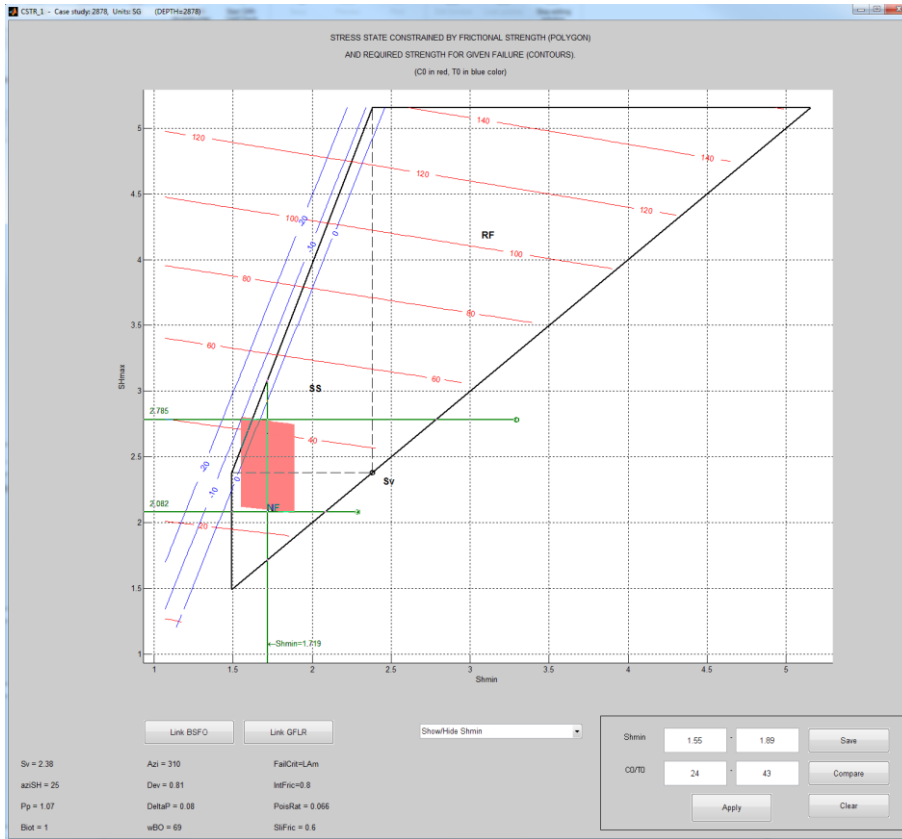


Figure 44: Stress polygon plot for prevailing conditions at 2878m MD.

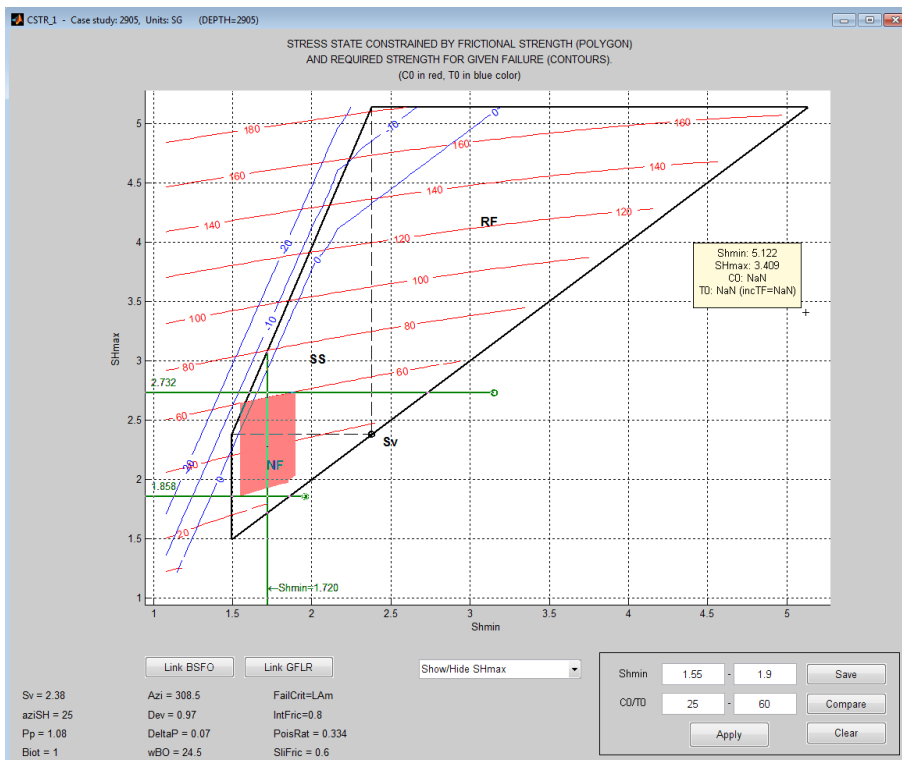


Figure 45: Stress polygon plot for prevailing conditions at 2905m MD.



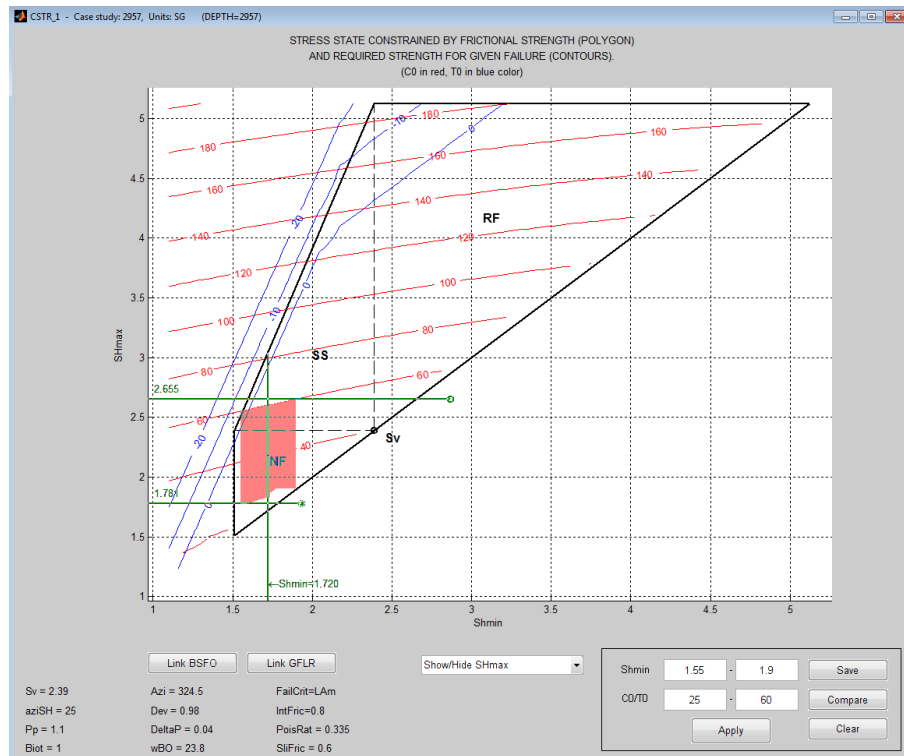


Figure 46: Stress polygon plot for prevailing conditions at 2957m MD.

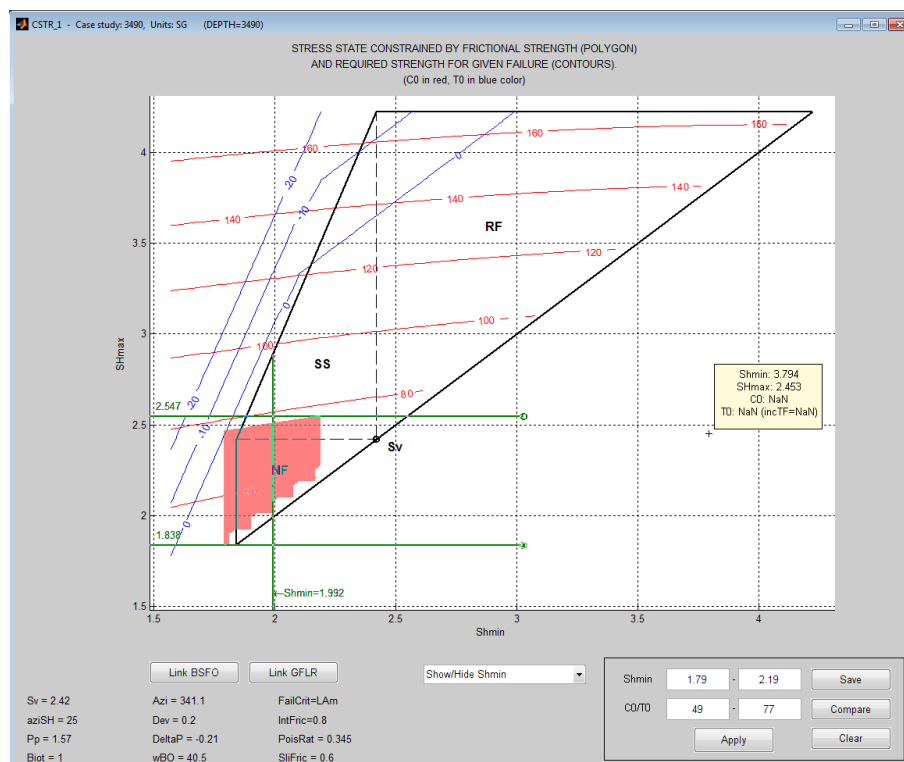


Figure 47: Stress polygon plot for prevailing conditions at 3490m MD.

# Appendix

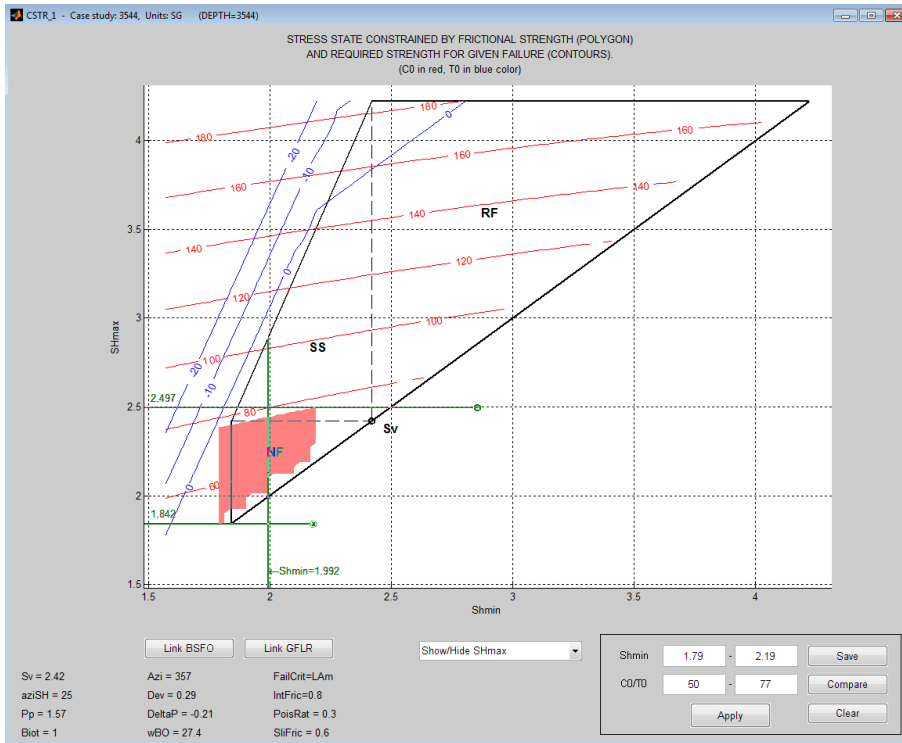


Figure 48: Stress polygon plot for prevailing conditions at 3544m MD.

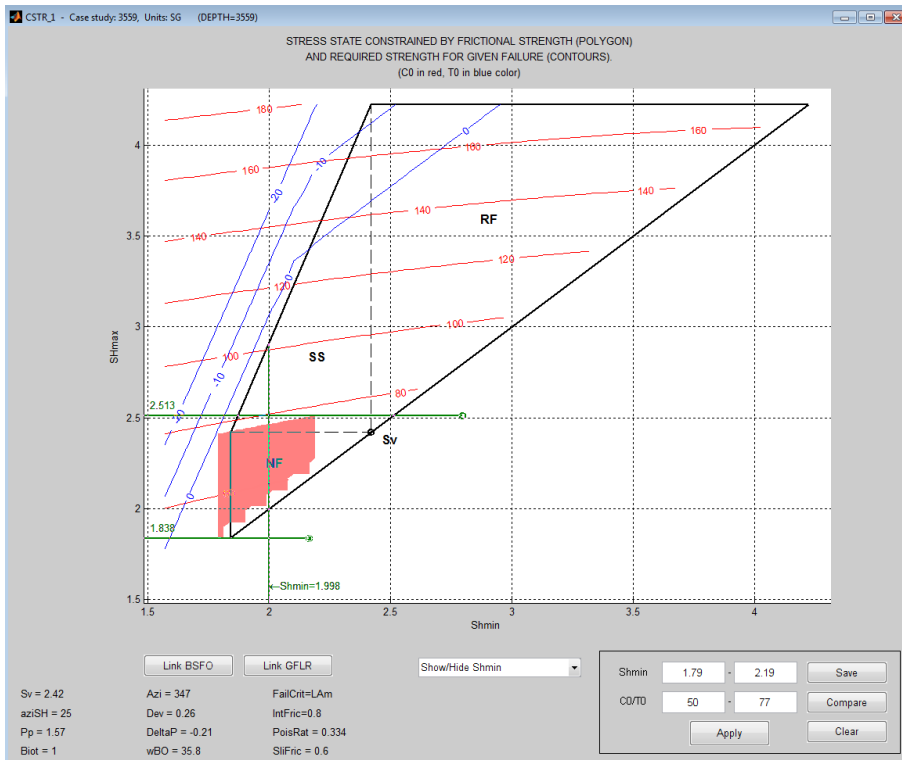


Figure 49: Stress polygon plot for prevailing conditions at 3559m MD.

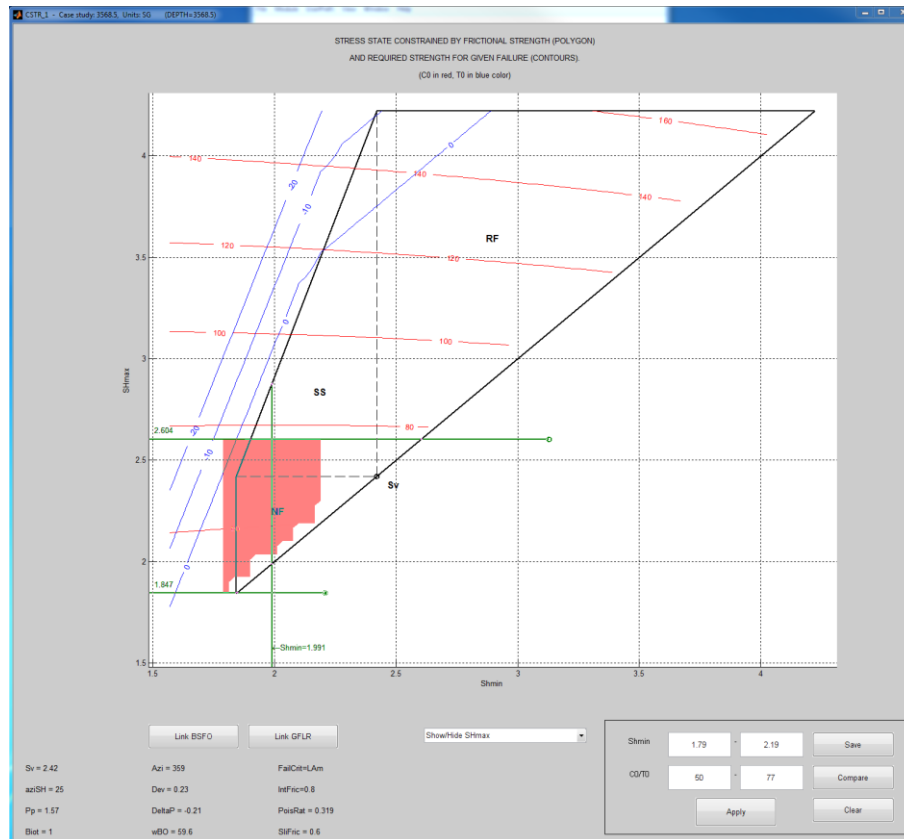


Figure 50: Stress polygon plot for prevailing conditions at 3568.5m MD.

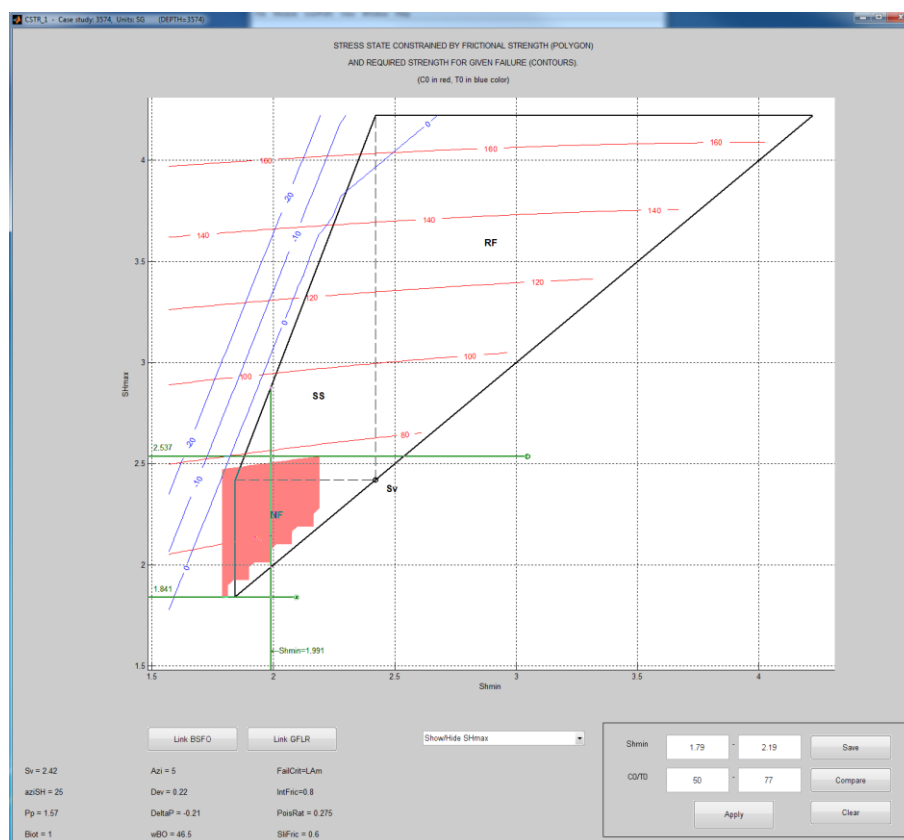


Figure 51: Stress polygon plot for prevailing conditions at 3574m MD.

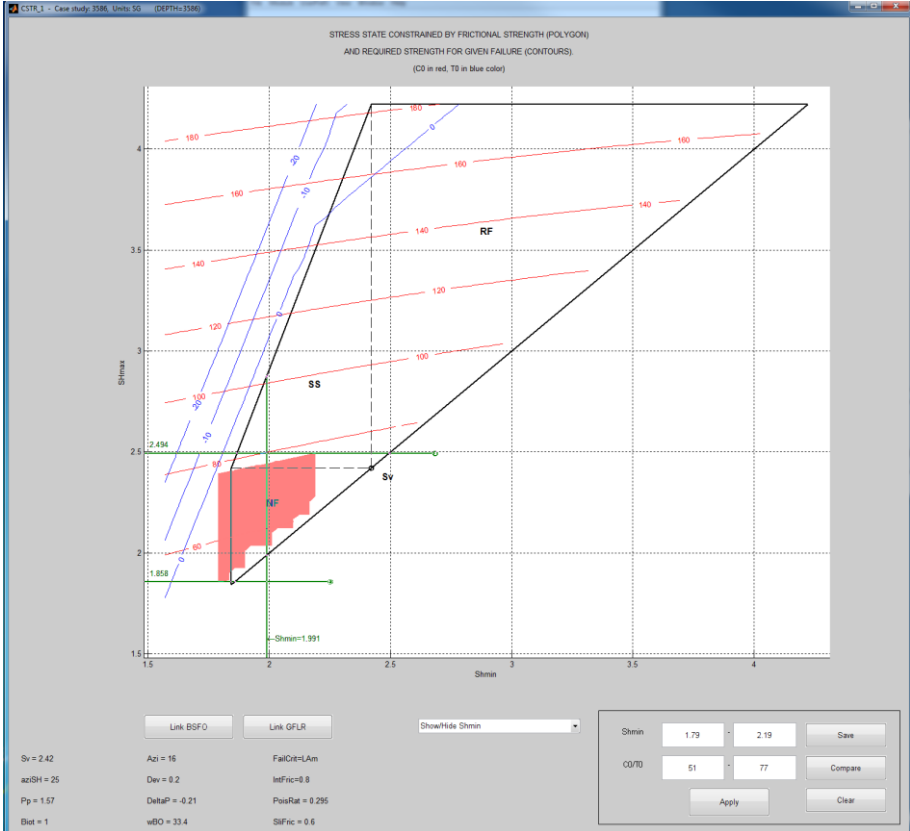
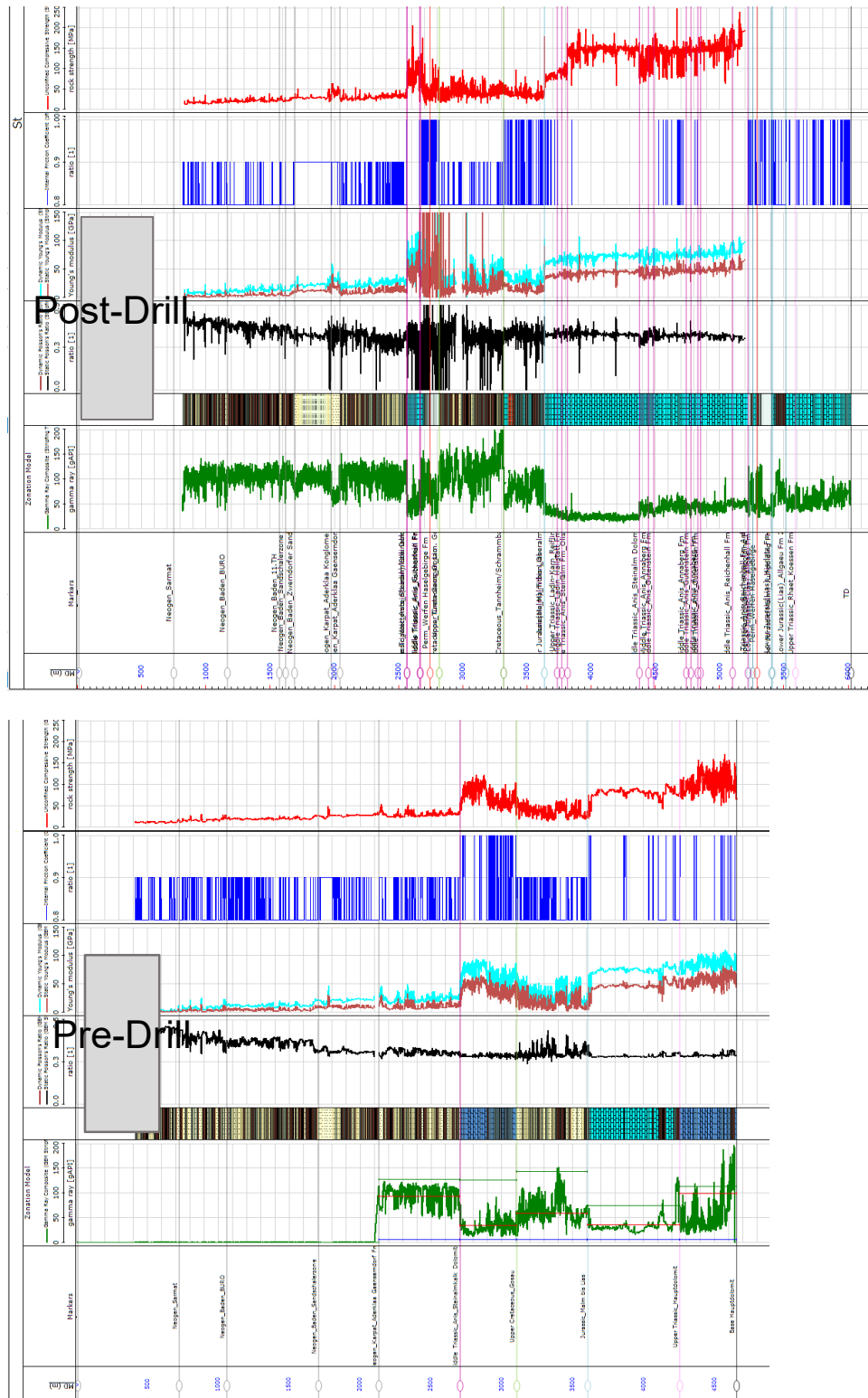


Figure 52: Stress polygon plot for prevailing conditions at 3586m MD.



**Figure 53:** Summary of the rock property logs for the pre- and post-drill model. Tracks showing from left to right: GR (green), lithology, dynamic and static Poisson's Ratio (identical logs, black), dynamic (turquoise) and static (ruby) Young's Modulus, Coefficient of internal friction (blue) and UCS (red). The Biot's Coefficient is assumed to be one for every lithology.

# Bibliography

- Addis, M.A., T.H. Hanssen, N. Yassir, D.R. Willoughby, and J. Enever. 1998. "A Comparison Of Leak-Off Test And Extended Leak-Off Test Data For Stress Estimation." In SPE-47235-MS. SPE: Society of Petroleum Engineers. <https://doi.org/10.2118/47235-MS>.
- Anderson, Ernest Masson. 1951. *The Dynamics of Faulting and Dyke Formation with Applications to Britain*. 206 p. Edinburgh: Oliver and Boyd. [//catalog.hathitrust.org/Record/001488761](http://catalog.hathitrust.org/Record/001488761).
- Atashbari, Vahid. 2016. "Origin of Overpressure and Pore Pressure Prediction in Carbonate Reservoirs of the Abadan Plain Basin." Adelaide: University of Adelaide.
- Baumgärtner, J., and M.D. Zoback. 1989. "Interpretation of Hydraulic Fracturing Pressure-Time Records Using Interactive Analysis Methods." *International Journal of Rock Mechanics and Mining Sciences & Geomechanics Abstracts* 26 (6): 461–69. [https://doi.org/10.1016/0148-9062\(89\)91422-8](https://doi.org/10.1016/0148-9062(89)91422-8).
- Croizé, Delphine. 2010. "Mechanical and Chemical Compaction of Carbonates - An Experimental Study." Oslo: University of Oslos.
- Eaton, Ben A. 1969. "Fracture Gradient Prediction and Its Application in Oilfield Operations." SPE-2163-PA, October. <https://doi.org/10.2118/2163-PA>.
- Eberstein, W.H. von, G.H. Mayo, M.A. Weaver, E. van Oort, and E.B. Kotara. 2004. "Method for Formation Pressure Control While Drilling," November. <http://www.google.ch/patents/US6823950>.
- Enever, J.R., N.A. Yassir, D.R. Willoughby, and M.A. Addis. 1996. "Recent Experience with Extended Leak-off Tests for in-Situ Stress Measurement in Australia." In *APPEA Journal*, 36:528–35. Darwin NT.
- Grauls, D. 1999. "Overpressures: Causal Mechanisms, Conventional and Hydromechanical Approaches." *Oil & Gas Science and Technology* 54 (6): 667–78.
- Grauls, D., and C. Cassagnol. 1993. "Identification of a Zone of Fluid Pressure-Induced Fractures from Log and Seismic Data - a Case History." *First Break* 11 (2): 59–68.
- Green, Sam, Alexander Edwards, and Stephen O'Connor. 2016. "Predicting Pore Pressure in Carbonates: A Review," January.
- Guo, F., N.R. Morgenstern, and J.D. Scott. 1993. "Interpretation of Hydraulic Fracturing Pressure: A Comparison of Eight Methods Used to Identify Shut-in Pressures." *International Journal of Rock Mechanics and Mining Sciences* 30: 627–31.
- Haimson, Bezalel, and Charles Fairhurst. 1967. "Initiation and Extension of Hydraulic Fractures in Rocks." SPE-1710-PA, September. <https://doi.org/10.2118/1710-PA>.

- Hayashi, K., and Bezalel C. Haimson. 1991. "Characteristics of Shut-in Curves in Hydraulic Fracturing Stress Measurements and Determination of in Situ Minimum Compressive Stress." *Journal of Geophysical Research* 96: 18311–21.
- Hickman, S., and M.D. Zoback. 1983. "The Interpretation of Hydraulic Fracturing Pressure- Time Data for in Situ Stress Determination. Hydraulic Fracturing Measurements." Washington, D.C, National Academy Press.
- Hottmann, C.E., and R.K. Johnson. 1965. "Estimation of Formation Pressures from Log-Derived Shale Properties." SPE-1110-PA, June. <https://doi.org/10.2118/1110-PA>.
- Knoop, Oliver. 2015. "Geological Work Program Exploration Well Stripfing Tief1/Tief 1a."
- Lacy, Lewis L. 1997. "Dynamic Rock Mechanics Testing for Optimized Fracture Designs." In SPE-38716-MS. SPE: Society of Petroleum Engineers. <https://doi.org/10.2118/38716-MS>.
- Lei, Xiao, Jun Cai, Shi Duo Yang, Yen Han Shim, Hong Xia Wu, and Yu Xi Wang. 2007. "Fully Integrated Solution for LWD Resistivity Image Application a Case Study from Beibu Gulf, China." In *Formation Evaluation in Horizontal Wells*. Mumbai.
- Li, Gang, Apiwat Lorwongngam, and Jean-Claude Roegiers. 2009. "Critical Review Of Leak-Off Test As A Practice For Determination Of In-Situ Stresses." In ARMA-09-003. ARMA: American Rock Mechanics Association.
- Lin, Weiren, Koji Yamamoto, Hisao Ito, Hideki Masago, and Yoshihisa Kawamura. 2008. "Estimation of Minimum Principal Stress from an Extended Leak-off Test Onboard the Chikyu Drilling Vessel and Suggestions for Future Test Procedures."
- McNally, G.H. 1987. Estimation of Coal Measures Rock Strength Using Sonic and Neutron Logs. *Geoexploration* 24, 381–395.
- Militzer, H., and R. Stoll. 1973. *Einige Beiträge der Geophysik Zur Primärdatenerfassung Im Bergbau*. Neue Bergbautechnik 3 (1).
- Nie, Xin, Changchun Zou, Li Pan, Zhaohui Huang, and Dongming Liu. 2013. "Fracture Analysis and Determination of In-Situ Stress Direction from Resistivity and Acoustic Image Logs and Core Data in the Wenchuan Earthquake Fault Scientific Drilling Borehole-2 (50–1370m)." *Tectonophysics* 593 (Supplement C): 161–71. <https://doi.org/10.1016/j.tecto.2013.03.005>.
- Rummel, F., and J. Hansen. 1989. "Interpretation of Hydrofrac Pressure Recordings Using a Simple Fracture Mechanics Simulation Model." *International Journal of Rock Mechanics and Mining Sciences & Geomechanics Abstracts* 26 (6): 483–88. [https://doi.org/10.1016/0148-9062\(89\)91425-3](https://doi.org/10.1016/0148-9062(89)91425-3).
- Strauss, Philipp. 2015. "Juvavischer Olistolith in Den Kalkalpen Unter Dem Wiener Becken Erbohrt." In *Arbeitstagung 2015*, 110. Mitterdorf im Müürztal.
- Strauss, Philipp, and König. 2015. "After Action Review Exploration Well Stripfing Tief 1."

## Bibliography

- Swarbrick, Richard E., Mark J. Osborne, and Gareth S. Yardley. 2004. "Comparison of Overpressure Magnitude Resulting from the Main Generating Mechanisms." In AAPG Memoir, 76:1–12.
- Tellez, C.P., Francis Laurent Elisabeth, Elena Bentosa, Diego Munoz, and Cesar Alberto Cortes. 2012. "Geomechanics Characterization of the Clastics and Carbonates Formation of Southern Fields of Mexico (2005 - 2009)." In SPE-153430-MS. SPE: Society of Petroleum Engineers. <https://doi.org/10.2118/153430-MS>.
- Traugott, M.O. 1997. "Pore/Fracture Pressure Determinations in Deep Water, Deep Water Supplement to World Oil,," August.
- Traugott, M.O., and P.D. Heppard. n.d. "Use Of Seal, Structural, and Centroid Information in Pore Pressure Prediction."
- White, Adrian J., Martin O. Traugott, and Richard E. Swarbrick. 2002. "The Use of Leak-off Tests as Means of Predicting Minimum *in-Situ* Stress." Petroleum Geoscience 8 (2): 189. <https://doi.org/10.1144/petgeo.8.2.189>.
- Zheng, Yan, Katja Schulze, and Manuel Blumenthal. 2012. "Geomechanical Earth Model (GEM) for the Stripfing Tief Area, Austria."
- Zoback, Mark D. 2010. Reservoir Geomechanics. Cambridge University Press.
- Zoback, Mark D., and Bezalel C. Haimson. 1982. "Status Of The Hydraulic Fracturing Method For In-Situ Stress Measurements." In ARMA-82-141. ARMA: American Rock Mechanics Association.
- "Diagnosing Wellbore Failure." n.d. Accessed October 12, 2017. <http://www.halliburton.com/public/consulting/contents/Posters/Wellbore-Failure-Portrait.pdf>.
- Nolen-Hoeksema, Richard. n.d. "Elements of Hydraulic Fracturing." Schlumberger Oilfield Review. Accessed October 1, 2017. [http://www.slb.com/resources/oilfield\\_review.aspx](http://www.slb.com/resources/oilfield_review.aspx).



# Acronyms

<i>AAR</i>	After Action Review
<i>BO</i>	Breakout
<i>CHT</i>	Cased Hole Test
<i>DDR</i>	Daily Drilling Report
<i>DEF</i>	Drilling Enhanced Fracture
<i>DGR</i>	Daily Geological Report
<i>DITF</i>	Drilling Induced Tensile Fracture
<i>ES</i>	Effective Stress
<i>ESR</i>	Effective Stress Ratio
<i>FBP</i>	Formation Breakdown Pressure
<i>FCP</i>	Fracture Closure Pressure
<i>FIT</i>	Formation Integrity Test
<i>FPP</i>	Fracture Propagation Pressure
<i>GEM</i>	Geomechanical Earth Model
<i>HC</i>	Hydrocarbon
<i>HF</i>	Hydraulic Fracturing
<i>ISIP</i>	Instantaneous Shut-In Pressure
<i>LOP</i>	Leak-Off Pressure
<i>LOT</i>	Leak-Off Test
<i>LWD</i>	Logging While Drilling
<i>MD</i>	Measured Depth
<i>MW</i>	Mud Weight
<i>MWD</i>	Measurement While Drilling
<i>NF</i>	Normal Faulting
<i>NPT</i>	Non-Productive Time
<i>NCT</i>	Normal Compaction Trend
<i>OHT</i>	Open Hole Test
<i>PPP</i>	Pore Pressure Prediction
<i>RF</i>	Reverse Faulting
<i>SS</i>	Strike-Slip
<i>TD</i>	True Depth

## Acronyms

<i>TVD</i>	True Vertical Depth
<i>UCS</i>	Unconfined Compressive Strength
<i>WL</i>	Wireline
<i>XLOT</i>	Extended Leak-Off Test

# Symbols

$c_b$	Compressibility of Rock	[1/Pa]
$c_g$	Compressibility of Individual Solid Grain	[1/Pa]
$\Delta t_{NCT}$	Measurement of Sonic Compressional Transit Time at Hydrostatic Pressure	[ $\mu$ s/ft]
$\Delta t_{obs}$	Measurement of Sonic Compressional Transit Time Obtained from Well Logging	[ $\mu$ s/ft]
$E$	Young's Modulus	[GPa]
$E_{dynamic}$	Dynamic Young's Modulus	[GPa]
$E_{static}$	Static Young's Modulus	[GPa]
$\mu_i$	Coefficient of Internal Friction	
$P_{NCT}$	Pressure for Normally Compacted Shales	[MPa], [SG]
$P_p$	Pore Pressure	[MPa], [SG]
$\zeta$	Density	[g/cm <sup>3</sup> ], [SG]
$S_{Hmax}$	Maximum Horizontal Stress	[MPa], [SG]
$S_{hmin}$	Minimum Horizontal Stress	[MPa], [SG]
$S_v$	Vertical Stress	[MPa], [SG]
$\nu$	Poisson's Ratio	
$\nu_{dynamic}$	Dynamic Poisson's Ratio	
$\nu_{static}$	Static Poisson's Ratio	
$x_{obs}$	Measurement Obtained from Well Logging	
$x_{NCT}$	Measurement at Hydrostatic Pressure	

# List of Figures

<b>Figure 1:</b> Seismic section of the Tallesbrunn high from SW to NE. ....	6
<b>Figure 2:</b> Potential geological interpretations of the seismic, explaining the noticeable structure and the flat reflectors.....	6
<b>Figure 3:</b> Interpretation of the seismic section of the STR T1 well, pre-drill. ....	8
<b>Figure 4:</b> Interpretation of the seismic section of the STR T1 well, post-drill.....	8
<b>Figure 5:</b> Overview of the workflow steps which are conducted during model building. ....	10
<b>Figure 6:</b> Borehole section of the Stripfing T1 wellbore, logged with a GVR™ LWD tool.....	21
<b>Figure 7:</b> Borehole section of the Stripfing T1 wellbore, logged with a FMI™ wireline logging tool. ....	23
<b>Figure 8:</b> Examples of borehole sections of the STR T1 well with different hole diameters, logged with FMI™ wireline logging.....	24
<b>Figure 9:</b> Borehole sections of the STR T1 well, showing drilling enhanced fractures on the left and drilling induced tensile fractures on the right. ....	25
<b>Figure 10:</b> Exemplary stress polygon plot generated by the use of the SFIB™ program.....	29
<b>Figure 11:</b> Geomechanical relevant drilling events collected during drilling the STR T1 well....	36
<b>Figure 12:</b> Time vs. depth plot of the STR T1 wellbore, including the geomechanical relevant drilling events. ....	37
<b>Figure 13:</b> Geomechanical relevant drilling events illustrated in a mud weight vs. depth plot in the JewelSuite™ program, here without the mud weight curves.....	38
<b>Figure 14:</b> Observed stratigraphy, gamma ray and lithology (from left to right) of the STR T1 post-drill model in comparison with the forecasted stratigraphy, lithology and gamma ray (from left to right) of the pre-drill model. ....	40
<b>Figure 15:</b> Segment of the petrophysical interpretation done with Techlog™, showing the visualization of bad hole sections.....	42
<b>Figure 16:</b> Illustration of the overburden density and the resulting overburden stress .....	43
<b>Figure 17:</b> Pore pressure workflow view with determined pore pressure curve. ....	45
<b>Figure 18:</b> Leak-off test conducted in the 18.625in hole section of the STR T1 well. ....	49
<b>Figure 19:</b> Leak-off test conducted in the 13.375in hole section of the STR T1 well. ....	49
<b>Figure 20:</b> Repeated leak-off test conducted in the 13.375in hole section of the STR T1 well. ....	50
<b>Figure 21:</b> Leak-off test conducted in the 9.625in hole section of the STR T1 well. ....	50
<b>Figure 22:</b> Leak-off test conducted in the 9.625in hole section of the STR T1a well. ....	51
<b>Figure 23:</b> Summary of vertical and horizontal stresses and pore pressure for STR T1. ....	51
<b>Figure 24:</b> Azimuth distribution for drilling induced tensile fractures and breakouts.....	56
<b>Figure 25:</b> Stress polygon plots generated by using the SFIB™ program to determine $S_{Hmax}$ calibration points for the max. horizontal stress determination workflow. ....	59
<b>Figure 26:</b> Exemplification of the timing of logging running and mud weight alteration. ....	61
<b>Figure 27:</b> Exemplification of the timing of logging running and mud weight alteration. ....	61
<b>Figure 28:</b> Illustration of the lowest mud weight the borehole has experienced before or during logging and which therefore serves as input MW for the BO prediction.....	62
<b>Figure 29:</b> Visualization of the input parameters of the wellbore stability calculation.....	63
<b>Figure 30:</b> Illustration showing the caliper log next to the calculated BO width (a) to compare the measured wellbore failure (BO) with the calculated one. ....	64
<b>Figure 31:</b> Comparison of the sidetrack (left) and the main hole (right) lithology. ....	66
<b>Figure 32:</b> Illustration showing mud weight [SG], calculated BO width and BO width limit (0 - 180° scale), caliper log [in] and drilling events (from left to right) for the sidetrack of the STR T1. ....	67
<b>Figure 33:</b> Comparison of the pre- (left) and post-drill (right) model stratigraphy, lithology and gamma ray log. ....	71

<b>Figure 34:</b> Comparison of overburden density (green) and resulting overburden stress .....	72
<b>Figure 35:</b> Summary of events and measurements used to constrain the pore pressure of the pre-drill model.....	73
<b>Figure 36:</b> Comparison of the pre- and post-drill model pore pressure determination. ....	74
<b>Figure 37:</b> Comparison of the maximum and minimum ESR points with trend lines and resulting max. and min. horizontal stresses for pre- (left) and post-drill (right) model. ....	75
<b>Figure 38:</b> Mechanisms of overpressure generation, cf. Grauls 1999 and Atashbari 2016.....	80
<b>Figure 39:</b> Illustration of the pore pressure determined from NCT and Eaton’s Method, using two different approaches to determine the trend in the overpressured section.....	85
<b>Figure 40:</b> Application of the centroid buoyancy workflow to evaluate the overpressure in the Ruhpolding formation of the Zwerndorf T1 wellbore. ....	87
<b>Figure 41:</b> Idealized pressure versus volume plot of an extended leak-off test, cf. White, Traugott, and Swarbrick (2002) and von Eberstein et al. (2004). ....	89
<b>Figure 42:</b> Stress polygon plot for prevailing conditions at 2795m MD.....	101
<b>Figure 43:</b> Stress polygon plot for prevailing conditions at 2870m MD.....	101
<b>Figure 44:</b> Stress polygon plot for prevailing conditions at 2878m MD.....	102
<b>Figure 45:</b> Stress polygon plot for prevailing conditions at 2905m MD.....	102
<b>Figure 46:</b> Stress polygon plot for prevailing conditions at 2957m MD.....	103
<b>Figure 47:</b> Stress polygon plot for prevailing conditions at 3490m MD.....	103
<b>Figure 48:</b> Stress polygon plot for prevailing conditions at 3544m MD.....	104
<b>Figure 49:</b> Stress polygon plot for prevailing conditions at 3559m MD.....	104
<b>Figure 50:</b> Stress polygon plot for prevailing conditions at 3568.5m MD.....	105
<b>Figure 51:</b> Stress polygon plot for prevailing conditions at 3574m MD.....	105
<b>Figure 52:</b> Stress polygon plot for prevailing conditions at 3586m MD.....	106
<b>Figure 53:</b> Summary of the rock property logs for the pre- and post-drill model. ....	107

# List of Tables

<b>Table 1:</b> Determination of the stress regime by applying the effective stress ratio, after Anderson's theory of faulting (Anderson 1951).....	29
<b>Table 2:</b> Evaluation of collected drilling data, cf. Tellez et al. 2012. ....	30
<b>Table 3:</b> Interpretation of caving appearance as a method to determine the causes of failure....	32
<b>Table 4:</b> Input data available for the post-drill model building of the Stripfing T1 wellbore.....	35
<b>Table 5:</b> Stratigraphy drilled by the STR T1 well. ....	39
<b>Table 6:</b> Empirical equations used to calculate the pseudo density log [ $\text{g}/\text{cm}^3$ ] from the compressional sonic log [DTCO, $\mu\text{s}/\text{ft}$ ].....	41
<b>Table 7:</b> Density trend in the Vienna Basin, developed for the STR T1 pre-drill model.....	42
<b>Table 8:</b> Reported LOTs for the STR T1 well, interpreted by the drilling department. ....	48
<b>Table 9:</b> Reported LOTs for the STR T1 well, interpreted as part of this thesis. ....	48
<b>Table 10:</b> Friction coefficients for different lithology types, values are borrowed from the pre-drill model. ....	53
<b>Table 11:</b> Equations used to calculate the static Young's Moduli for different lithology .....	53
<b>Table 12:</b> Equations used to derive the UCS for different lithology types from compressional sonic slowness measurements; borrowed from the pre-drill model. ....	54
<b>Table 13:</b> Image logging running depth and used method for the STR T1 wellbore. ....	54
<b>Table 14:</b> Summary of the pressure values which can be obtained from the pressure vs. volume plot analysis of an extended leak-off test. ....	90
<b>Table 15:</b> Stratigraphy forecasted for the STR T1 wellbore (pre-drill model). ....	99
<b>Table 16:</b> Equations used to derive pseudo shear sonic [ $\text{km}/\text{s}$ ] from compressional sonic [ $\text{km}/\text{s}$ ] for the pre-drill model workflow. ....	99
<b>Table 17:</b> Input values for the stress polygon analysis conducted to determine the maximum horizontal stress for the STR T1 wellbore.....	100